Spring 2021

Biophysical Characterization of the Par-4 Tumor Suppressor: Evidence of Structure Outside the Coiled Coil Domain and Interactions with Platinum Chemotherapeutics

Andrea Megan Clark
Old Dominion University, andrea_korell@yahoo.com

BIOPHYSICAL CHARACTERIZATION OF THE PAR-4 TUMOR SUPPRESSOR: EVIDENCE OF STRUCTURE OUTSIDE THE COILED COIL DOMAIN AND INTERACTIONS WITH PLATINUM CHEMOTHERAPEUTICS

by

Andrea Megan Clark
B.S. May 2016, Salisbury University
M.S. August 2020, Old Dominion University

A Dissertation Submitted to the Faculty of
Old Dominion University in Partial Fulfillment of the
Requirements for the Degree of

DOCTOR OF PHILOSOPHY

CHEMISTRY

OLD DOMINION UNIVERSITY
May 2021

Approved by:

Steven M. Pascal (Director)

Lesley H. Greene (Member)

Alvin A. Holder (Member)

Erin B. Purcell (Member)

Harold C. Riethman (Member)

ABSTRACT

BIOPHYSICAL CHARACTERIZATION OF THE PAR-4 TUMOR SUPPRESSOR: EVIDENCE OF STRUCTURE OUTSIDE THE COILED COIL DOMAIN AND INTERACTIONS WITH PLATINUM CHEMOTHERAPEUTICS

Andrea Megan Clark
Old Dominion University, 2021
Director: Dr. Steven M. Pascal

Prostate apoptosis response-4 (Par-4) is an apoptosis-inducing tumor suppressor protein. Full-length Par-4 has previously been shown to be a predominantly intrinsically disordered protein (IDP) under neutral conditions, with significant regular secondary structure evident only within the C-terminal coiled coil domain. However, IDPs can gain ordered structure through the process of induced folding, which often occurs under non-neutral conditions. Previous work has shown that the Par-4 leucine zipper, which is a subset of the C-terminal coiled coil domain, is disordered under neutral conditions, but forms a dimeric coiled coil at acidic pH. Increase in ionic strength was also shown to increase leucine zipper formation. Building on this work, we undertook to study the effects of environment on a naturally occurring Par-4 segment, the cl-Par-4 fragment. During apoptosis, intracellular full-length Par-4 is cleaved at aspartic acid 131 by caspase-3, generating a 24 kilodalton fragment (cl-Par-4). Cl-Par-4 enters the nucleus and inhibits pro-survival genes, thereby preventing cancer cell proliferation.

Here, the structure of cl-Par-4 was investigated using circular dichroism (CD) spectroscopy, dynamic light scattering (DLS), intrinsic tyrosine fluorescence, and size exclusion chromatography with multi-angle light scattering (SEC-MALS). Biophysical characterization showed that under conditions of low salt and neutral pH, cl-Par-4 forms large soluble aggregates. We have clearly identified two disparate conditions under which cl-Par-4 forms non-aggregated

largely helical structures. First, with low salt and acidic pH, c l-Par-4 folds into a predominantly alpha helical and coiled coil structure. Second, at neutral pH and high ionic strength, cl-Par-4 forms highly helical tetramers. Together, these results suggest that the cellular environment influences the *in vivo* structure and self-association state of cl-Par-4 and that the tetramer may be the active conformation under specific intracellular conditions.

A third area of research involves the chemotherapeutic drug cisplatin and its trans isomer transplatin. We have shown that both bind directly to full-length Par-4 and the caspase-cleaved fragment. It appears that this binding interaction occurs through coordination of platinum to sulfur ligands in the protein, such as methionine and/or cysteine residues. This direct binding of cisplatin and transplatin could also subsequently influence apoptotic activity and Par-4 structure.

This dissertation is dedicated to my husband Tristin and my family and friends for their love and continued support.

ACKNOWLEDGEMENTS

There are several people who have helped with the successful completion of this dissertation. I wish to thank my advisor Dr. Steven Pascal for his guidance and support during my time in his lab. I would like to thank Dr. Komala Ponniah for her guidance and training in the Pascal Laboratory. To my committee members Dr. Greene, Dr. Purcell, Dr. Holder, and Dr. Riethman for their guidance and support on my research. I would like to acknowledge current and previous Pascal Lab members who have helped with this dissertation, specifically Meghan Warden, Andrea Yawn, Christiana Ntangka, Laura Sweet, Emily Raitt, Benjamin Smith, Krishna Raut, and Rebecca Richardson. I would like to thank the Department of Chemistry and Biochemistry at ODU. This work was supported by Old Dominion University startup funds to Dr. Steven M. Pascal. In addition, I would like to thank the Virginia Space Grant Consortium for support via a VSGC graduate fellowship. I would also like to thank Dr. Alvin Holder for his gift of cisplatin (Sigma Aldrich) which was purchased with funds from the National Institute of General Medical Sciences of the National Institutes of Health under Award Number T34GM118259. Lastly, I would like to thank my husband Tristin for his support, love, and encouragement.

NOMENCLATURE

Par-4	Prostate apoptosis response-4
cl-Par-4	Caspase-cleaved Par-4
FL-Par-4	Full-length Par-4
SAC	Selective for apoptosis induction in cancer cells
CC	Coiled coil
LZ	Leucine zipper
NLS2	Nuclear localization signal 2
NES	Nuclear export sequence
GRP78	Glucose regulated protein 78
IDP	Intrinsically disordered protein
cisPt	Cisplatin
transPt	Transplatin
CD	Circular dichroism
DLS	Dynamic light scattering
SEC-MALS	Size exclusion chromatography with mutli-angle light scattering
SDS-PAGE	Sodium dodecyl sulfate polyacrylamide gel electrophoresis
ITC	Isothermal titration calorimetry

TABLE OF CONTENTS

LIST OF TABLES

LIST OF FIGURES

Figure Page

CHAPTER 1

INTRODUCTION

INTRINSICALLY DISORDERED PROTEINS (IDPS) AND THEIR UNUSUAL BIOPHYSICS

In contrast to the lock-and-key model for protein structure, not all proteins exist in one set three-dimensional structure [1-3]. Natural proteins can often exist in one of three major protein forms: functional and folded, nonfunctional and misfolded, or functional and intrinsically disordered [1, 4]. Intrinsically disordered proteins (IDPs) are a class of proteins that lack stable three-dimensional structure and are considered natively unfolded [2, 3, 5, 6]. IDPs often lack significant ordered secondary, tertiary, or quaternary structure and rather, exist in random coil structures with enhanced conformational flexibility [1]. Proteins may also have intrinsically disordered protein regions (IDPRs) along with ordered domains. IDPs and IDPRs often function in cell signaling and therefore, are more abundant in eukaryotes [1, 7, 8]. IDPs and IDPRs often have a decreased number of order-promoting residues such as Trp, Cys, Ile, Phe, Tyr, Asn, Val, and Leu and instead are enriched in disorder-promoting residues such as Lys, Pro, Arg, Gly, Glu, Ser, Gln, and Ala. [1, 5, 9, 10].

The conformational behavior of IDPs and IDPRs greatly contrasts that of ordered globular proteins. Conformational flexibility allows IDPs to accommodate multiple binding interactions and form flexible ensembles which is important in cell signaling pathways [6, 11-13]. IDPs often represent a mixture of partially folded protein segments [4]. IDPs can undergo a functional disorder to order transition called induced folding which can be triggered by environmental changes or substrate binding, resulting in the formation of intermediate pre-molten globule (PMG) and molten

globule (MG) conformations or a predominantly folded structure [14-18]. IDPs are often highly unstructured in physiological conditions but gain structure in un-physiological conditions such as extreme temperature, acidic or basic pH, or extreme ionic strength [5, 19].

IDPS AND HUMAN DISEASE: "DISORDER IN DISORDERS" CONCEPT

There is an enrichment of IDPs in human diseases such as cancer, cardiovascular disease, and neurodegenerative disease [6]. Approximately 79% of cancer-associated proteins and 66% of cell-signaling proteins contain regions of disorder that are thirty residues in length or longer [6]. Failure of a protein to adopt its functional conformational state can lead to protein misfolding, gain of toxic functions, aggregation, and loss of normal function [6]. Many IDPs function in cell signaling pathways where intrinsic disorder can serve as a regulatory mechanism with "on-off" switch-type interactions, highlighting the importance of cell signaling and intrinsic disorder in a wide range of diseases [20, 21]. Examples of IDPs and proteins with IDPRs associated with cancer include p53, PTEN, BRCA1, HPV proteins, and EWS [22-24]. IDPs including alpha synuclein and amyloid β are associated with neurodegenerative diseases [25]. Prions implicated in scrapie, bovine spongiform encephalopathy, and Creutzfeldt-Jakob disease are among the IDP class of proteins [6, 26-29].

INTRINSICALLY DISORDERED PROSTATE APOPTOSIS RESPONSE-4 (PAR-4) TUMOR SUPPRESSOR

Par-4 is a pro-apoptotic tumor suppressor protein that was first identified in studies of prostate cancer [30-32]. In normal mammalian tissue, Par-4 is ubiquitously expressed, localized in the

cytoplasm of healthy cells, and spontaneously secreted [30, 31, 33, 34]. Par-4 contains two nuclear localization sequences (NLS1 and NLS2), a Vasa domain, a selective for apoptosis induction in cancer cells (SAC) domain, a coiled coil (CC) domain with a leucine zipper (LZ), and a nuclear export sequence (NES) (Figure 1) [31, 34, 35]. The SAC domain is the minimum fragment necessary to induce apoptosis [35-37]. The Par-4 CC contains a heptad repeat characteristic of a LZ [34]. The isolated C-terminal LZ can interconvert between a partially ordered monomer (POM) and a coiled coil dimer (CCD) and forms a more stable dimer under acidic conditions [38-41]. X-ray crystallography studies have confirmed dimer formation in the entire CC domain [42]. However, little is known about the structure of the remainder of the protein except that most of the full-length Par-4, outside of the CC, appears to be disordered in vitro [38, 39]. Most identified protein interactions involving Par-4 are mediated via the CC and LZ [31, 42]. These include interactions with Wilms' tumor 1 (WT1), atypical isoforms of protein kinase C (aPKC), DAP-kinases (Dlk/ZIP), and THAP1 [43-47].

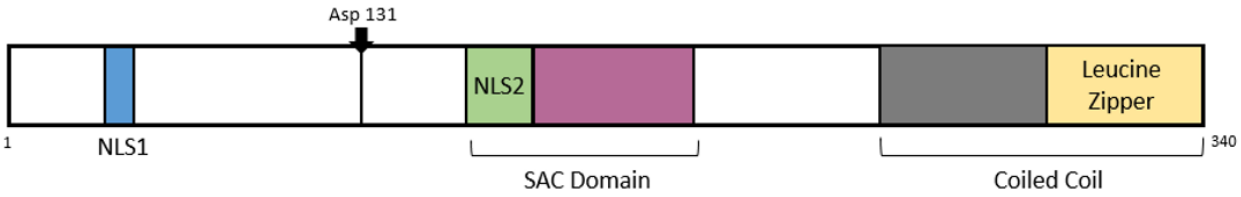

Fig. 1. Domain structure of full-length Par-4.

In the Par-4 LZ, negative charge-charge repulsion between aspartic and glutamic acid residues at the *g* and *e* positions of the helical wheel contribute to conformational instability of the dimer (Figure 2). Interestingly, extreme conditions such as high ionic strength or acidic pH are known to help highly polar IDPs fold by shielding or preventing charge-charge repulsion [2, 4, 5] [48-50].

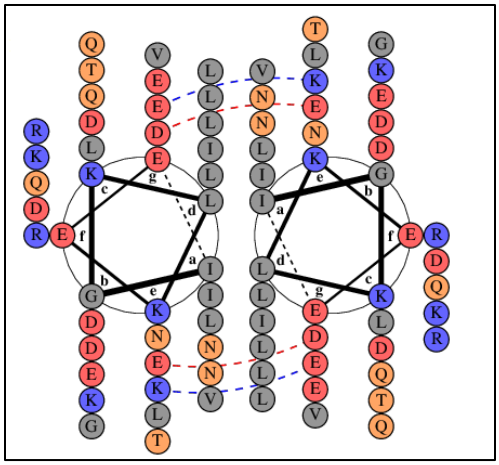

Fig. 2. Helical wheel representation of the Par-4 leucine zipper parallel dimer (DrawCoil 1.0) [51, 52]. Blue and red indicate basic and acidic residues, respectively. Red dashed lines represent inter-helical charge-charge repulsion and blue dashed lines represent salt bridges.

PAR-4 AND APOPTOSIS INDUCTION

Apoptosis induction by Par-4 is highly specific and is occurs through both extracellular and intracellular mechanisms (Figure 3) [53, 54]. GRP78 is primarily found in the ER of healthy cells but translocates to the cell surface of cancer cells due to ER stress [33, 53]. The interaction between GRP78 and the SAC domain of Par-4 at the cell surface initiates the apoptotic Fas/FasL-FADD pathway, activating both the intrinsic and extrinsic caspase cascades. [33, 54, 55].

Additionally, several post-translational modifications of Par-4 are important for cancer cell apoptosis. Phosphorylation of Par-4 at T163 by PKA serves as an activating phosphorylation whereas phosphorylation at S228 or S231 by Akt/PKB or CK2 prevents nuclear translocation of Par-4 [36, 56]. After activation of the caspase-cascade and phosphorylation by PKA, cytoplasmic full length Par-4 is cleaved by caspase-3 at D131, which generates caspase-3-cleaved Par-4 (cl-Par-4), a 24 kilodalton “activated” fragment [57, 58]. The small 15 kilodalton Par-4 amino-terminal fragment (PAF) remains in the cytoplasm [57, 58]. The cl-Par-4 fragment retains the SAC domain which includes NLS2, the CC with the LZ, and the linker domain which connects the SAC and CC domains

[35, 57]. Nuclear translocation of cl-Par-4 via NLS2 allows inhibition of pro-survival pathways that mediate cancer cell survival including NF-κB and Bcl-2 [35, 44, 54, 56, 57, 59].

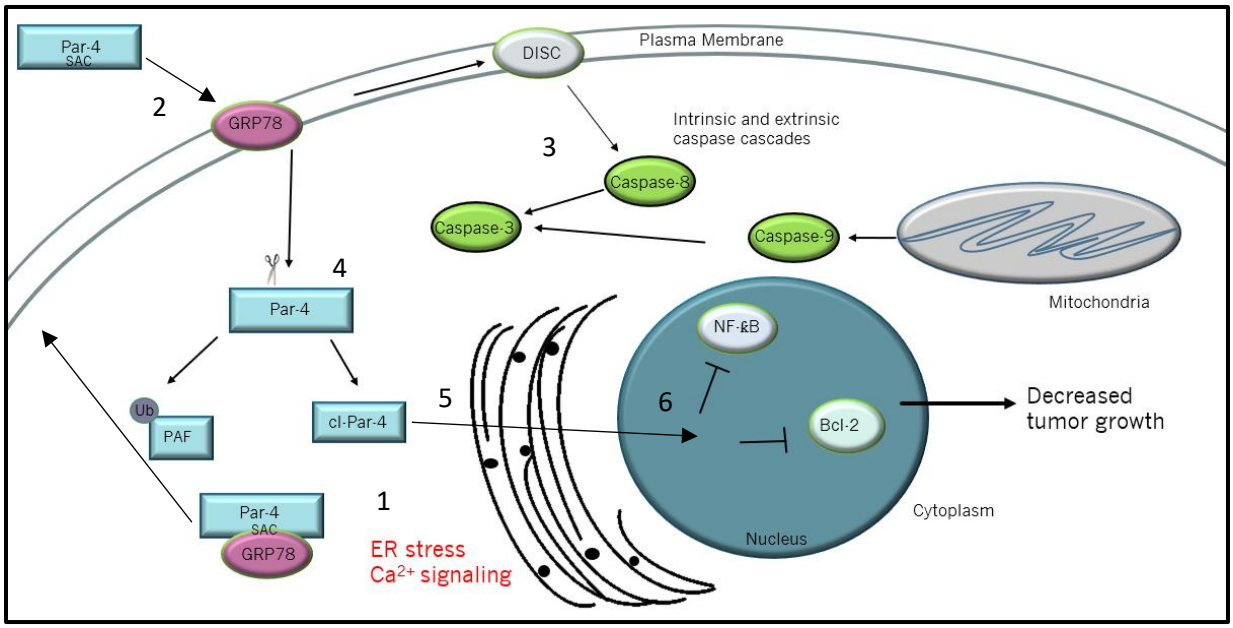

Fig. 3. Apoptosis induction by Par-4.

PAR-4 AND CANCER THERAPY

The *Par-4/PAWR* gene is found on the unstable chromosome 12q21.2, which can be mutated or deleted in cancers, contributing to low Par-4 levels [60]. However, Par-4 downregulation often occurs through mechanisms other than gene mutation or deletion. Par-4 down-regulation can result from over-activated oncogenes such as Ras, epigenetic silencing, or post-translational modifications that render the protein inactive [36, 61]. Par-4 down-regulation occurs in a variety of cancers including prostate, breast, and endometrial cancers, renal cell carcinoma, acute and chronic leukemia, and neuroblastoma [62-65]. Low Par-4 levels have been shown to correlate to metastasis, increased chance of cancer recurrence, and resistance to chemotherapeutics [64, 66].

For example, Par-4 is epigenetically silenced by the transcription factor TWIST, which promotes cancer recurrence in mouse breast cancer models [61]. However, tumor growth decreased after restoring Par-4 expression to apoptosis-inducing levels [61]. Additionally, purified recombinant Par-4 has been shown to decrease tumor growth in mice models [67]. Recently, Par-4 with an extended sequence was engineered to extend the half-life, making this engineered construct more stable in therapeutics [68]. Therefore, restoring apoptosis-inducing levels of Par-4, and the utilization of recombinant Par-4, are attractive therapeutic strategies to combat cancer.

SYNERGISTIC ANTI-TUMOR EFFECT OF PAR-4 AND CISPLATIN

Recent studies have shown a correlation between Par-4 and cisplatin efficacy. Cisplatin (cis-diamminedichloridoplatinum [II], cisPt) is a platinum-based chemotherapeutic agent that targets proliferating cells (Figure 4) [69, 70]. The mechanism of action occurs through cross-linking of purine DNA bases, which inhibits DNA synthesis [69, 70]. CisPt is used to treat many cancers including lung, breast, ovarian, and brain cancers, along with carcinomas and lymphomas [70].

Downregulation of Par-4 conferred resistance to cisPt treatment in pancreatic cancer cells, while overexpression of Par-4 conversely prevented resistance to cisPt treatment [71]. Combined treatment of Par-4 and cisPt had an inhibitory effect on human Wilms' tumor cells, via Par-4-induced sensitization to cisPt [72]. CisPt treatment of ovarian and endometrial cancer cells increased cellular levels of cl-Par-4 [73]. In chemosensitive cells, cisPt treatment enhanced caspase-induced cleavage of FL-Par-4 and increased cellular levels of cl-Par-4 [73]. However, it is not known whether these correlations between Par-4 and cisPt activities are the result of direct interaction, or whether intermediaries may be involved.

INTERACTIONS OF PLATINUM CHEMOTHERAPEUTICS WITH PROTEINS

Multiple negative side effects are associated with cisPt treatment [69, 70]. One source of negative side effects is binding to cellular proteins, which occurs because cisPt has high affinity towards S- and N-donors [74]. After cisPt hydrolysis upon exposure to aqueous solution, the resulting reactive cationic species readily reacts with the nitrogen or sulfur sites found in methionine, histidine, and cysteine residues [74]. This is problematic in cancer treatment, wherein cisPt can be trapped in complexes with cellular proteins instead of cross-linking DNA in proliferating cells.

Characterizing platinum-protein interactions and the effect on Pt/protein function will further our understanding of how cancer cells become resistant to platinum chemotherapeutics and could be used to design therapeutic agents with reduced affinity for cellular proteins. It has been established that cisPt is highly reactive with plasma proteins. After injection into the bloodstream, approximately 65 to 98 % of the platinum is bound to proteins [75]. CisPt-protein interactions have been characterized for bovine serum albumin, ribonuclease A, lysozyme, ubiquitin, myoglobin, BRCA1, and the copper chaperone Atox1, among others [74, 76-81]. CisPt binding can alter both protein structure and function [74].

After administration into the bloodstream, cisplatin can convert to the trans isomer (transPt) over time (Figure 4). Transplatin is clinically ineffective in cancer treatment [82, 83]. Therefore, the cytotoxicity of transPt is lower than that of cisPt. CisPt and transPt often have different preferential binding sites and binding affinities for proteins [84]. For example, transPt binds urease with a higher affinity than cisPt and the binding sites are also different [85]. CisPt and transPt both bind ubiquitin, but cisPt forms four distinct adducts while transPt forms one distinct adduct [84]. The binding sites in ubiquitin and binding kinetics also vary based on the isomer [84]. Since ligand

chemistry and geometry of platinum chemotherapeutics dictate interactions with protein and DNA, further studies are needed to understand drug resistance and side effects.

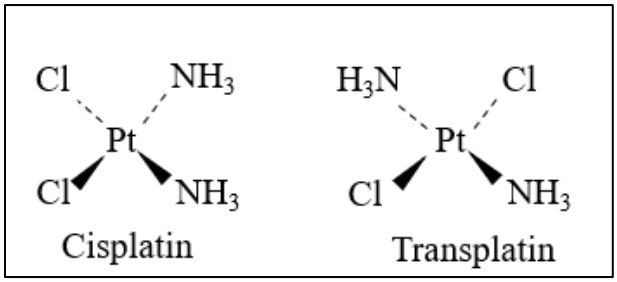

Fig. 4. Structure of cisplatin (cisPt) and transplatin (transPt). Cisplatin has square planar geometry with two ammine ligands and two chloro ligands oriented in a cis planar configuration around the central platinum ion. Transplatin has the same ligands but oriented in a trans configuration around the central platinum.

RESEARCH AIMS

The aim of this dissertation project was to study the caspase-cleaved Par-4 tumor suppressor using biophysical techniques including circular dichroism (CD) spectroscopy, dynamic light scattering (DLS), fluorescence spectroscopy, and size exclusion chromatography with mutli-angle light scattering (SEC-MALS). These techniques were used to identify conditions that induce folding of cl-Par-4 into a predominantly folded conformation, likely characteristic of the active conformation, and study the self-association state of Par-4. CD, DLS, UV-visible absorption spectroscopy (UV-vis), gel filtration, and gel electrophoresis experiments were used to identify and characterize direct interaction of the chemotherapeutic drug cisplatin and its trans isomer with both the full-length Par-4 protein (FL-Par-4) and cl-Par-4. Taken together, this is the first study to

characterize cl-Par-4 using biophysical techniques, the first evidence of tetramer formation in cl-Par-4, and the first evidence of direct interaction between platinum chemotherapeutics and the Par-4 tumor suppressor.

CHAPTER II

BIOPHYSICAL CHARACTERIZATION OF CL-PAR-4 AT ACIDIC PH

PREFACE

The content of this chapter was published in *Biomolecules* in December 2018. Reprinted with permission from Clark, A.M., Ponniah, K., Warden, M.S., Raitt, E.M., Yawn, A.C., and Pascal, S.M. (2018) Acidic pH-induced folding of the caspase-cleaved Par-4 tumor suppressor: evidence of structure outside of the coiled coil domain.

INTRODUCTION

The aim of the research described in the following chapter was to use biophysical techniques to study the effect of pH on the folding and structure of the caspase-cleaved fragment of Par-4, an apoptosis-inducing tumor suppressor protein. As mentioned in Chapter 1, extracellular full-length Par-4 binds GRP78 at the cell surface which initiates the apoptotic process and activates the caspase cascade [33, 55]. After activation of the caspase-cascade, intracellular full-length Par-4 is cleaved at aspartic acid 131 (D131) by caspase-3 [57]. This generates the 24 kilodalton caspase-cleaved fragment (cl-Par-4) and a small 15 kilodalton amino terminal fragment (PAF). Cl-Par-4 then predominantly localizes in the nucleus where inhibition of pro-survival pathways occurs while full-length Par-4 and the PAF remain primarily in the cytoplasm [86]. Subsequent interactions of the Par-4 coiled coil (CC) domain with atypical isoforms of PKC, Bcl-2, and WT1 are important in preventing pro-survival pathways and decreasing tumor growth [34, 44, 54].

While the isolated racine Par-4 C-terminal CC domain has previously been studied, little is known about the remainder of the protein outside of the CC. In this study, cl-Par-4 was studied in neutral pH and acidic pH and changes in conformation and hydrodynamic size were monitored using CD, DLS, and tyrosine fluorescence. IDPs are often unstructured in physiological conditions of low salt and neutral pH, yet extreme conditions such as acidic or basic pH have been shown to induce folding of IDPs [4, 5]. This is referred to as a "turned out" response to environment. Cancer cells have also been shown to have an acidic microenvironment and other tumor suppressors such as p53 have been found inside of acidic organelles [87]. Lysosomes have a pH as low as 4.5 and Par-4 can localize in exosomes which derive from the lysosome-endosome pathway [88-90]. Therefore, it is possible that an intracellular acidic environment could influence cl-Par-4 structure.

Techniques used to study the effect of pH on cl-Par-4 include CD spectroscopy, DLS, and tyrosine fluorescence. Secondary structure changes were monitored by CD spectroscopy, changes in hydrodynamic size were monitored by DLS, and changes in the microenvironment around tyrosine residues in the SAC and linker domains were monitored by tyrosine fluorescence. The work in the present study represents an important step in understanding conditions that induce folding of the Par-4 tumor suppressor, specifically the caspase-cleaved fragment, and how this relates to the protein's physiological structure and function.

MATERIALS AND METHODS

Expression and purification of cl-Par-4

To prepare the human cl-Par-4 construct (residues 132-340), full length human Par-4 was used as a template and amplified by PCR with the forward primer 5'-GACCCATGGGTGTTCCGGAGAAGGGCAAAAGC – 3' and the reverse primer 5'-

CAGAAGCTTTTAGCGGGTCAGTTGGCCCACCAC-3'. The PCR product was digested with NcoI and HindIII restriction enzymes and subsequently ligated into a modified H-MBP-3C expression vector [91]. After DNA sequence verification, cl-Par-4 was expressed in BL21(DE3) CodonPlus *E. coli* cells grown in LB media supplemented with 100 μg/mL ampicillin at 37 °C, 250 rpm. Cells were induced at an OD_{600} of 0.8-0.9 with 0.5 mM isopropyl thio-β-D-galactoside (IPTG) and grown for an additional 18 hours at 15 °C, 250 rpm. After centrifugation, the cell pellet was resuspended in pH 7.4 lysis buffer containing 10 mM Tris, 300 mM NaCl, 20 mM imidazole, 1 mM TCEP, and 1 mg/mL lysozyme. Cells were sonicated with a 10 sec pulse/59 sec rest at 40% amp for 30 repetitions and then centrifuged at 16,000 rpm. The supernatant (containing soluble protein) was filtered through both a 0.8 μm and 0.45 μm syringe filter.

Protein purification was achieved via IMAC using a His-Trap HP column (GE Healthcare) and the His-MBP-cl-Par-4 was eluted with buffer containing 300 mM imidazole. Fractions containing cl-Par-4 were identified using SDS-PAGE and then combined. Then the 3C protease was added to cleave the His-MBP tag and the sample was dialyzed in pH 7.5 buffer containing 10 mM Tris, 1 M NaCl, 1 mM TCEP, at 4 °C overnight. Cleavage was verified via SDS-PAGE (cl-Par-4 band at 24 kilodaltons) and the sample was dialyzed against 10 mM Tris, 1 M NaCl, 20 mM imidazole and 1 mM TCEP, pH 7.4 buffer and loaded onto a His-Trap HP column to remove the His-MBP tag.

The purified cl-Par-4 was dialyzed against 10 mM Tris, 1 M NaCl, 1 mM TCEP, pH 7.0 buffer, and concentrated by centrifugation at 3500 rpm with a Vivaspin Turbo 15 (Sartorius). To determine protein concentration, the absorbance at 280 nm was obtained and the extinction coefficient of 6400 $M^{-1}cm^{-1}$ was used in calculations. Purified cl-Par-4 was lyophilized in pH 7.0 buffer with 10 mM Tris, 1 M NaCl, 1 mM TCEP, and re-solubilized in ultrapure H_20.

Secondary Structure Predictions

Secondary structure predictions were performed on the cl-Par-4 amino acid sequence using DisEMBL and GOR4 analysis [92, 93].

Circular Dichroism Spectroscopy

CD spectra were recorded on a Jasco J-815 CD spectrometer. Cl-Par-4 was at a concentration of 0.2 mg/mL (8.3 µM) in native buffer (20 mM NaCl, 10 mM Tris, 1 mM TCEP) from pH 4-10, and native buffer with 0.1% SDS at pH 7. Far UV-CD spectra were recorded from 260-190 nm at a scan speed of 20 nm/min with a bandwidth of 1 nm, and samples were recorded at 25 °C. Additional CD spectra were obtained for pH 4 and pH 7 at 5, 25, 45, 65, and 85 °C to assess thermal stability. Three scans were recorded for each sample and averaged after baseline subtraction. The scans were smoothed using a means-movement function of 25 and deconvoluted using the Selcon3 algorithm (DichroWeb server) [94].

Dynamic Light Scattering and Zeta Potential

DLS measurements were recorded using a NanoBrook Omni particle sizer and zeta potential analyzer. Cl-Par-4 was at a concentration of 0.2 mg/mL (8.3 µM) in native buffer with pH ranging from 4-10 for DLS and zeta potential measurements. For each sample, five scans were recorded in 1 cm path length plastic cuvettes at 25 °C and averaged. The highest peak of the histogram was recorded as the mean diameter. To determine the experimental isoelectric point (pI), five zeta potential measurements were recorded and averaged for each pH value.

Fluorescence Spectroscopy

Fluorescence measurements were recorded using a Varian Cary Eclipse Fluorescence Spectrophotometer. Cl-Par-4 was at a concentration of 0.2 mg/mL (8.3 μM) in native buffer at pH 4 or 7. Spectra were obtained using 1 cm path length, 400 μL fluorescence cuvettes. Tyrosine was selectively excited at 220 nm (determined as the maximum excitation wavelength) and the emission spectrum was recorded over the range of 250-400 nm, using excitation and emission slits of 10 nm and 20 nm, respectively. Three emission scans were recorded for each sample and averaged after baseline subtraction. All scans were obtained at 25 °C The fluorescence intensity at 310 nm was recorded from 20-95 °C with a temperature rate increase of 1 °C/min using the same excitation and slit parameters as above to monitor thermal stability.

GalaxyWEB Modeling

Template-based models were generated using GalaxyTBM on the GalaxyWEB server using the racine Par-4 CC crystal structure (pdb 5fiy_A) as a template and allowing the remainder of the protein to fold computationally [42, 95]. Five structures were produced and then visually inspected for features consistent with the CD, DLS, and fluorescence results for cl-Par-4 at acidic pH.

RESULTS

Secondary Structure Predictions: Mix of Order/Disorder Outside of the CC Domain

DisEMBL was used to predict regions of high disorder in cl-Par-4 (Figure 5b). Disorder probability above 0.43 (dashed line) approximately separates regions of order and disorder. Some disorder is expected in the SAC domain and high disorder is predicted for the linker domain. In

contrast, the CC and LZ have low disorder probability. GOR4 was used to predict secondary structure in cl-Par-4: 48.8% helical content, 41.7% random coil, and 9.5% extended strand (Figure 5c shows helicity).

The SAC domain has some helical propensity, while very low helicity is expected within the linker domain. The CC and LZ have high helical propensity; however, decreased helical propensity between residues 180-190 occurs due to charge-charge repulsion across the dimer interface. DisEMBLE and GOR4 data are consistent, with regions of high disorder aligning with regions of low helical propensity.

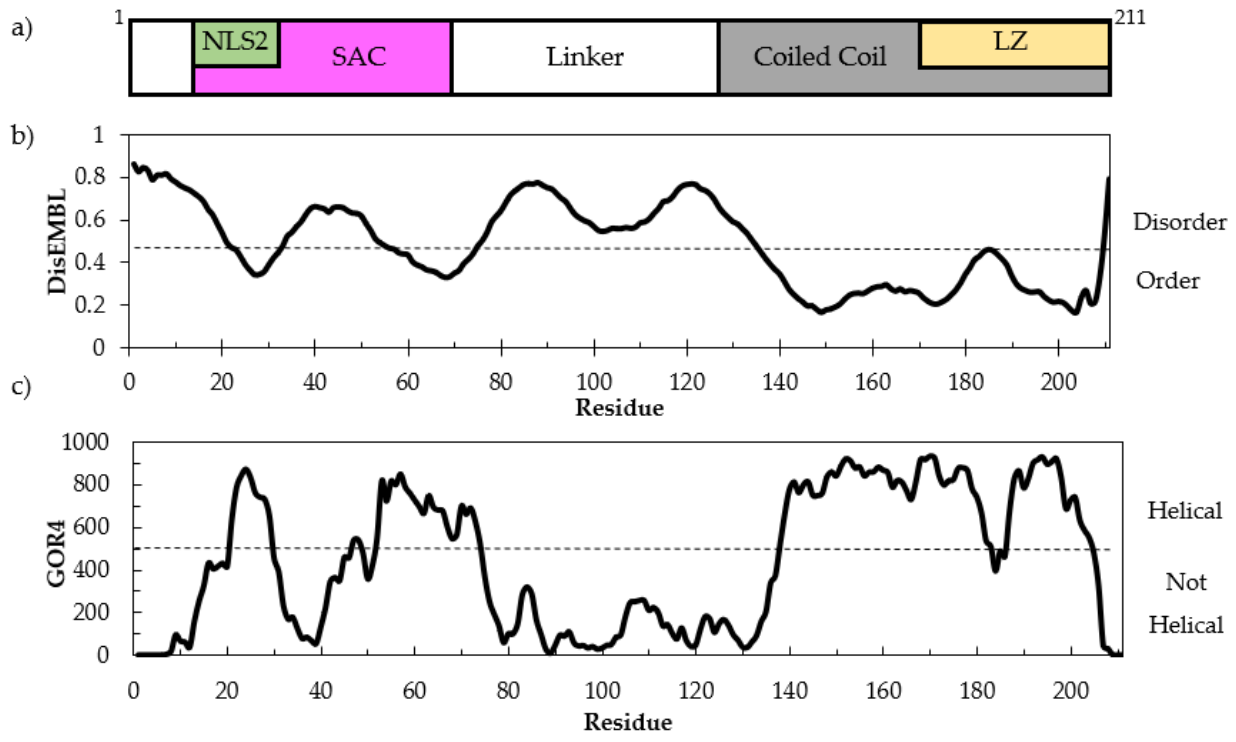

Fig. 5. Secondary structure predictions for cl-Par-4. (a) block diagram of cl-Par-4 domain structure. (b) DisEMBL disorder prediction of cl-Par-4. (c) GOR4 alpha helix analysis of cl-Par-4 amino acid sequence.

Circular dichroism: more intense negative dichroism in acidic pH

CD spectroscopy was used to study the effect of pH on the secondary structure of cl-Par-4 (Figure 6a). Minima at 222 and 208 nm were observed at neutral pH and more extreme pH (pH 4 and pH 10), consistent with partial alpha helical secondary structure. However, dichroism is more intense at pH 4. Decreased dichroism intensity at pH 7 and pH 10 could be related to the formation of large cl-Par-4 aggregates. CD spectra were also recorded under denaturing conditions of 0.1% SDS. With 0.1% SDS, an intense minimum at 205 nm dominates, although a local minimum appears near 222 nm. This CD spectrum under denaturing conditions is therefore consistent with a primarily disordered conformation for cl-Par-4, with some residual secondary structure. By comparison, cl-Par-4 CD spectra at all pH values tested appears to have more regular secondary structure than in denaturing conditions. This suggests that some order survives at all pH values tested.

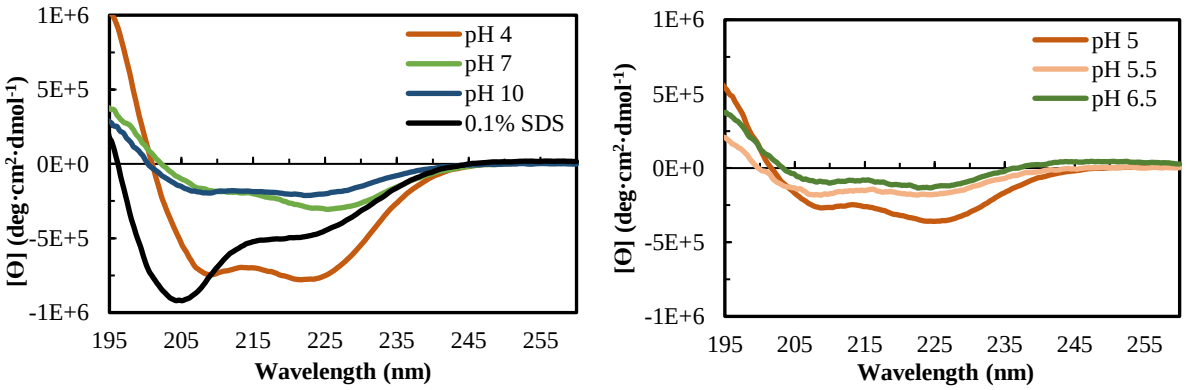

(a) (b)

Fig. 6. Circular dichroism spectroscopy of cl-Par-4 at pH 4-10. (a) CD analysis of cl-Par-4 at pH 4, 7, 10, and in SDS. (b) CD analysis at pH 5, 5.5, and 6.5, near the pI of 5.39.

A ratio of ellipticity at 222 and 208 nm ($\Theta_{222}/\Theta_{208}$) greater than 1 indicates coiled coil (CC) formation. Ratios are 1.2, 1.6, and 1.1 at pH 4, 7, and 10, respectively. The high ratio at pH 7 could be influenced by beta secondary structure which also produces negative dichroism near 222 nm. Under SDS denaturing conditions, the $\Theta_{222}/\Theta_{208}$ ratio is 0.60, and therefore does not suggest CC formation.

Since there is a distinct loss of dichroism intensity at pH values above the pI (5.39), CD spectra were recorded at pH 5.0, 5.5, and 6.5 (Figure 6b). Data was not acquired at pH 6.0 due to sample precipitation. Below the pI at pH 5.0, minima at 222 and 208 nm are more intense and the $\Theta_{222}/\Theta_{208}$ ratio is 1.3. This is consistent with helical CC formation. In contrast, minima at 222 and 208 nm are less intense at pH above the pI. The $\Theta_{222}/\Theta_{208}$ ratios are 1.0 at pH 5.5 and 1.3 at pH 6.5. These results show that observed dichroism becomes less intense at higher pH, although at least some of the effect is likely due to scattering. The change in shape however suggests that coiled coil formation, as opposed to simple helical formation, also is affected by pH with larger $\Theta_{222}/\Theta_{208}$ ratios observed near pH 7.

The thermal stability of cl-Par-4 at pH 7 and pH 4 was investigated by CD (Figure 7). At pH 7, the CD spectra at 5 °C has intense minimum near 225 nm and less intensity near 208 nm (Figure 7a). Minor spectral changes occur between 5 to 45 °C; however, an intense band near 200 nm arises at 65 °C and 85 °C, characteristic of disorder. In contrast, spectra at pH 4 show intense minima at both 208 and 222 nm up to 65 °C, with significant disorder only arising at 85 °C (Figure 7b). Deconvolution of the thermal stability CD data shows that at neutral pH, there is approximately 2/3 calculated helical content with 20% disorder at 5 °C (Figure 7c). However, the effect of large soluble aggregates on the dichroism intensity could influence this value. Helicity decreases between 25-45 ºC to approximately ½, with increased beta content (sheet + turn) to

approximately 20%. At 65 °C, helicity decreases to 40% with increased beta content to 31% and disorder to almost 30%. Helicity further decreases at 85 °C to approximately 1/4 with increase in beta content to 40%, and 34% disorder. At acidic pH (Figure 7d), there is approximately 80% helicity with marginal disorder from 5 to 45 ºC. Helicity starts to decrease and beta/disorder content increase at 65 °C. At 85 °C, helicity decreases to approximately 20% with increased beta and disorder contents to approximately 40% each.

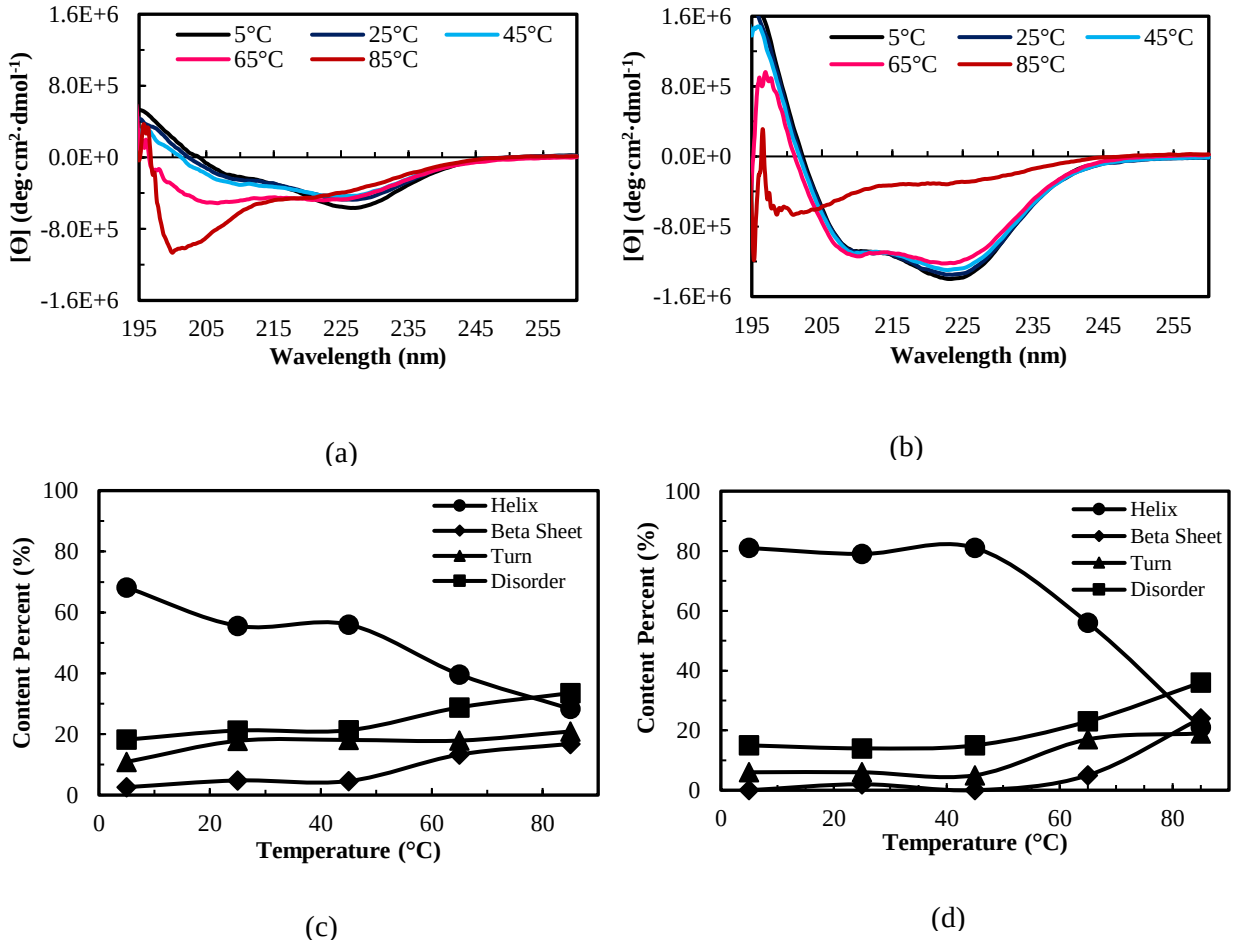

Fig. 7. Relationship of cl-Par-4 thermal stability and pH assessed by CD. (a) CD versus temperature at pH 7. (b) CD versus temperature at pH 4. (c) Secondary structure versus temperature at pH 7. (d) Secondary structure versus temperature at pH 4.

DLS: the hydrodynamic properties of cl-Par-4 are pH dependent

To assess the hydrodynamic properties and aggregation state of cl-Par-4 at different pH conditions, DLS measurements were obtained. The measured R_s values are 43 nm at pH 4, 483 nm at pH 7 and 339 nm at pH 10 (Figure 8a). Under 0.1% SDS denaturing conditions at pH 7, the R_s was 28.3 nm. From zeta potential measurements, the experimental pI was determined (Figure 8b). As pH increased from 4 to 10, zeta potential decreased from 15.4 mV to -20.01 mV and the experimental pI was determined to be pH 5.35. This is consistent with theoretical pI of 5.39.

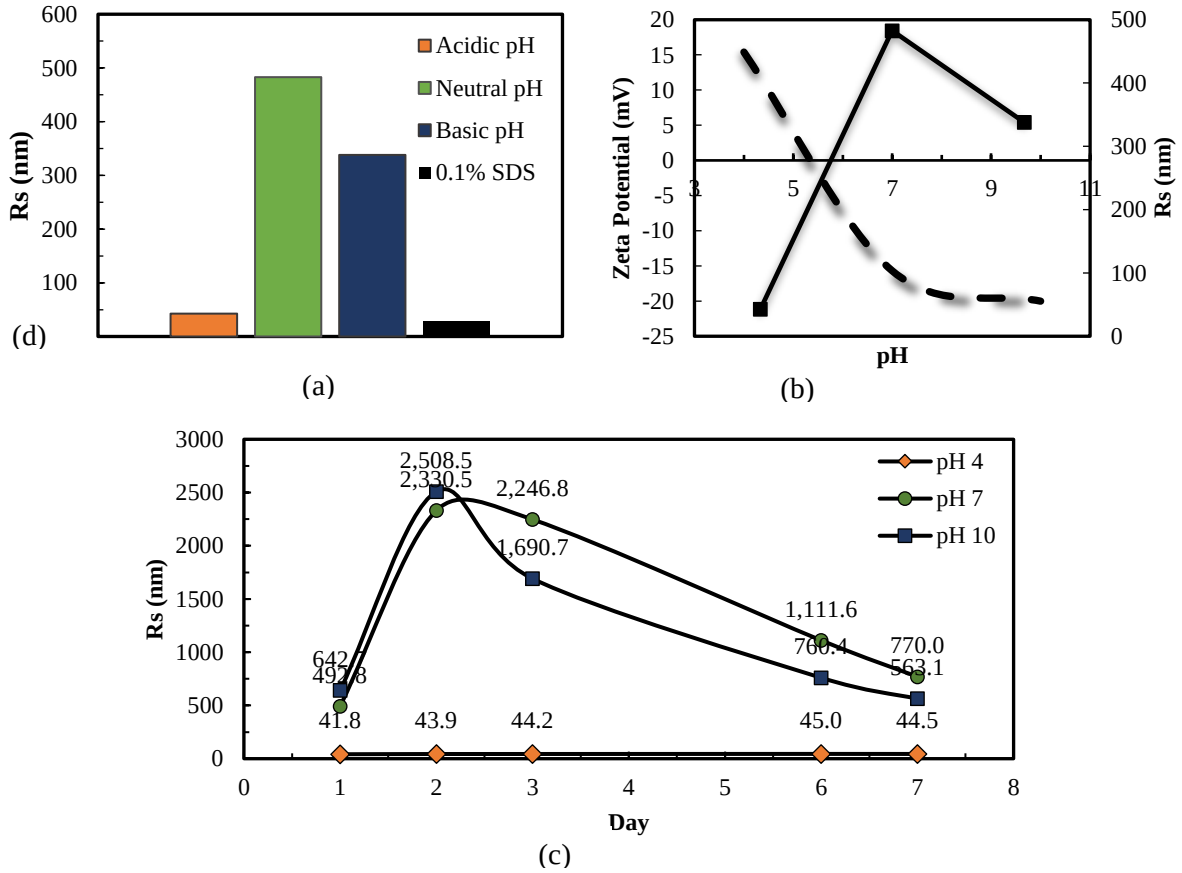

Fig. 8. Dependence of cl-Par-4 hydrodynamic size on pH. (a) Measured R_s of cl-Par-4 under native and denaturing conditions by DLS. (b) Relationship of zeta potential (dashed) to pH and R_s (solid line). (c) Measured R_s over seven days at pH 4, 7, and 10.

Additionally, there was minor variation in hydrodynamic size at acidic pH, with the R_s ranging from 41.8 to 45.0 nm over seven days (Figure 8c). In contrast, the R_s changed substantially over seven days at pH 7 and 10, with significant variation in measured R_s. The large R_s at pH 7 and 10 suggest that aggregation occurs at pH values above the pI of 5.35 where cl-Par-4 has a net negative charge. The large R_s likely suggests a non-globular or rod-shaped conformation. Decreased hydrodynamic size in acidic pH suggests a more compact conformation when cl-Par-4 has a net positive charge. Additionally, the R_s of all non-denatured samples were larger than the partially unfolded SDS denatured form, indicating cl-Par-4 exists in a polymeric state when non-denatured. At least some of this self-association is mediated by the CC dimerization motif.

Effect of pH on tyrosine fluorescence intensity

Fluorescence emission is dependent upon solvent exposure of the aromatic residues. If the aromatics are buried within the hydrophobic core of the protein, the emission has higher intensity. However, if the aromatics are exposed to the solvent, the emission intensity decreases. Since cl-Par-4 has tyrosine residues in the SAC and linker domains, tyrosine fluorescence can be used to monitor folding these regions, which are predicted to be partially disordered based on DisEMBLE and GOR4 analysis. Tyrosine was selectively excited at 220 nm and the emission was recorded from 250-400 nm at 25 °C for cl-Par-4 in 20 mM NaCl at pH 7 and pH 4 (Figure 9a).

The emission maximum near 310 nm was more intense at pH 4, than at pH 7. Thermal denaturation was also investigated (Figure 9b) by monitoring tyrosine emission at 310 nm as temperature increased from 20 to 95 °C. At both pH 7 and pH 4, fluorescence emission decreased linearly with increased temperature. While the emission spectra seem to indicate better solvent protection of tyrosine residues in acidic pH, the observed difference could reflect aggregation

rather than a change of solvent accessibility of the tyrosine residues at neutral pH. However, it does appear that at both neutral and acidic pH there is substantial solvent protection of tyrosine residues at low temperatures, which is reduced at higher temperatures.

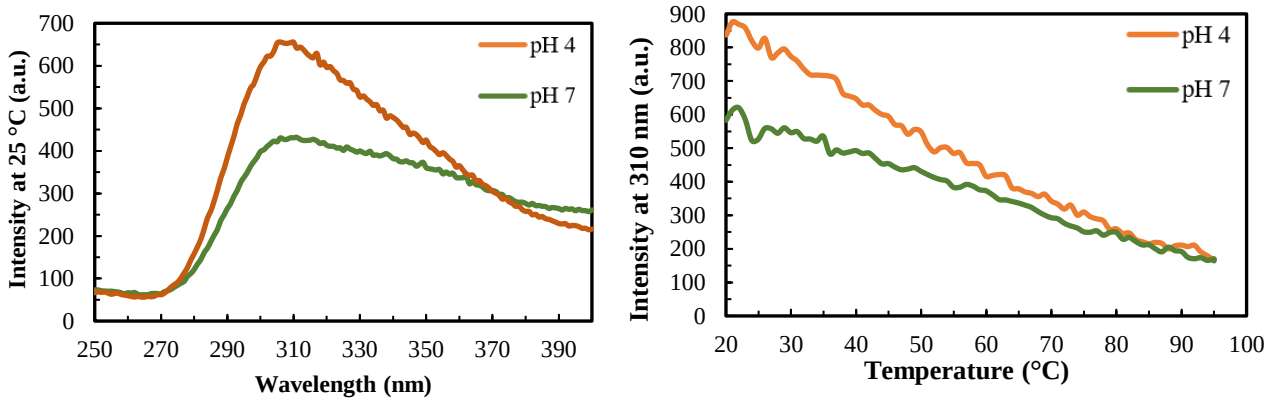

(a) (b)

Fig. 9. Intrinsic tyrosine fluorescence of cl-Par-4 at pH 4 and 7. (a) Tyrosine fluorescence at pH 4 and 7 over 250-400 nm (b) Thermal denaturation at pH 4 and 7 monitored by emission at 310 nm.

GalaxyWEB model of the cl-Par-4 dimer at acidic pH

To further assess the conformation of cl-Par-4 at acidic pH, template-based models were generated using GalaxyTBM on the GalaxyWEB server [95]. The racine Par-4 CC crystal structure (pdb 5fiy_A) was used as a template and the remainder of the protein folded computationally [42]. An ensemble of five structures were generated and visually inspected for features consistent with the biophysical results obtained for cl-Par-4 at acidic pH. The structure shown in Figure 10 is best representative of the conformation at acidic pH: a relatively compact conformation with partially helical SAC and linker domains attached to the C-terminal CC.

In this model, NLS2 is accessible for nuclear import receptor binding which is necessary for nuclear import. Additionally, the NES is likely masked by homodimerization mediated by the

CC, preventing nuclear export of cl-Par-4. However, the exact self-association state of cl-Par-4 in acidic pH is not known, only that cl-Par-4 exists in a polymeric state with some self-association mediated by the CC dimerization motif.

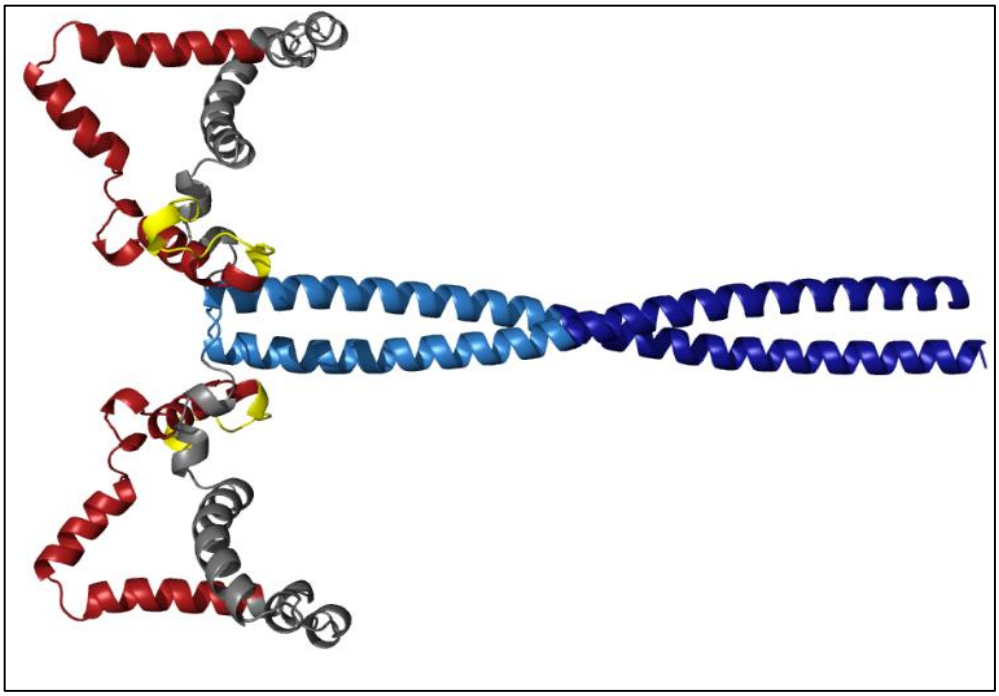

Fig. 10. GalaxyWEB model of the cl-Par-4 dimer at acidic pH. The SAC domain is red, the NLS2 is yellow, linker domain gray, CC light blue and LZ dark blue

DISCUSSION

Intrinsic disorder in cl-Par-4

Disorder-to-order transitions serve a major role in IDP function, such as regulation of cell signaling and ligand binding [1, 3]. Common features of IDPs include reduced sequence complexity and high net charge, and often increased stability at extreme temperature and pH [1, 2,

96]. This last feature is clearly related to the high content of charged residues, since extreme pH will change the charge distribution. In most cases, this will reduce the number of charged side chains, thus reducing charge-charge repulsions that inhibit folding of the protein.

Full-length Par-4 has been classified as mostly intrinsically disordered, although it contains a helical CC at its C-terminus [38, 39, 42]. However, during apoptosis, a 24 kilodalton fragment, cl-Par-4, is generated which then predominantly localizes in the nucleus where inhibition of pro-survival pathways occurs [57]. There is little structural information known about the caspase-cleaved fragment and it is unclear whether cl-Par-4 is predominantly disordered as is the full-length protein. DisEMBLE disorder prediction of cl-Par-4 showed high disorder probability in the linker domain and some disorder in the SAC domain, which coincide with regions of low helix propensity by GOR4 analysis (Figure 5b,c) [92, 97]. Additionally, GOR4 analysis predicts approximately 42% disorder under physiological conditions (Figure 5c) [97].

Consistent with the secondary structure predictions in Figure 5, results in the present study show evidence for some disorder in cl-Par-4. First, based on SDS-PAGE analysis, cl-Par-4 displays an apparent molecular weight of 31 kilodaltons which is approximately 30% higher than expected. This is consistent with previous studies on the racine Par-4 constructs including full length, SAC, and deleted LZ, which each showed apparent molecular weights on SDS-PAGE at least 30% higher than predicted based on primary structure [39]. This behavior is due to the unique negatively charged amino acid composition typical of IDPs, which reduces the affinity of SDS binding, preventing full denaturation and decreasing electrophoretic mobility [2, 98, 99]. CD (Figure 6a) and DLS (Figure 8a) analysis are also consistent with only partial disorder in the presence of SDS. Thermal denaturation (Figure 7) was better able to unfold cl-Par-4, confirming that a significant degree of structure remains in the presence of the SDS denaturant.

Instability at neutral pH

CD spectra of cl-Par-4 obtained at pH 7 show less intense negative dichroism at 222 and 208 nm and decreased thermal stability compared to CD obtained in acidic conditions (Figures 6a, 7a). DLS experiments showed large measured R_s, which varies with time (Figure 8). IDPs have a larger R_s than a globular protein of the same molar mass. However, the R_s value here is far larger than expected for a disordered monomer, and is consistent with the formation of soluble aggregates [100, 101].

Decreased intensity in the tyrosine fluorescence emission spectra is also consistent with the formation of large aggregates (Figure 9). A high $\Theta_{222}/\Theta_{208}$ ratio from CD experiments suggests CC formation, although this ratio could be influenced by beta content. Less intense negative dichroism and increased Rs values occurred at all pH values tested above the experimentally determined pI of 5.35 (Figure 6b, Figure 8c). Taken together, the data demonstrates that at pH above the pI, cl-Par-4 forms large soluble aggregates with a degree of conformational flexibility.

Depicted in Figure 2 (Chapter I) is a helical wheel diagram of the LZ region of Par-4. LZs are a special type of coiled-coil oligomerization motif with leucine residues in the *d* position. [102-104]. Dashed lines represent inter-helical interaction between charged residues at the *e* and *g* positions. The D-E charge repulsion contributes to the conformational instability observed above the pI, as previously determined for the LZ and CC constructs [38, 40, 41].

In summary, the aggregation at pH above the pI can be explained via electrostatic repulsion across the LZ dimer interface. This repulsion reduces dimer stability, which apparently promotes a more disordered interaction of hydrophobic regions that are systematically buried at the dimer interface at low pH.

Acidic pH-induced folding

Electrostatic repulsion within the cl-Par-4 CC domain is abrogated at low pH due to partial titration of the acidic side chains involved [40, 41]. Due to the associating negative charges, the pKa of the repelling D-E acidic side chains in the CC domain is expected to be higher than normal and should be somewhere in the range of 5-6. In acidic conditions, negative dichroism at 222 and 208 nm was more intense, specifically at pH below the pI (Figure 6a,b). While CD spectroscopy shows thermal stability up to at least 65 °C, the 222 nm band does become systematically less intense with increasing temperature (Figure 7b). This suggests a reduction in CC content at higher temperatures. Some IDPs, such as nerve growth factor and αs-casein, gain structure upon increased temperature [105, 106]. Our results show the opposite trend: increased temperature results in partial loss of secondary structure in cl-Par-4, providing further evidence of ordered structure.

DLS shows a monodisperse conformation with an R_s value intermediate between the largely disordered monomer in SDS and the aggregate at neutral pH (Figure 8). Thermal unfolding experiments monitored by fluorescence showed that tyrosine residues in the SAC and linker domains are solvent protected at room temperature (Figure 9a,b). Together, these data suggest that at acidic pH, cl-Par-4 forms a single, stable conformation of fixed self-association state, with substantial CC and perhaps additional non-coiled helical regions. The amount of helix present requires that at least part of the SAC and linker domains have helical character.

To further assess the conformation at acidic pH, template-based models were generated via GalaxyTBM on the GalaxyWEB server [95]. The racine Par-4 CC crystal structure (pdb 5fiy_A) was used as a template and the remainder of the protein was allowed to fold computationally [42]. An ensemble of five structures was generated and visually inspected for features consistent with the above biophysical results for cl-Par-4 at acidic pH. At least part of the SAC and linker domains

must fold under acidic conditions since the CC only comprises approximately 37% of the protein fragment, while CD analysis indicates approximately 80% helical content. The structure shown in Figure 10 is representative of the type of conformation that may occur at acidic pH: a relatively compact conformation with partially helical SAC and linker domains attached to the CC.

Caspase-cleavage of FL-Par-4 is important for apoptosis

Interestingly, increased caspase-3 activation occurs during apoptosis due to the release of cysteine proteases from the lysosome, during cytosolic acidification [107-111]. Thus, cl-Par-4 could be generated under acidic conditions. For subsequent nuclear entry, another protein such as a nuclear import receptor must bind the NLS of cl-Par-4 [34, 112, 113]. The NLS would likely be accessible in a folded non-aggregated conformation such as that represented in Figure 11 but may not be accessible in the aggregate present at neutral pH.

Consistent with this possible mechanism, the RASSF2 tumor suppressor binds a cl-Par-4-sized fragment of Par-4, via the NLS [114]. This binding interaction enhances nuclear localization of the Par-4 fragment, leading to cancer cell apoptosis [114]. In contrast, the NES is most likely masked by homo-dimerization mediated by the CC, preventing nuclear exit of cl-Par-4 [55]. Taken together, these results indicate that caspase-induced cleavage of Par-4, creating cl-Par-4, simultaneously exposes the cl-Par-4 NLS and sequesters the NES, obligating nuclear localization. The folded conformation shown here is consistent with exposure of the NLS at its N-terminus, and sequestration of the NES within the CC dimerization domain. Furthermore, we have shown that at acidic pH, aggregation of cl-Par-4 is inhibited, producing a molecular size more consistent with the ability to traverse the nuclear pores.

Intracellular Acidic Environments

Though acidic pH can induce cl-Par-4 folding *in vitro*, the physiological relevance of the acidic-induced structure of cl-Par-4 remains to be determined. Some clues to the importance of folding at acidic pH can be obtained through discussion of other proteins with similar characteristics. First, many *in vitro* studies have shown IDPs preferentially folding at acidic pH [87, 115]. Examples include α synuclein, prothymosin α, and the cytoplasmic domain of BAP29 [115-118]. The general principle is that acidic pH can alleviate charge-charge repulsion in IDPs, allowing for stable folding [1, 2, 5]. Other proteins are known to have both stable structure and to function in an acidic environment. For instance, acid endonucleases function in cell death and have optimal activity as low as pH 4.9 [119, 120]. As a second example, dimer formation of the apoptosis-regulating Bcl-2 family proteins is stabilized at pH 4 [121].

Many other proteins, including tumor suppressors, have been detected in lysosomes, endosomes or exosomes, which can be highly acidic. Perhaps the best-known example is the p53 tumor suppressor, which can be found in the highly acidic lysosomes in human breast cancer cells [87, 122]. It has been suggested that the p53 conformation at acidic pH could function in lysosomal membrane permeabilization, which often occurs in early apoptosis [87, 123]. The PTEN protein is an example of a tumor suppressor that is transported via exosomes [124]. Exosomes can be used for intercellular transfer of tumor suppressors, which helps to prevent tumor proliferation [125, 126]. Since exosome biogenesis occurs through the lysosome-endosome pathway (pH 4-6 range), the relevant pH is consistent with the acidic pH in our study [89, 127-132].

Therefore, it is interesting to note that while most studies of Par-4 have focused on intracellular function, full length Par-4, along with Par-4 fragments of 33 and 14 kilodaltons (based on SDS-PAGE) have also been found in secreted exosomes (termed apoxosomes) [88]. These fragments

have not yet been positively identified; however, the SDS-PAGE-based sizes are consistent with those created by caspase-induced cleavage, including the cl-Par-4 fragment. Additionally, p62 forms a ternary complex with PKCζ and Par-4 (through the Par-4 C-terminus), helping to regulate the interaction of aPKC with the NF-κB pathway [133]. Interestingly, atypical isoforms of protein kinase C (aPKCs) and p62 localize to late endosomal compartments [43, 133-135], suggesting that Par-4 may also localize to late endosomes due to this binding interaction. Therefore, it is quite plausible that future studies will positively identify cl-Par-4 in these acidic organelles. Also, the fact that typical exosome size is less than 100 nm [136] suggests that cl-Par-4 under neutral conditions (R_s >400 nm) may be too large for transport via exosomes. However, the folded conformation at acidic pH would be of a more suitable size.

It has also been well documented that the cytosol of cancer cells can be more acidic than that of healthy cells, particularly during apoptotic processes [110, 111, 119, 137-141]. For instance, one study showed apoptotic human histiocytic lymphoma cells with a cytosolic pH of 5.7 [122, 129]. While the precise degree of acidification may vary in different tumors, cancer-related acidification of the cytosol could potentially help to promote IDP folding. Finally, it should be noted that *in vivo* folding of cl-Par-4 may be influenced by factors other than pH, including post-translational modification or binding interactions with other proteins or ions. This could help to reduce the conformational instability observed at neutral pH. However, these factors are not required for stable folding of cl-Par-4 at acidic pH.

CHAPTER III

DEPENDENCE OF CL-PAR-4 STRUCTURE ON IONIC STRENGTH: EVIDENCE OF TETRAMER FORMATION

PREFACE

The content of this chapter was published in the *FEBS* journal in June 2019. Reprinted with permission from Clark, A.M., Ponniah, K., Warden, M.S., Raitt, E.M., Smith, B., and Pascal, S.M. (2019) Tetramer formation by the caspase-activated fragment of the Par-4 tumor suppressor, the FEBS journal. Copyright 2019

INTRODUCTION

The aim of the research described in the following chapter was to study the effect of ionic strength on the structure of cl-Par-4, the caspase-cleaved fragment of the Par-4 tumor suppressor. Biophysical techniques including CD spectroscopy, DLS, tyrosine fluorescence, and SEC-MALS were used. As discussed in Chapter II, cl-Par-4 forms aggregates under typical physiological conditions, but adopts a predominantly alpha helical conformation in acidic pH [51]. Disordered proteins often fold under extreme conditions such as extreme pH, temperature, or ionic strength due to various stabilizing factors [2, 4, 5, 19]. For instance, high salt can increase folding of highly polar IDPs by shielding charge-charge repulsion [48-50].

Over time, some proteins on earth have adapted to life in extreme environments like high salt [142, 143]. These halophilic proteins are influenced by electrostatic interactions and often form random coil structures, both common among intrinsically disordered proteins (IDPs) like

Par-4. This suggests a possible link between halophilic protein adaption and the folding and structural flexibility of IDPs [143]. One of NASA's mission directorates addresses the question "Does life exist outside of Earth?" It is plausible that if proteins could exist outside of earth, they would have characteristics comparable to that of IDPs, which interestingly encompasses many medically relevant proteins. Therefore, the objective of this research was to use a medically relevant human protein, Par-4, as a model of protein folding in extreme conditions characteristic of an extraterrestrial environment. In this chapter, the effect of ionic strength on cl-Par-4 conformation at neutral pH was studied. Results show that cl-Par-4 is highly susceptible to aggregation in low salt conditions, forming large oligomers. However, cl-Par-4 forms predominantly alpha helical tetramers in high salt. This observation raises the possibility that Par-4 tetramerization may be critical for its apoptotic activity.

MATERIALS AND METHODS

Expression and purification of cl-Par-4

Cl-Par-4 was expressed and purified according to published procedures using the H-MBP-3C expression vector and BL21(DE3) CodonPlus *E. coli* cells [51]. Cl-Par-4 was purified using a His-Trap HP column (GE Healthcare) and dialyzed against high salt, pH 7 buffer (10 mM Tris, 1 M NaCl, 1 mM TCEP). Cl-Par-4 was lyophilized and re-solubilized in ultrapure H_20.

Circular Dichroism

Far-UV CD experiments were performed as in Chapter II. Stock protein was diluted to 0.2 mg/mL (8.3 µM) in pH 7 buffer with 10 mM Tris-HCl, 1 mM TCEP, and NaCl ranging from 20 mM to 3 M.

Intrinsic Tyrosine Fluorescence

Fluorescence spectra were recorded as in Chapter II. Protein was at a concentration of 0.2 mg/mL (8.3 µM) in pH 7 buffer with 10 mM Tris-HCl, 1 mM TCEP, and 20 mM or 1 M NaCl.

SEC-MALS

A Superdex 200 column (GE healthcare, Uppsala, Sweden) with a 24 mL column volume (CV) was equilibrated with 1 CV of buffer at a flow rate of 0.1 mL/min before injecting the sample. BSA was used as a standard. After filtration with a 0.45 µm syringe filter, 500 µL of cl-Par-4 at 3 mg/mL (125 µM) was loaded onto the column. Running buffer contained 10 mM Tris, pH 7 and either 20 mM or 1 M NaCl. SEC experiments were done at 4 °C with a flow rate of 0.3 mL/min for 0.02 M NaCl and a flow rate of 0.2 mL/min for 1 M NaCl to prevent increased pre-column pressure.

After protein elution, light scattering and refractive index measurements were recorded. Light scattering was recorded at three angles (43.6°, 90°, and 136.4°) using a mini-DAWN with a 690 nm laser (Wyatt Technology). Using Astra software, the molar masses (MM) and radius of gyration (R_g) values were calculated for the eluted fractions. Double log plots of MM versus Rg were obtained from Astra software. Fractions were collected and analyzed by SDS-PAGE.

GalaxyWEB Modeling

GalaxyHomomer on the GalaxyWEB server for protein structure prediction was used to generate the cl-Par-4 tetramer model. An oligomeric state of four (tetramer) was specified at input, and models were generated based on the cl-Par-4 amino acid sequence and template-based modeling, using pdb 5dol (YabA) as a template.

RESULTS

CD: More intense negative dichroism in high ionic strength

The effects of ionic strength on cl-Par-4 secondary structure were investigated using CD spectroscopy (Figure 11a). There was minor change in negative dichroism between 0.02 to 0.25 M NaCl. Minima at 222 and 208 nm became more intense as NaCl concentration increased, specifically in the range of 0.35 M to 3 M.

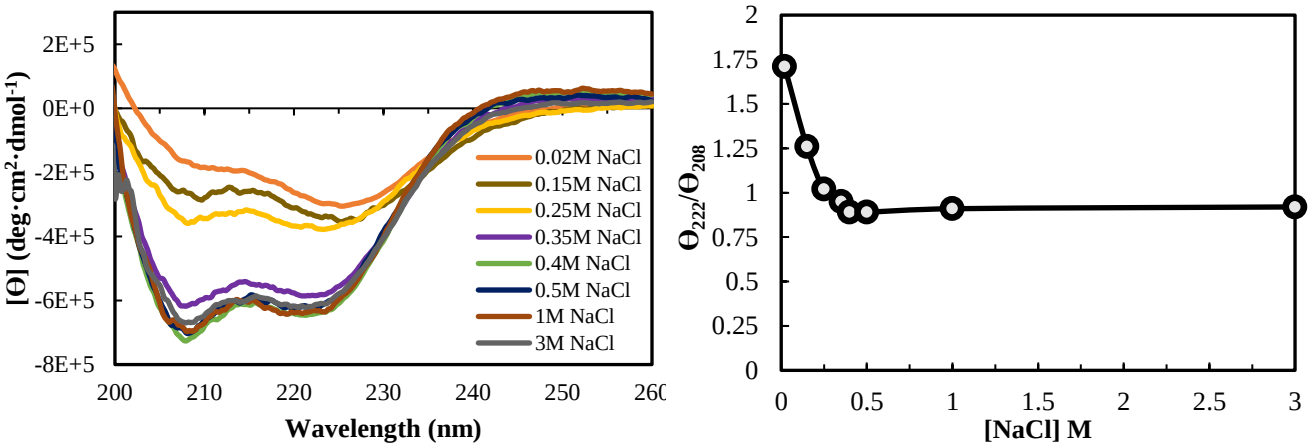

(a) (b)

Fig. 11. Minima at 222 and 208 nm become more intense with increasing ionic strength at pH 7. (a) CD spectra of cl-Par-4 in ionic strength ranging from 20 mM to 3 M NaCl (b) $\Theta_{222}/\Theta_{208}$ ratios in 0.02-3 M NaCl.

Less intense negative dichroism in low ionic strength could be related to scattering of large soluble aggregates. The $\Theta_{222}/\Theta_{208}$ ratios were assessed to monitor CC formation (Figure 11b). Ratios decreased from 1.71 to 0.92 as salt increases from 0.02 M to 3 M. This would seem to suggest that CC formation occurs at low salt (0.02-0.25 M) but not in high salt (0.35-3 M). However, ratios in low salt could be influenced by beta content.

The change in $[\Theta]_{222}$ as temperature was increased from 25 to 85 °C was studied in 0.15 M, 0.5 M, and 1 M NaCl (Figure 12). In 0.15 M NaCl, temperature-induced changes in $[\Theta]_{222}$ were modest. However, in 0.5 and 1 M NaCl, there is a significant loss of $[\Theta]_{222}$ intensity with increased temperature. The melting temperature (Tm) appears to be near 55 °C at 0.15 M and 1 M NaCl. Extraction of Tm at 0.5 M NaCl was not possible with this data.

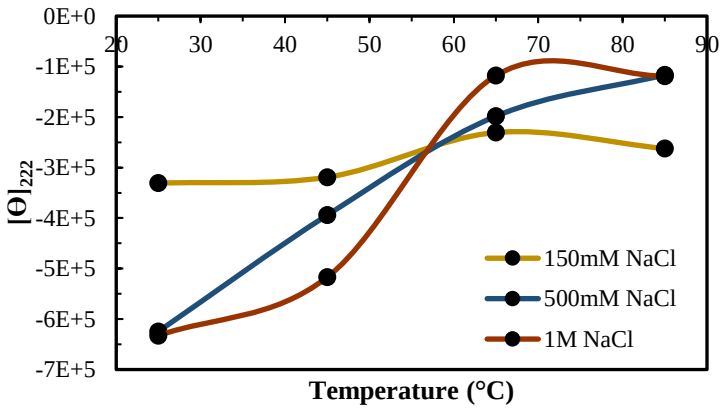

Fig. 12. Thermal stability analysis of cl-Par-4 by CD. $[\Theta]_{222}$ versus temperature at three salt concentrations are shown.

DLS: Ionic strength changes the hydrodynamic properties of cl-Par-4

To assess the dependence of cl-Par-4 hydrodynamic size on ionic strength, DLS measurements were obtained of cl-Par-4 in varying ionic strength buffers at pH 7 (Figure 13). Large R_s measurements (greater than 400 nm) were observed in low salt of 0.02-0.25 M NaCl, which are characteristic of large aggregates. The hydrodynamic size of cl-Par-4 significantly decreased in high salt (0.5 to 1 M NaCl) with small R_s values in the range of 115 to 86 nm. This is consistent with a non-aggregated, more compact conformation. Additionally, there is significant variation in size in low ionic strength, suggesting multiple conformations and flexibility. However, low error in high salt shows better reproducibility between samples and one consistent conformation.

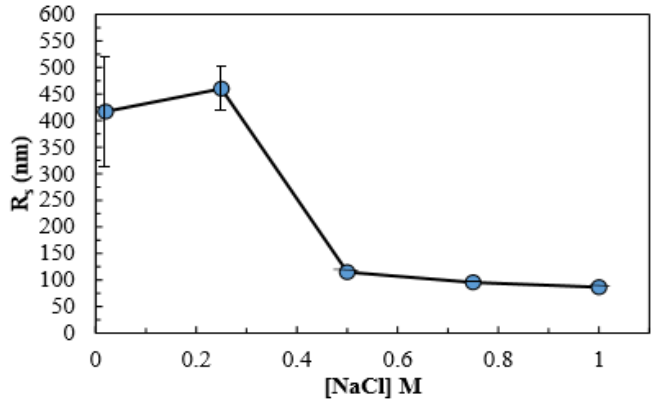

Fig. 13. Dependence of cl-Par-4 hydrodynamic size on ionic strength. Measured Stokes radius (R_S) values from 0.02 to 1 M NaCl are shown. The standard deviations from 0.02 M to 1 M NaCl are 129, 25, 3, 3, and 15 nm.

Effect of NaCl concentration on tyrosine fluorescence

Tyrosine fluorescence emission spectra were obtained in the range of 250-400 nm (Figure 14). The difference in fluorescence intensity from 0.02 M to 1 M NaCl might suggest the tyrosine residues in the SAC and linker domains have different levels of solvent exposure. However, decreased intensity in low ionic strength could be due to aggregation, rather than a change of solvent accessibility of the tyrosine residues in the SAC and linker domains, as discussed in the previous chapter.

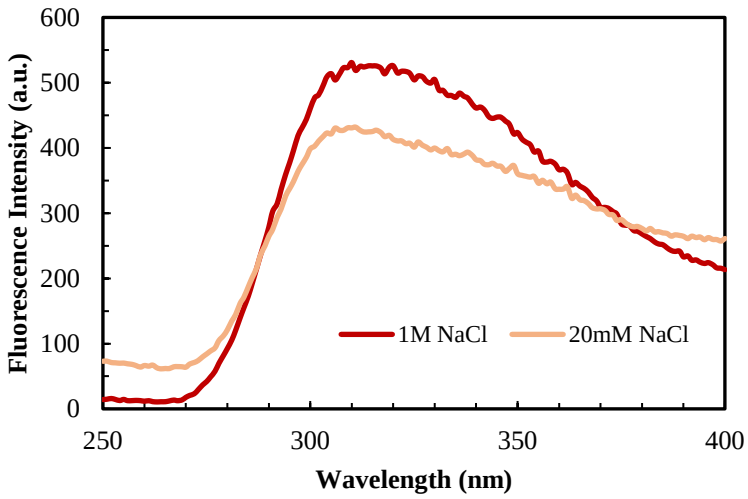

Fig. 14. Tyrosine fluorescence of cl-Par-4 in the presence of 0.02 M (orange) and 1 M (red) NaCl following excitation at 220 nm.

SEC-MALS: Mixed high-order oligomers in low salt

To identify the oligomeric association of 125 µM cl-Par-4, SEC-MALS experiments were performed to determine molar mass (MM) and radius of gyration (Rg). A mixture of large aggregates form in low salt of 0.02 M NaCl, which is consistent with DLS data. The major peak eluted after 70 minutes and scattered light intensely, indicating a large molecular size (Figure 15a). MM measurements could not accurately be calculated for the small second and third peaks that eluted between 71-75 minutes. The major peak had a MM ranging from 389 to 424 kilodaltons (Table 1, Figure 15b). Plotting the elution profile as a function of MM shows variation in MM as the sample eluted from the column (Figure 15b), suggesting a somewhat heterogeneous sample. Mw/Mn is the polydispersity ratio, and the value was 1.3 ± 35% for this sample, consistent with heterogeneity. Since the MM of monomeric cl-Par-4 is 24 kilodaltons, the results are consistent with a primary species ranging from 16mer to 18mer (theoretical MM is 384 and 432 kilodaltons, respectively). The average Rg for this sample was 128 nm (Table 1).

When the SEC-MALS experiment was repeated with a second 125 µM cl-Par-4 sample, also in low salt (0.02 M NaCl), the fraction that eluted near 70 minutes had a somewhat larger MM of 517 kilodaltons, consistent with a 22mer (theoretical 22mer MM is 528 kilodaltons), and an Rg of 155 nm (Figure 15c, Table 1). Figure 15c is also consistent with a heterogeneous sample based on variation in measured MM as the sample eluted. An Mw/Mn of 1. In both low salt samples, individual MM measurements had an error in the range of 24-39%. Though these results are inexact, clearly, SEC-MALS consistently predicts higher-order oligomers in low salt, while the observation of multiple peaks consistently suggests the presence of multiple, possibly interconverting, aggregated species. This is not unexpected for a disordered protein which is highly flexible and not expected to have a fixed quaternary structure.

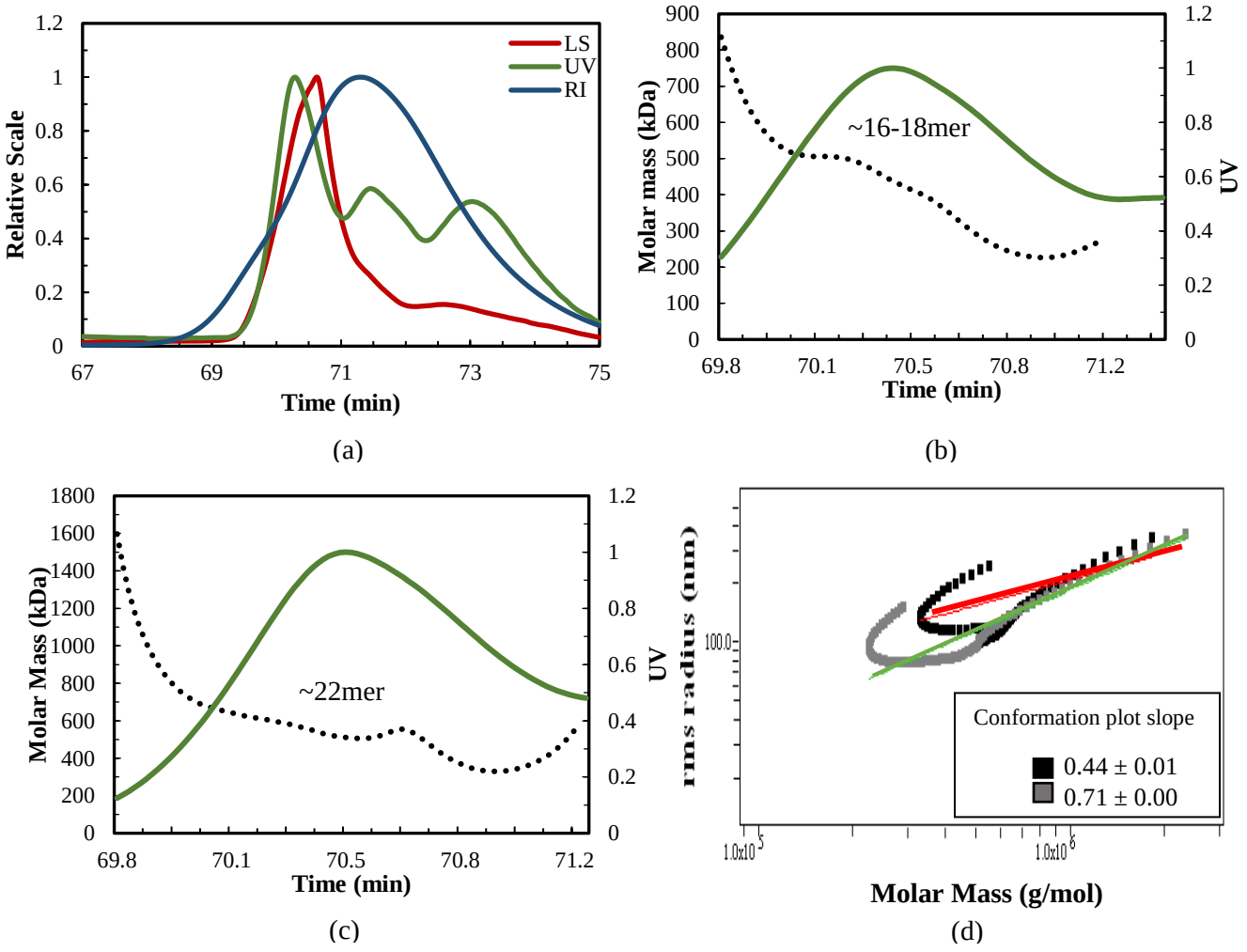

Fig. 15. SEC-MALS of 125 µM cl-Par-4 in 0.02 M NaCl (a) Elution profile of cl-Par-4 from Superdex 200 gel filtration column with light scattering (LS), UV, and refractive index (RI) measurements. (b) and (c) show molar mass analysis of the major peak from part (a) for two separate runs. (b) M_w (weight average molar mass -black dots) and UV (green) versus time. The molar mass at the peak maximum is approximately 424 kilodaltons, consistent with an 18mer. (c) M_w molar mass plot of a second sample showing a mass of approximately 515 kilodaltons at the peak maximum, consistent with a 22mer. Variation in weight average molar mass measurements in (b) and (c) suggest the presence of a range of oligomers. (d) Conformation plot in 0.02 M NaCl

for samples shown in (b) and (c). Fitted slopes are 0.44 (black/red) and 0.71 (gray/green), respectively.

Parameters	R1 (error %)	R2 (error %)
M_n (g/mol)	3.4e5 ± 25%	4.9e5 ± 32%
M_w (g/mol)	4.3e5 ± 24%	5.5e5 ± 39%
Avg MM (g/mol)	3.9e5	5.2e5
M_w/M_n	1.3 ± 35%	1.1 ± 50%
R_n (nm)	106.8 ± 9%	146.1 ± 7%
R_w (nm)	119.8 ± 6%	152.5 ± 7%
R_z (nm)	156 ± 4%	167.7 ± 6%
Avg R (nm)	127.5	155.4

Table 1. SEC-MALS measurements of 125 µM cl-Par-4 in 0.02 M NaCl. Shown are M_n and M_w values which refer to number average MM and weight average MM. M_w/M_n is the polydispersity ratio. R_n, R_w, and R_z are the number, weight, and z-average radius of gyration values. Two separate runs are shown for low salt which gave a range of oligomers: 16mer-22mer. The average molar mass and radius values are shown with standard deviation (± SD %); however, there is high error for individual measurements and high polydispersity in the samples.

A double log conformation plot of MM versus radius provides information about protein shape where a slope of 0.33 indicates spherical, 0.5 indicates coil, and 1 indicates rod-like. The conformation plot of cl-Par-4 in low salt shows slopes of 0.44 and 0.71 (Figure 15d). At least some of the difference between the slopes are due to fitting uncertainty, since visually, the slopes appear more similar than the numbers suggest. However, both of these values suggest at least some coil-like character.

SEC-MALS: helical tetramer formation in 1 M NaCl

Smaller oligomers were the primary species detected in 1 M NaCl (Figure 16, Table 2). A peak with weak UV intensity eluted after 28-30 minutes, which scattered intensely, consistent with a small amount of aggregation. The largest UV signal came from the second peak which eluted after 40 minutes. This major peak scattered less intensely, which correlates to a smaller species. The average MM for the major peak was 94 kilodaltons which is consistent with tetramer formation (theoretical MM is 96 kilodaltons) (Figure 16b, Table 2).

In total, four 125 μM cl-Par-4 samples were run in 1 M NaCl, each with similar results. Within each run (Figure 16b shows the first run), and across the four runs (Table 2), less variation in MM measurement was observed, indicating a more homogeneous sample than in low salt. However, the slight shoulder on the right edge of the main peak would appear to represent a smaller species such as dimer. This suggests the presence of a small amount of dimer-tetramer interconversion as the sample elutes.

The average calculated Rg of the tetramer was 30 nm (Table 2), significantly smaller than the observed Rg of the aggregates. The conformation plot (Figure 16c) has a slope of 0.26, close to 0.33 for spherical proteins. Slopes from additional experiments in high salt include 0.30 and 0.37, which all suggest a mostly spherical protein. The Mw/Mn ratios were approximately 1.05 ± 10% depending on the sample, which is consistent with largely homogeneous samples. Additionally, most of the individual MM measurements had 10% error or below; therefore, we can ascribe tetramer state with some certainty. Less sample-to-sample variation in high salt indicates a more stable structure, with less conformational/associative interconversion than at low salt.

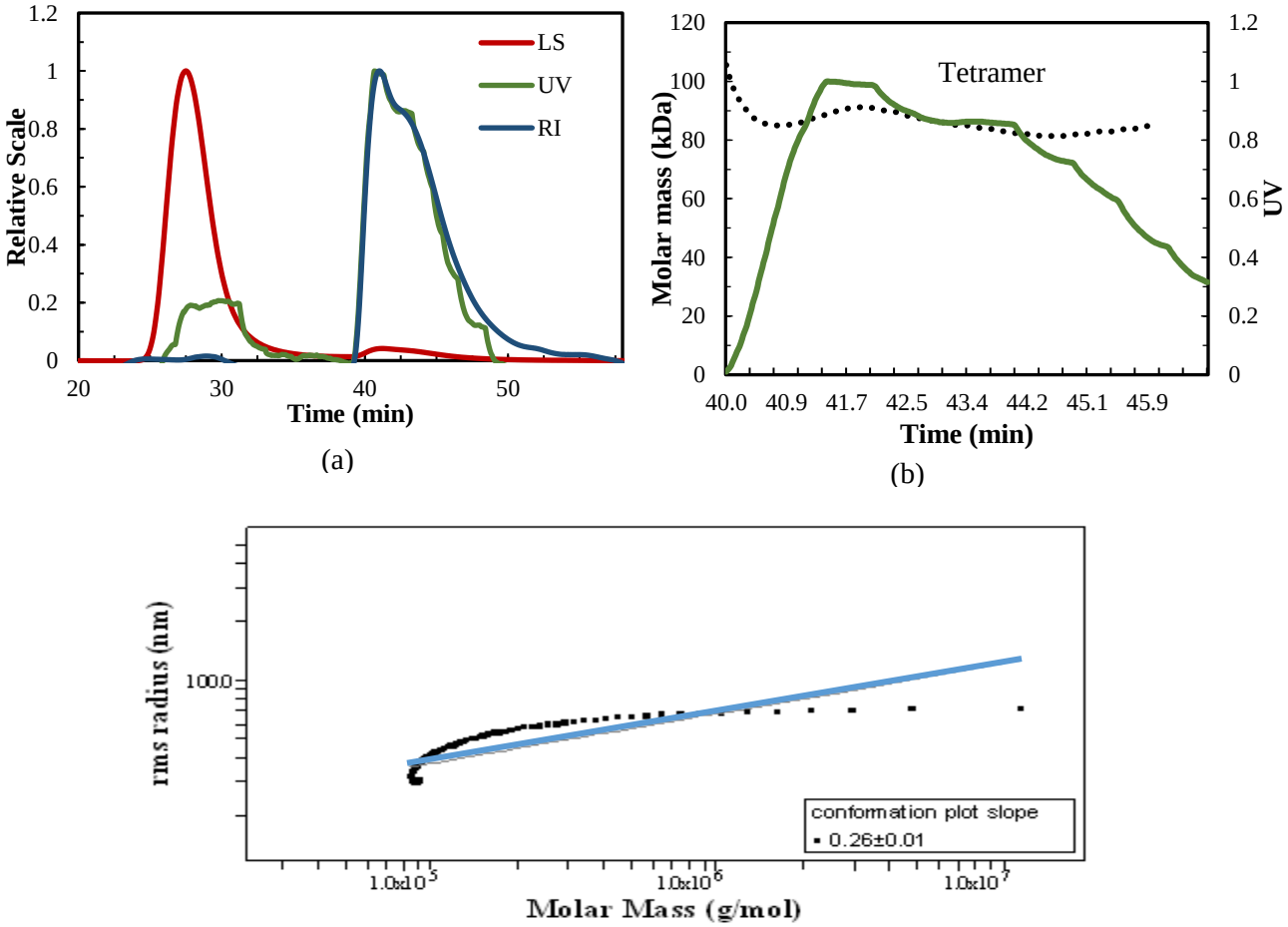

Fig. 16. SEC-MALS of 125 µM cl-Par-4 in 1 M NaCl. (a) Elution profile of cl-Par-4 from a Superdex 200 gel filtration column in 1 M NaCl with LS, UV, and RI measurements. (b) M_w molar mass analysis of the major peak that eluted between 40-45 minutes with molar mass (black) and UV (green) versus time. The molar mass at the peak maximum is approximately 91 kilodaltons, consistent with a tetramer. (c) Conformation plot in 1 M NaCl with a slope (blue line) of 0.26.

Parameters	R1 (error %)	R2 (error%)	R3 (error %)	R4 (error %)
M_n (g/mol)	9.1e4 ± 7%	7.6e4 ± 4%	8.2e4 ± 6%	7.8e4 ± 3%
M_p (g/mol)	8.6e4 ± 7%	8.3e4 ± 4%	9.1e4 ± 6%	8.6e4 ± 3%
M_w (g/mol)	9.6e4 ± 7%	7.9e4 ± 4%	8.7e4 ± 6%	8.3e4 ± 3%
M_z (g/mol)	1.8e5 ± 23%	8.8e4 ± 9%	1.1e5 ± 13%	1.1e5 ± 8%
Avg MM(g/mol)	1.1e5	8.2e4	9.2e4	9.0e4
M_w/M_n	1.06 ± 10%	1.04 ± 6%	1.05 ± 10%	1.06 ± 4%
R_n (nm)	32.7 ± 22%	24.3 ± 23%	24.9 ± 37%	31 ± 10%
R_w (nm)	33.5 ± 21%	25.2 ± 22%	26.1 ± 34%	32 ± 10%
R_z (nm)	36.5 ± 19%	27.5 ± 18%	28.8 ± 28%	35.3 ± 8%
Avg R(nm)	34.2	25.7	26.6	32.8

Table 2. SEC-MALS measurements of 125 µM cl-Par-4 in 1 M NaCl. Molar mass, M_w/M_n, and radius measurements reported for 1 M NaCl are from four separate samples that all were predominantly tetramers. The average molar mass was 9.4e4 g/mol (94 kilodaltons) which is close to the theoretical molar mass of 96 kilodaltons for a tetramer. The average radius is 29.8 (~30 nm). Low error in individual runs and in averaging the runs, correlates to one predominant self-association state with reproducibility in SEC-MALS measurements.

Homology model of the cl-Par-4 tetramer

Using Clustal Omega and BLAST, we identified that the YabA protein (pdb 5dol) has high sequence similarity to cl-Par-4, specifically to the CC domain (Figure 17) [55-57]. Shown below the alignment is the domain structure of cl-Par-4: SAC domain (14-69), linker region (70-130), and the coiled coil (CC) with a leucine zipper (131-209). The YabA sequence is aligned with the CC region of cl-Par-4 (sequences obtained from UniProt.org). Between residues 168-204 in the cl-Par-4 CC, there is 59% sequence similarity to YabA and 38% sequence identity. The YabA tetramer forms via anti-parallel alignment of two parallel CC dimers [58]. Tetramer formation in cl-Par-4 may occur in a similar manner.

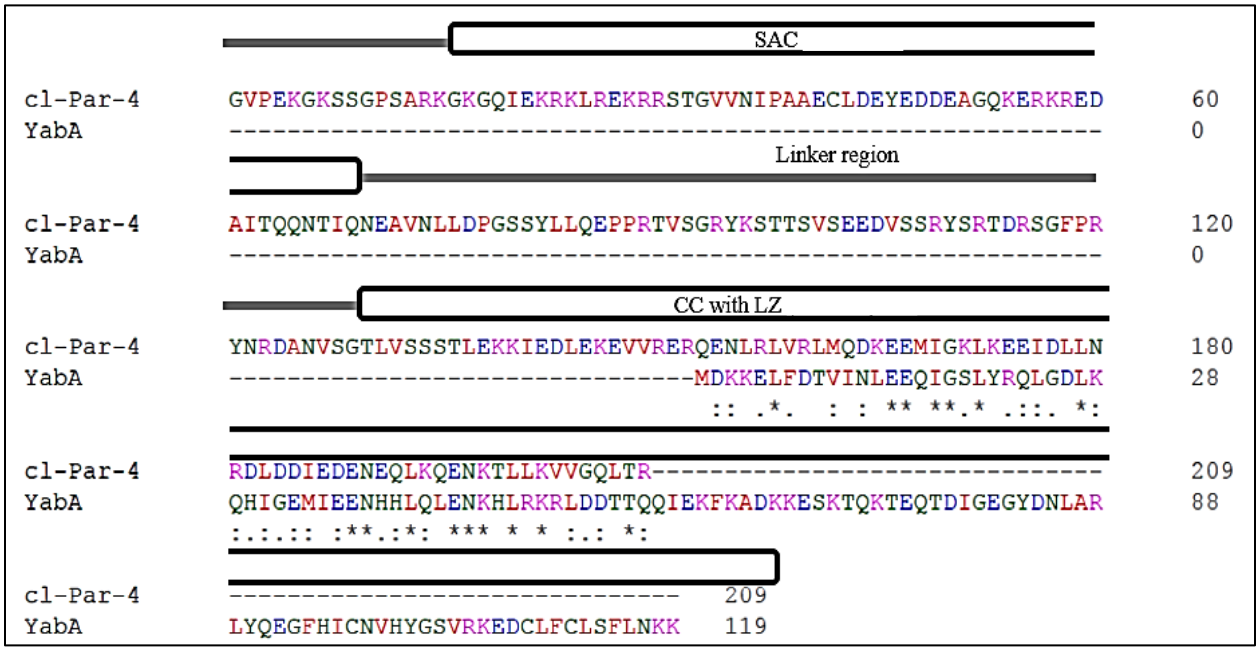

Fig. 17. Sequence alignment of cl-Par-4 with YabA (pdb 5dol) using Clustal Omega [144, 145]. Nonpolar, uncharged residues are red. Polar, uncharged along with nonpolar, aromatic are green. Basic residues are pink, while acid residues are blue. The asterisks (*) show fully conserved residues, a colon (:) shows positions that have amino acids with similar properties, and a period (.) shows positions with conservation between amino acids with partially similar properties.

Using GalaxyHomomer modeling software [59], the YabA tetramer was used as a template to generate a tetramer model of cl-Par-4 (Figure 18). In the model, each parallel oriented dimer pair (AB and A'B') resembles a pair of tweezers formed by the CC domains, and the two tweezers interact in a scissors-like fashion. The SAC and linker domains are shown as mostly helical but extending away from the coiled coil. They could instead be folded back towards the geometrical center of the tetramer, which would result in a more compact spherical shape.

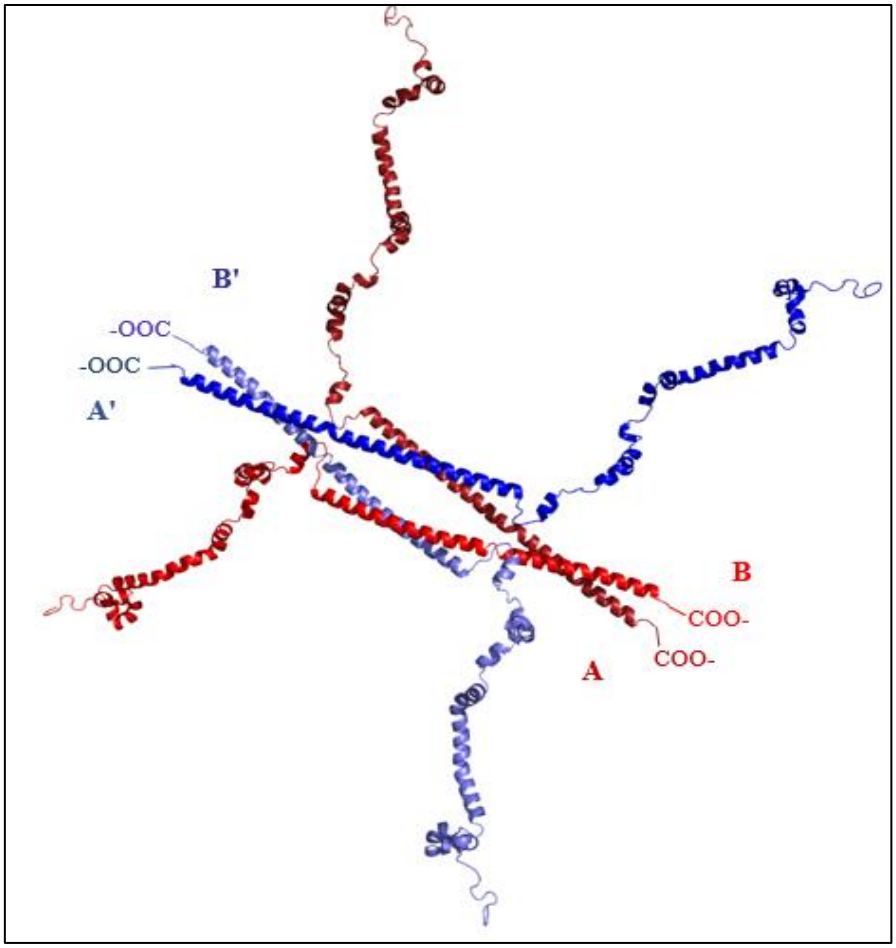

Fig. 18. Cl-Par-4 tetramer model. The model was generated via GalaxyWEB homomer modeling software using the YabA tetramer as a template.

Dimer 1 (red) is made up of chains A and B with their CC domains oriented in a parallel fashion. Dimer 2 (blue) is a similar parallel arrangement of chains A' and B'. The two dimers interact with each other in an antiparallel orientation to form a central tetrameric region, with the LZ regions at the C-termini remaining dimeric. In this model, the SAC and linker domains are shown as largely helical but extending away from the CC regions. These domains may instead fold back toward the geometric center, resulting in a more compact sphere-like structure.

DISCUSSION

Ionic strength influences cl-Par-4 dichroism, hydrodynamic size, and fluorescence

In the present study, ionic strength-induced folding of cl-Par-4 was investigated. High salt can be used to dissociate large protein oligomers and increase solubility. [146]. In our initial studies of cl-Par-4, we found that high salt was necessary during purification to prevent the formation of insoluble aggregates. This suggested that high salt was inducing a more stable three-dimensional structure. Upon further investigation (the present study), we found that in low salt and neutral pH, cl-Par-4 forms large soluble aggregates. In low ionic strength conditions, CD spectra show less intense negative dichroism (Figure 11), DLS analysis showed increased hydrodynamic size (Figure 13), and fluorescence shows decreased tyrosine fluorescence emission (Figure 14). The opposite trend is observed for cl-Par-4 in high ionic strength: more intense negative dichroism, decreased Rs, and increased tyrosine fluorescence emission.

Less intense negative dichroism in low ionic strength conditions could be related to scattering of large cl-Par-4 oligomers. CD of cl-Par-4 in high ionic strength is characteristic of a predominantly alpha helical protein (Figure 11). However, in high ionic strength, negative dichroism was more intense at 208 nm than at 222 nm, making the $\Theta_{222}/\Theta_{208}$ ratios in high ionic strength are less than 1. The large R_S in low salt is characteristic of non-globular aggregates. However, a decrease in hydrodynamic size in high salt up to 1 M NaCl is consistent with a more compact conformation and a decrease in self-association state. The SAC and linker domains represent potential sites for induced folding and could, for instance, serve as a flexible hinge, a type of structure observed in other long CC proteins [147]. Increased ionic strength likely minimizes negative-negative charge repulsion in the LZ due to contacts between acidic side chains discussed in Chapter II.

Cl-Par-4 forms large soluble aggregates at neutral pH

After identifying aggregate formation in low salt, SEC-MALS was used to identify the degree of self-association. Large molar mass measurements indicated that high-order oligomers in a range near 16mer to 22mer can form in low salt (Figure 15, Table 1) that have a non-globular shape, somewhat characteristic of coil or a rod shape. This data could indicate, for instance, a "folded rod" which is not spherical, but has some partially folded regions [147].

It is plausible that partially disordered pre-formed dimers and/or tetramers further self-associate in a destabilizing environment such as low salt to form large partially disordered aggregates. Many factors such as electrostatic repulsion and CC destabilization, hydrophobic interactions, and helix sliding could potentially result in protein aggregation and loss of function [148-150].

Ionic strength-induced tetramer formation

Possibly the most intriguing conclusion from this study is that cl-Par-4 forms a tetramer in 1 M NaCl (Figure 16, Table 2). This is the first evidence of tetramer formation in the Par-4 tumor suppressor. Based on our biophysical data, the tetramer is mostly alpha helical and more globular than is the structure in low salt. The observance of a tetramer at high salt is consistent with results reported for other proteins, e.g. mellitin and Ndel1 [151-153]. Tetramer formation by another tumor suppressor, p53, is well-established and determined to be the active conformation [154, 155]. Additionally, many IDPs undergo a structural transition (induced folding) either when bound to a physiological partner or due to changes in cellular environment [14, 15, 99]. Here, data clearly demonstrates that high salt is sufficient to induce folding of cl-Par-4 into stable tetramers.

This folding process likely serves a role in Par-4 regulation and function. Extracellular Par-4 enters tumor cells by binding GRP78 at the cell surface, and then is modified post-translationally through phosphorylation and the caspase-induced cleavage that produces the cl-Par-4 fragment [53, 54, 56, 57]. It has been proposed that a post-translational signal initiates tetramer formation in the p53 tumor suppressor [154]. A similar post-translational signal may initiate tetramerization of Par-4 *in vivo*. This could potentially occur in the full-length protein as well as in the cl-Par-4 fragment, or caspase-cleavage may be required for tetramer formation to occur.

Clearly, a compact tetramer could more easily translocate to the nucleus than could a large and disordered aggregate. Tetramer formation could also make NLS2 more accessible. Also, similar to p53, the nuclear export sequence (NES), which resides in the Par-4 CC region, would likely become masked within the CC of the tetramer, preventing export of Par-4 from the nucleus [156]. Once in the nucleus, tetramer formation could facilitate pro-apoptotic binding interactions, as seen in other apoptotic proteins such as the Bcl-2 relative Bak [157, 158]. Par-4 nuclear interactions with, e.g., WT1, ζpKC isoforms, and Dlk occur within the leucine zipper (LZ) region of the CC [31, 43, 45, 62, 133], which our proposed tetramer model suggests would be accessible for substrate binding (Figure 8).

Higher order oligomerization could itself serve a regulatory role. As an example, the HypT transcription factor forms dodecamers in low salt, but dissociates into tetramers and dimers upon DNA binding [146]. This dissociation process can be initiated *in vitro* via exposure to 0.8 to 1.5 M NaCl [146]. Large cl-Par-4 oligomers could similarly serve as a storage form, which dissociate into active tetramers upon substrate-binding. It has been proposed that Par-4 can be transported out of cells within exosomes [88, 133]. Since the average diameter of an exosome is less than 100 nm [136], only the folded structures identified in either acidic pH or high salt would be suitable

for exosome transport. Therefore, it is interesting to note that exosomes arise from late endosomal compartments that are more acidic than the cytosol [127], an environment more conducive to the compact structural form.

In summary, it is highly likely that both ionic strength and pH, among other factors, influence the *in vivo* structure and regulation of Par-4. Additional biophysical and functional characterization of both full-length Par-4 and cl-Par-4 are necessary to establish the role and significance of tetramerization more definitively in Par-4 localization and apoptotic function.

CHAPTER IV

DIRECT INTERACTION OF PLATINUM CHEMOTHERAPEUTICS WITH FULL LENGTH PAR-4 AND CASPASE-CLEAVED PAR-4

INTRODUCTION

The aim of the research described in the following chapter was to identify and characterize the direct interaction of cisplatin (cisPt) and transplatin (transPt) with the full length Par-4 protein (FL-Par-4) and the caspase-cleaved fragment of Par-4 (cl-Par-4). As discussed in Chapter I, cisPt is a platinum-based chemotherapeutic agent that cross-links the DNA of proliferating cells, inhibiting DNA synthesis [69, 70]. CisPt is widely used in cancer therapy and is used to treat lung, breast, ovarian, and brain cancers, along with carcinomas and lymphomas [70, 159].

CisPt and transPt are highly reactive to S- and N-donors and can therefore bind cellular proteins [74, 160]. It has been proposed that sulfur-containing biomolecules such as methionine could function as a cisPt drug reservoir, ultimately transporting cisPt to DNA [160]. Pt-protein interactions can affect the biodistribution and cellular uptake of drug, produce negative side effects, contribute to resistance processes, and alter the structure and function of the protein [74]. Therefore, characterizing interactions between platinum chemotherapeutics and cellular proteins, specifically IDPs, is of high importance. As described in Chapter I, recent studies have shown that Par-4 combined with cisPt have a synergistic anti-tumor effect [72]. However, it is unknown whether the correlations between Par-4 and cisplatin activities are due to direct interaction, or whether intermediaries may be involved.

FL-Par-4 has six sulfur-containing residues that serve as potential platinum binding sites: five methionine (M) residues and one cysteine (C) residue (Figure 19). Cl-Par-4 retains three potential

cisplatin binding sites: one cysteine in the selective for apoptosis induction in cancer cells (SAC) domain and two methionine residues in the C-terminal coiled coil (CC) domain. While most previous studies have characterized interactions of cisPt with globular proteins, the interaction of cisPt with IDPs has not been extensively studied. In this study, analytical and biophysical techniques were used to characterize the interaction of cisPt and transPt with Par-4. Platinated cl-Par-4 and FL-Par-4 oligomers were detected and the interaction likely occurs through S-Pt coordination. This is the first evidence of direct interaction between cisPt and transPt with Par-4.

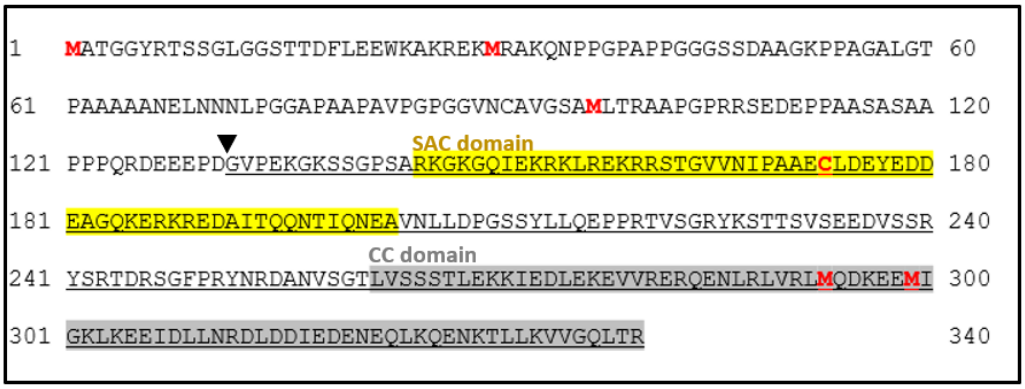

Fig. 19. Par-4 sequence and domain structure**.** The six sulfur-containing residues are highlighted in red: five methionine. Yellow indicates SAC domain and gray indicates the CC domain. The cl-Par-4 fragment is underlined (cleavage site marked by triangle).

MATERIALS AND METHODS

Cisplatin and transplatin

The cisPt and transPt stock solutions were prepared by dissolving cisPt (Sigma Aldrich) or transPt (Sigma Aldrich) in phosphate buffered saline (PBS) at neutral pH with 140 mM NaCl to a

final concentration of 1.67 mM (cisPt) and 0.84 mM (transPt). Stock solutions were stored at room temperature in the dark and then diluted for Par-4 cisPt/transPt binding studies.

Expression and purification of FL-Par-4 and cl-Par-4 proteins

FL-Par-4 and cl-Par-4 were expressed in BL21(DE3) *E. coli* cells using the modified H-MBP-3C expression vector according to published procedures (described in Chapters II and III) [51, 161]. FL-Par-4 did not require high NaCl for solubility, and therefore was dialyzed into 300 mM NaCl, 10 mM Tris, 1 mM TCEP, pH 7 buffer. Absorbance measurements at 280 nm and a molar extinction coefficient of 14440 $M^{-1}cm^{-1}$ were used to determine FL-Par-4 concentration.

Gel analysis of cross-linking and thermal stability

Protein samples were incubated with or without varying molar ratios of cisplatin or transplatin for one hour. Samples containing 25 µM cl-Par-4 and 27 µM FL-Par-4 were prepared in pH 7 buffer containing 120 mM NaCl (cl-Par-4) or 195 mM NaCl (FL-Par-4) and 10 mM Tris. Loading dye was added to the protein samples which were then loaded onto a denaturing 4-12% SDS-PAGE gel under non-reducing conditions with no boiling of samples. For thermal stability/dissociation studies, samples were either heated at 90 °C for 5 minutes or kept at room temperature. Gels were run at 240 V for 35 minutes and then stained with Coomassie blue to assess cross-linking of Par-4 by cisPt or transPt.

UV-vis spectroscopy, dynamic light scattering and circular dichroism

Cl-Par-4 (8.3 µM) and FL-Par-4 (4.1 µM) protein samples were incubated with cisPt or transPt for one hour at room temperature in buffer containing 10 mM Tris-HCl, pH 7 and varying

NaCl concentration. UV-vis spectroscopy experiments were performed on a Schimadzu double beam UV-Vis spectrophotometer. Three scans were recorded from 240 to 400 nm using 1 cm pathlength quartz cuvettes and baseline subtracted. DLS experiments were performed on a NanoBrook Omni particle sizer. Five scans were recorded in 1 cm pathlength plastic cuvettes and then averaged. Far-UV CD and corresponding UV-visible absorption experiments were obtained on a Jasco J815 CD spectrometer using 0.1 cm pathlength quarts cuvettes. Far-UV CD and UV-vis scans were acquired from 190-260 nm with a scan speed of 20 nm/min. Three scans were recorded for each sample and baseline was subtracted. CD spectra were smoothed using a means-movement function of 25 and deconvoluted with Selcon3 (DichroWeb server) [94]. Experiments were performed at room temperature.

Gel filtration

Gel filtration experiments were performed on a Superdex 200 column (GE Healthcare) with a column volume of 24 mL. The column was equilibrated with 30 mM NaCl, pH 7 buffer at a flow rate of 0.1 mL/min for 1 CV prior to sample injection. Aliquots containing 500 µL of 83 µM cl-Par-4 and 500 µL of 16 µM FL-Par-4 were treated with a range of molar equivalents of cisPt or transPt and then loaded onto the column. Untreated samples were used as a control. Experiments were performed at 4 °C and a flow rate of 0.3 mL/min was used. A280 measurements were obtained. MALS analysis of FL-Par-4 in 300 mM NaCl, pH 7 buffer was performed as in Chapter III.

Isothermal Titration Calorimetry

ITC experiments were performed using a Micral ITC 200. The sample cell was filled with 16 µM FL-Par-4, the reference cell was filled with 30 mM NaCl, 10 mM Tris, pH 7 buffer, and the

syringe was filled with 320 µM cisPt solution. The temperature was set to 23 °C. Multiple injections of cisPt were made into the sample cell which contained FL-Par-4. Each injection of cisPt into the sample cell was made over 4 seconds with an interval of 60 seconds between injections. The titration curves were analyzed to determine thermodynamic parameters.

RESULTS

Effect of Pt-binding on cl-Par-4 absorption, hydrodynamic size, and secondary structure

UV-visible absorption spectroscopy, dynamic light scattering (DLS), and Far-UV circular dichroism (CD) experiments were performed to assess the effect of cisPt on the UV-vis absorbance spectra, hydrodynamic size, and secondary structure of cl-Par-4. Cl-Par-4 at 8.3 µM in either 150 mM or 1 M NaCl, pH 7 buffer was incubated with 10 molar equivalents of cisPt at room temperature for 1 hour followed by UV, DLS, and CD measurements.

Absorption spectra in were obtained in the range of 240 to 400 nm to assess scattering of large cl-Par-4 oligomers. In 150 mM NaCl buffer, UV-vis absorption spectra in the near UV region show no substantial change in absorbance between the untreated control and cisPt-treated cl-Par-4 (Figure 20a). UV-vis measurements obtained in parallel with far-UV chirality measurements showed no substantial change in absorbance (Figure 20b). This confirms that in circular dichroism experiments, any changes in dichroism intensity are due to change in chirality and not in scattering.

Far-UV CD experiments did show a change in dichroism upon cisPt treatment, with negative dichroism becoming less intense (Figure 20c). DLS experiments showed no substantial change in the stokes radius (Rs) upon cisPt treatment with minor change from 1460 to 1422 nm upon Pt treatment (Figure 20d). Shown in Figure 20e is the difference between the two dichroism

plots in Figure 20c. This molar ellipticity difference is approximately $1e^5$ deg·cm^2·dmol^{-1} and could be related to the S-Pt dichroism.

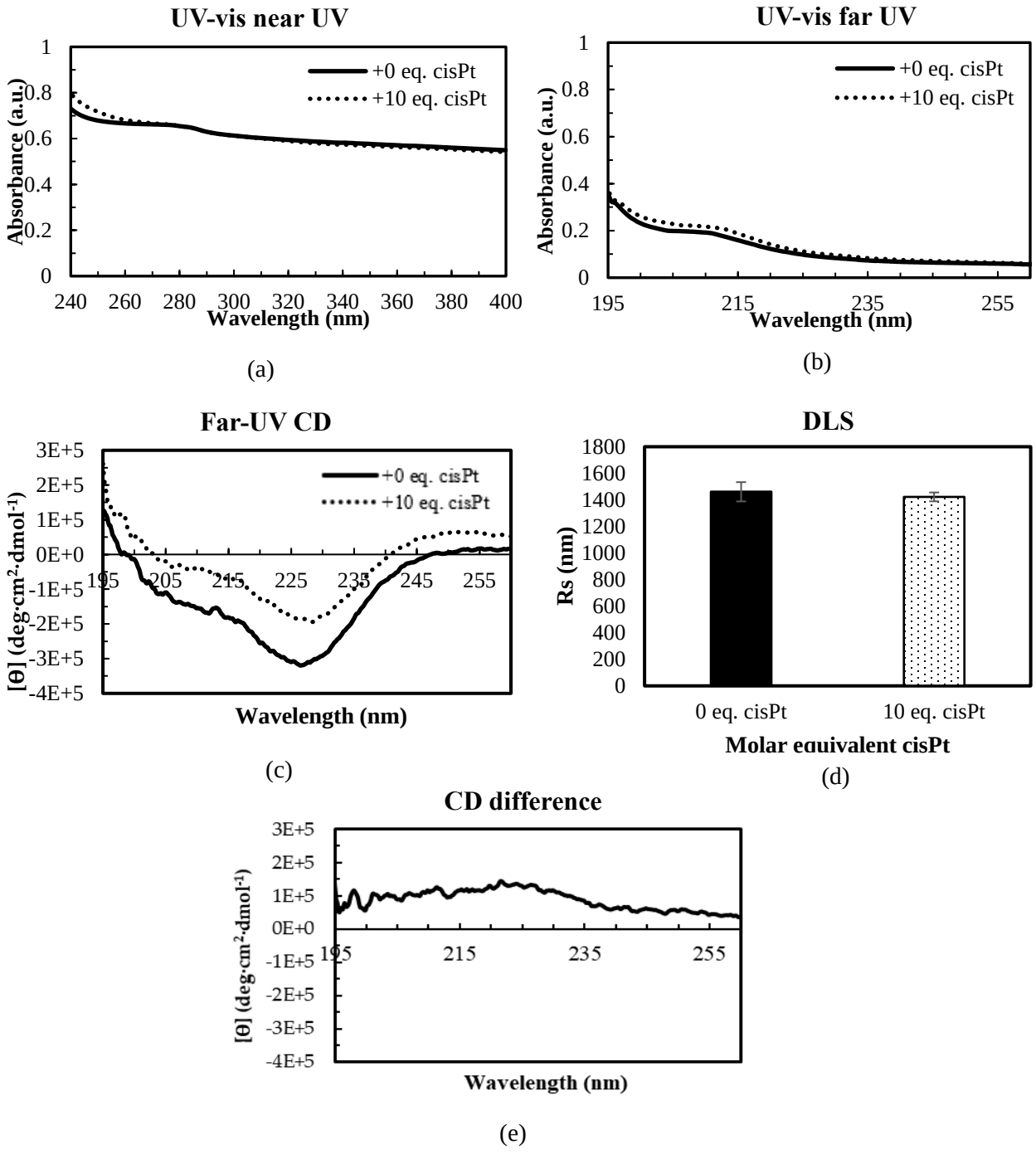

Fig. 20. In low ionic strength, cisplatin induces changes in dichroism but does not change the self-association state of cl-Par-4. Cl-Par-4 at 8.3 µM in 150 mM NaCl, pH 7 buffer was treated with

10 molar equivalents of cisplatin (dotted) or untreated (solid) and incubated for one hour at room temperature and then analyzed by (a) UV-visible spectroscopy in the near UV region from 240 – 400 nm and (b) UV-visible spectroscopy in the far UV region from 195 to 260 nm (c) Far-UV CD (d) DLS. Panel (e) shows the difference between the two dichroism plots in panel (c). Pathlengths are 1 cm (a,d) and 0.1 cm (b,c).

The effect of cisPt treatment on 8.3 µM cl-Par-4 in 1 M NaCl, pH 7 buffer was also assessed since cl-Par-4 has been shown to form stable structure in extreme conditions of 1 M NaCl [162]. UV-vis absorption spectra in the near UV range of 240 to 400 nm showed minor change in absorbance upon cisPt treatment (Figure 21a). In 1 M NaCl, absorbance in the range of 320 to 400 nm was less intense compared to Figure 20a, likely due to decreased scattering of large particles. UV-vis measurements obtained in parallel with far-UV chirality measurements showed similar absorbance (Figure 21b), confirming any changes in dichroism in Figure 21c are due to changes in chirality and not in scattering. CD spectra showed no substantial change in secondary structure (Figure 21c), with dichroism overlapping for untreated and cisPt-treated cl-Par-4. Two cl-Par-4 species were detected by DLS measurements (Figure 21d) with Rs values of 700 and 74 nm (untreated) and 734 and 71 nm (cisPt treated). No major change in Rs was detected between treated and untreated cl-Par-4.

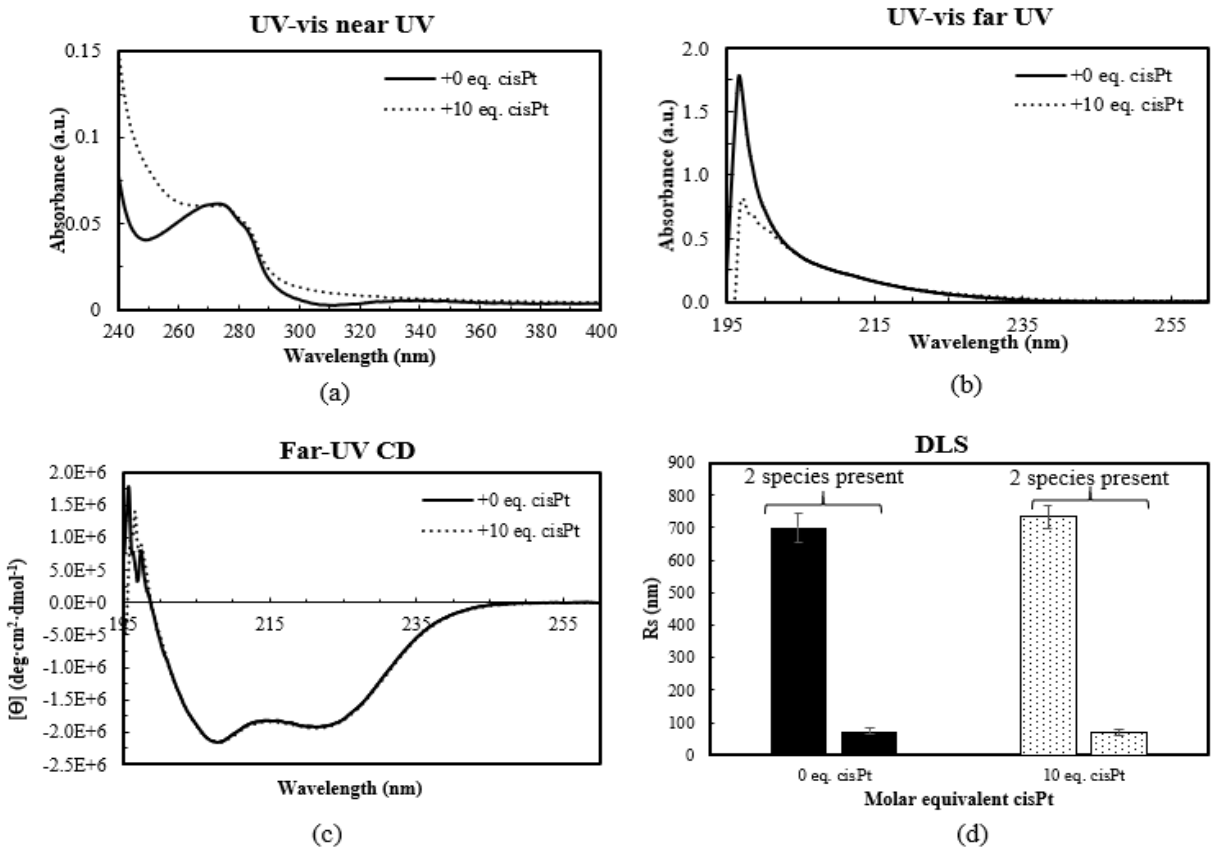

Fig. 21. At high ionic strength, cisplatin does not change the structure or self-association state of cl-Par-4 significantly**.** Cl-Par-4 at 8.3 µM in 1 M NaCl, pH 7 buffer was treated with 10 equivalents of cisplatin (dotted) or untreated (solid) and incubated for one hour at room temperature and then analyzed by (a) UV-visible spectroscopy in the near UV region from 240-400 nm, (b) UV-vis spectroscopy in the far UV region from 195 to 260 nm, (c) Far-UV CD, and (d) DLS. Pathlengths are (a,d) 1 cm and (b,c) 0.1 cm.

Shown in Figure 22 are additional CD experiments of cisPt-treated cl-Par-4 performed in low ionic strength conditions ranging from 40 mM to 150 mM NaCl at neutral pH. Protein samples were at 8.3 µM. In all experiments shown, the intensity of negative dichroism either increases or decreases upon cisPt treatment (dotted line) compared to the untreated control (solid line). In

Figures 22a,b, the intensity of negative dichroism decreased upon cisPt treatment similar to Figure 20c. Negative dichroism for the untreated control (solid line) was of similar intensity in both experiments (Figure 22a,b), indicative of a similar starting structure before treatment.

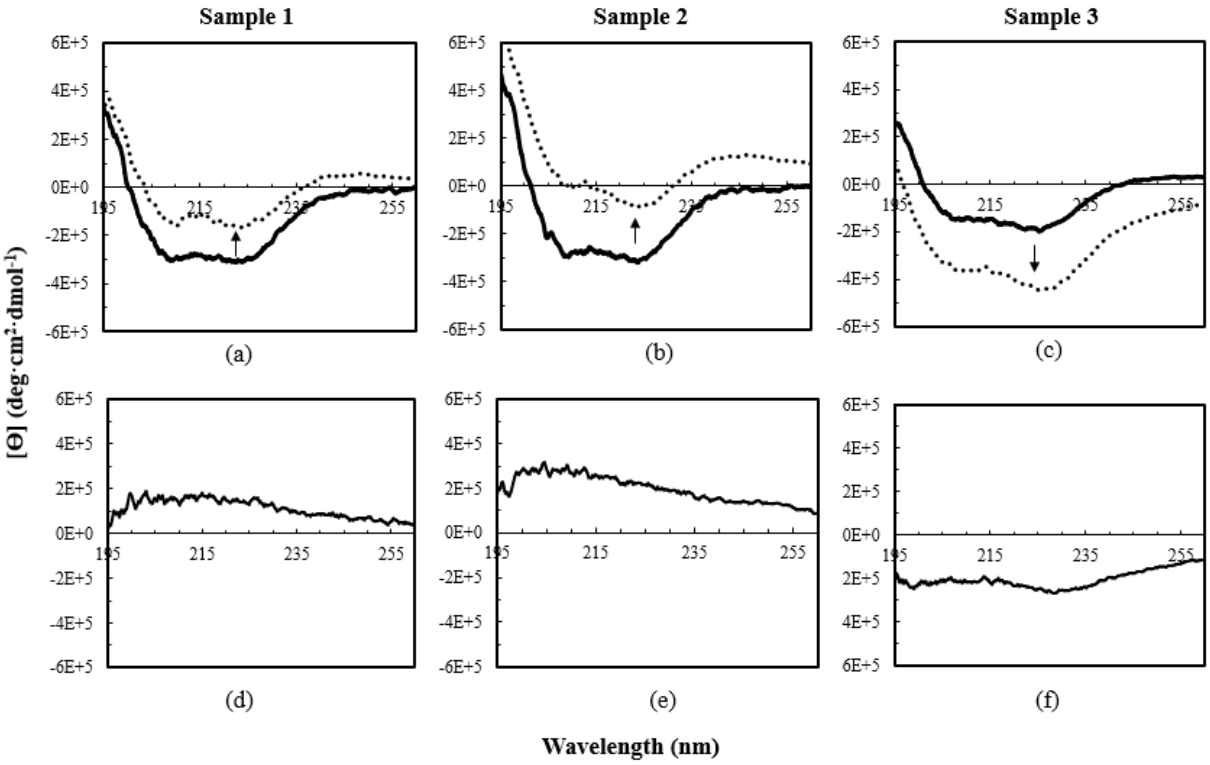

Fig. 22. Intensity of cl-Par-4 negative dichroism increases or decreases upon cisPt treatment**.** CD of 8.3 μM cl-Par-4 without (solid line) and with (dotted line) one equivalent of cisplatin at pH 7, under the following ionic strength conditions: (a) with 150 mM NaCl (sample 1); (b) with 150 mM NaCl (sample 2); (c) with 40 mM NaCl. The difference between the two plots in panel (a) is shown in panel (d). Similarly, panels (e) and (f) show difference plots for data from panels (b) and (c), respectively. The pathlength of cuvettes used was 0.1 cm.

However, cisPt-treatment can also increase the intensity of negative dichroism (Figure 22c). In Figure 22c, negative dichroism of the untreated control is less intense than samples 1 and 2 and therefore is likely in a difference conformation or self-association state. This suggests that the effect of cisPt-binding on dichroism intensity may be related to the initial protein conformation and self-association state, or even to the initial state of cisPt. The formation of large soluble oligomers may prevent accessibility of certain Pt-binding sites. Figures 22d-f show the difference plot of cisPt-treated and untreated cl-Par-4 in Figures 22a-c. This global shift in dichroism intensity is likely related chirality of the S-Pt bond and the dihedral bond angle influences an upward versus downward shift.

Identification of Pt-induced cl-Par-4 oligomers

To determine if cisPt and transPt can induce the formation of cl-Par-4 cross-links, gel electrophoresis experiments were performed (Figure 23). Cl-Par-4 was prepared at a concentration of 25 μM in pH 7 buffer containing 120 mM NaCl. On a denaturing gel, monomeric cl-Par-4 migrates primarily as a single form, with a band near 30 kilodaltons. After incubation with 10 to 40 molar equivalents of cisPt, aggregated species (platinated cl-Par-4 oligomers) are detected on a denaturing gel, and the intensity of the monomeric band decreased (Figure 23a).

A similar result was obtained when treated with transPt (Figure 23b). Platinated cl-Par-4 oligomers were detected on a denaturing gel upon treatment with 10 to 30 molar equivalents of transPt. The platinated oligomers have sizes ranging from 66-70 kDa and greater than 116 kDa. The larger oligomers could possibly represent a cl-Par-4 dimer and tetramer. This result suggests that platinated cl-Par-4 oligomers are formed when the platinum center of cisPt or transPt cross-

links cl-Par-4 subunits. Aggregates formed in the presence of cisPt and transPt are SDS-resistant or at least partially SDS-resistant.

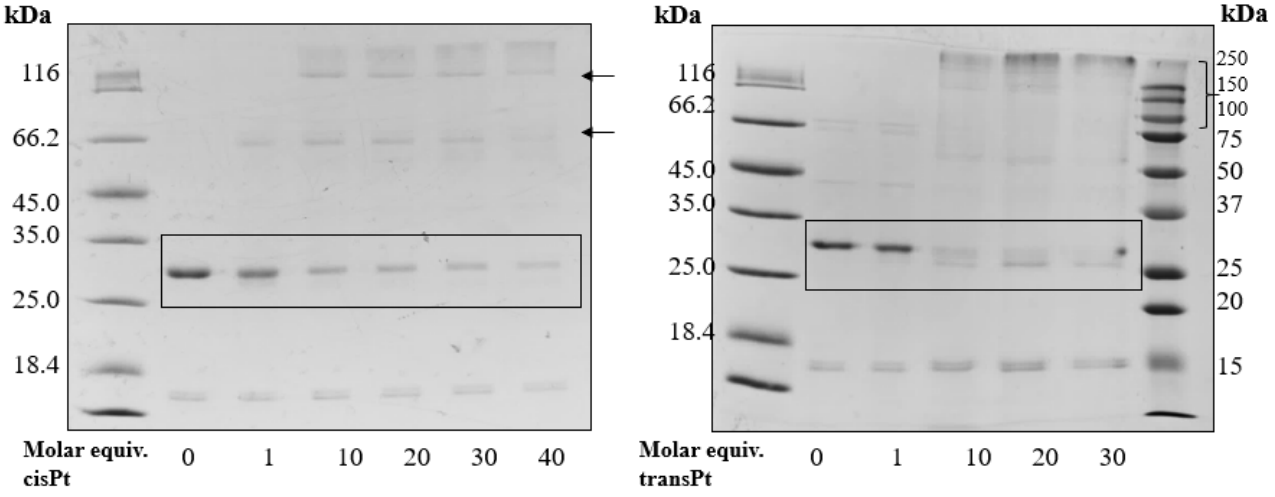

(a) (b)

Fig. 23. At high concentration, cisplatin and transplatin cross-link cl-Par-4. SDS-PAGE of 25 µM cl-Par-4 treated with (a) cisPt and (b) transPt prepared in pH 7 buffer containing 120 mM NaCl.

Next, thermal stability of the platinated cl-Par-4 oligomers was assessed by gel electrophoresis (Figure 24). Cl-Par-4 was prepared at a concentration of 25 µM in pH 7 buffer containing 120 mM NaCl and then incubated with or without cisPt or transPt. Again, the intensity of the monomeric band near 30 kilodaltons decreased upon Pt treatment. Minor differences in intensity of the monomeric band were detected for untreated cl-Par-4 upon heating. Dissociation of platinated cl-Par-4 oligomers upon heating suggests that Pt-induced cl-Par-4 cross-links are not resistant to denaturation. Cl-Par-4 oligomers formed upon cisPt treatment dissociate into bands of

various sizes upon denaturation, while cl-Par-4 oligomers formed upon transPt treatment dissociate primarily into monomer.

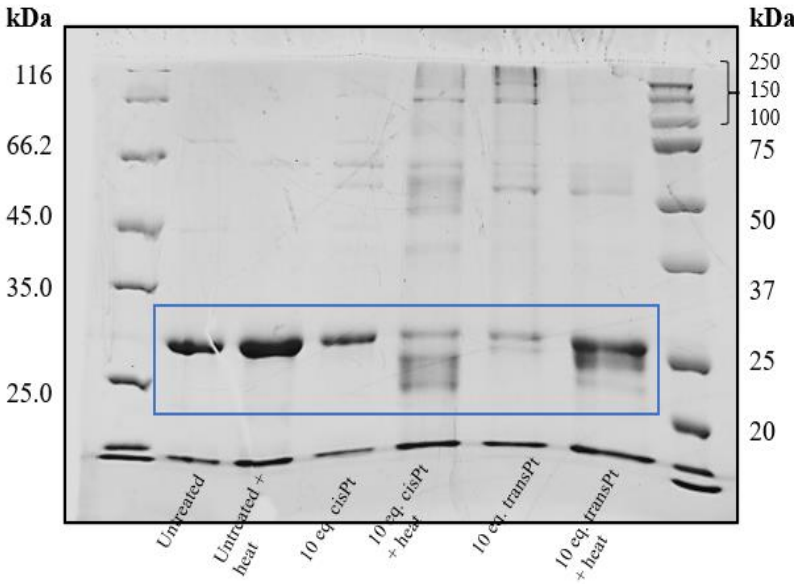

Fig. 24. Thermal stability of platinated cl-Par-4 oligomers. SDS-PAGE analysis of Pt-treated and untreated 25 µM cl-Par-4 prepared in pH 7 buffer containing 120 mM NaCl. Samples were heated at 90°C for 5 min and compared to the unheated control samples.

Analysis of platinated cl-Par-4 oligomers by gel filtration

SDS-PAGE experiments showed that cisPt and transPt can cross-link cl-Par-4 and DLS experiments in low ionic strength conditions produced large Rs values, consistent with a large oligomeric cl-Par-4 species. Therefore, gel filtration experiments were performed to assess if Pt-binding affects the aggregation state of cl-Par-4 by monitoring changes in the retention time of Pt-treated cl-Par-4. Additionally, increased absorbance at 280 nm of the eluting species has been used to detect S-Pt coordination in other proteins.

Chromatographic profiles obtained for 83 µM cl-Par-4 treated with varying molar ratios of cisPt and transPt are reported in Figure 25 and compared to the untreated control. The SEC elution profile of untreated cl-Par-4 was consistent with published SEC results for cl-Par-4: in low ionic

strength, cl-Par-4 has a retention time of 21 mL, representing large soluble oligomers in the range of 16 to 22mer [162]. Treatment of cl-Par-4 with 1 molar equivalent of cisPt produced peaks with retention times of 15.5, 19, and 21.5 mL with similar intensity to the untreated control. Treatment of cl-Par-4 with 10 molar equivalents of cisPt produced peaks with similar retention times. However, the absorbance for the peak with a retention time of 21.5 mL increased.

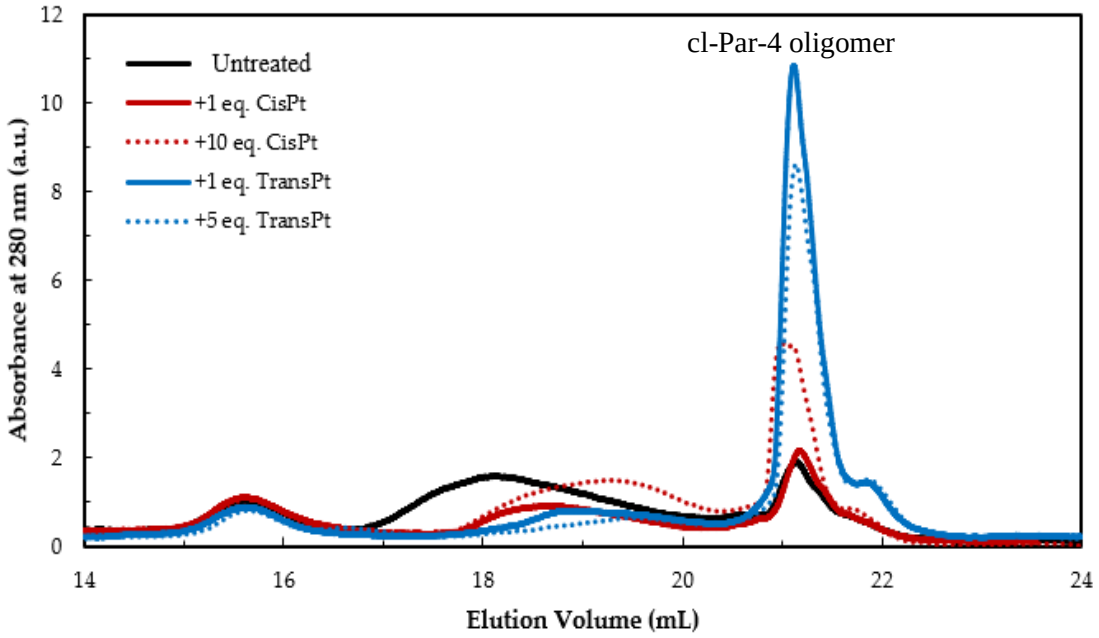

Fig. 25. Cl-Par-4 forms large oligomers with increased absorbance upon cisPt and transPt treatment. Gel filtration pattern of 83 µM cl-Par-4 treated with cisPt (red) and transPt (blue) in 30 mM NaCl, pH 7 buffer. The solid black line represents the untreated control.

This increase in absorbance at 280 nm might correspond to S-Pt coordination between cisPt and sulfur-containing residues in cl-Par-4. The peak with a retention time of 18 mL for the control eluted at 19 mL upon cisPt treatment of both 1 and 10 molar equivalents. Treatment with 1 molar equivalent likely produced one platinated species, while treatment with 10 molar equivalents

produced two platinated species. Similar results were obtained when cl-Par-4 was treated with the trans isomer, transPt. The peak with a retention time of 18 mL was not detected upon transPt treatment. However, transPt treatment resulted in increased absorbance for the peak eluting at 21.5 mL. The major peaks are symmetric and therefore, likely correlate to one oligomerization state.

Biophysical analysis of the FL-Par-4-Pt interaction

FL-Par-4 at 4.1 µM in 30 mM NaCl, pH 7 buffer was incubated with cisPt or transPt for one hour at room temperature and then CD and DLS measurements were obtained. There was no substantial change in the secondary structure of Par-4 treated with 10 molar equivalents of either cisPt or transPt (Figure 26a). All spectra show negative dichroism near 222 nm and 208 nm with positive dichroism near 195 nm, characteristic of an alpha helical conformation.

Deconvolution of CD spectra using Selcon3 provided calculated percentages of secondary structure: approximately 80% alpha helical and the remaining 20% comprised of beta sheet, turn, and disorder [94]. While most CD spectra obtained of cisPt-treated FL-Par-4 show no change in dichroism intensity, changes in intensity of negative dichroism are occasionally detected. UV measurements obtained in parallel with Far-UV CD showed no change in absorbance (Figure 26b), confirming changes in dichroism intensity are due to changes in chirality and not in scattering.

The hydrodynamic size of Pt-treated Par-4 was assessed by DLS (Figure 26c). The average Rs did decrease slightly upon Pt treatment. The untreated control had an average Rs of 1331 nm, while cisPt and transPt treated Par-4 had Rs values of 1168 nm and 1108 nm, respectively. However, all Rs values are large, consistent with an oligomeric species.

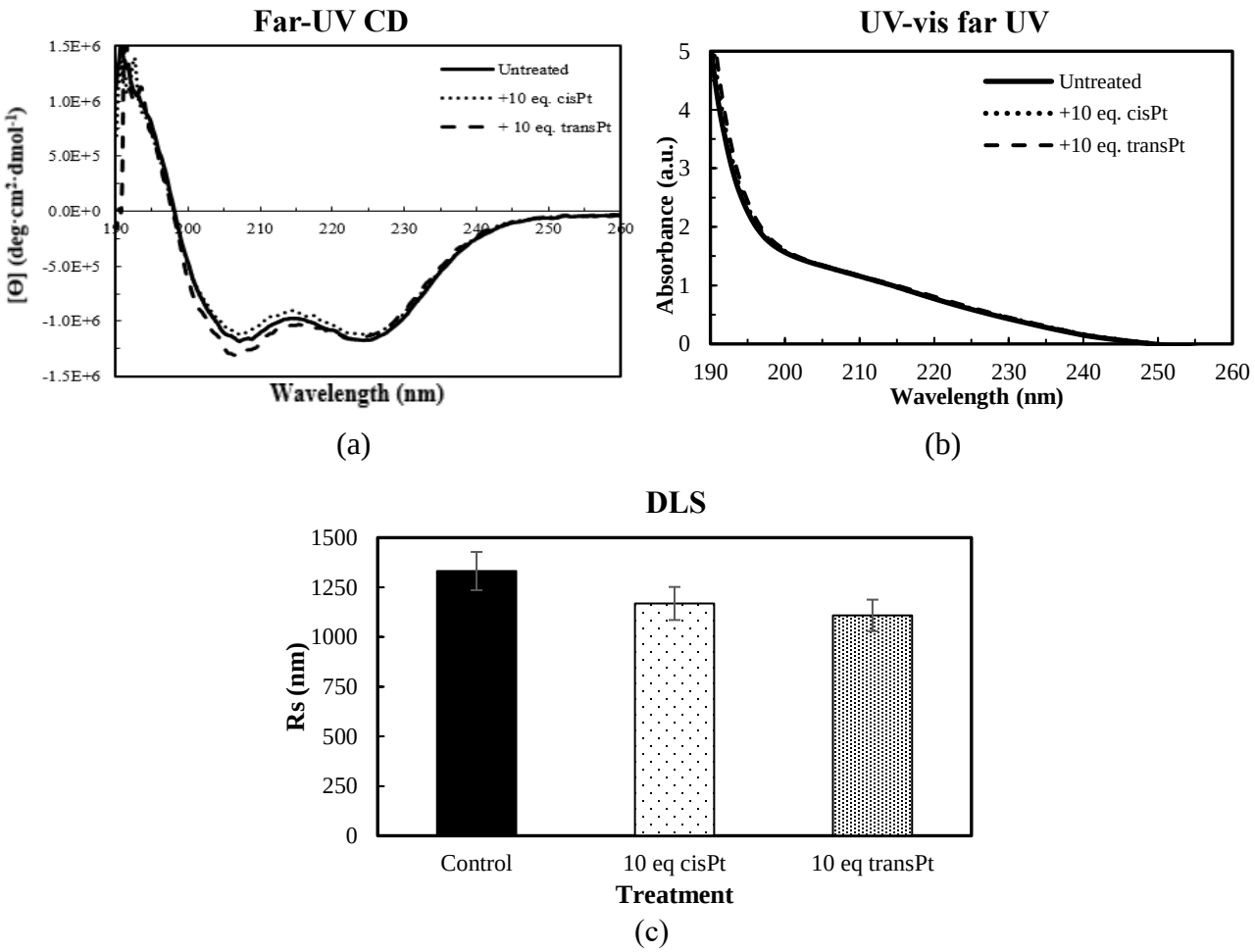

Fig. 26. No substantial change in FL-Par-4 hydrodynamic size or dichroism upon cisplatin or transplatin treatment. FL-Par-4 at 4.1 µM in 30 mM NaCl, pH 7 buffer was treated with 10 equivalents of cisplatin (dotted), transplatin (dashed), or untreated (solid) and incubated for one hour at room temperature and then analyzed by (a) Far-UV CD (b) UV-vis absorbance spectra in the far UV region and (c) DLS. The pathlength was 0.1 cm (a,b) and 1 cm (c).

While most CD spectra obtained of cisPt-treated FL-Par-4 did not show a change in dichroism intensity, in one experiment the intensity of negative dichroism increased upon cisPt treatment (Figure 27). FL-Par-4 was at a concentration of 4.1 µM in pH 7 buffer containing 30 mM NaCl, 10 mM Tris. In this experiment, the untreated FL-Par-4 control (solid line) varies in

shape and intensity compared to Figure 26. Upon treatment with 1 molar equivalent of cisPt, negative dichroism became more intense. This shift in dichroism intensity is comparable to results obtained for cl-Par-4 and suggests that the effect of cisPt-binding could be related to initial protein conformation. Shown in Figure 27b is the difference in CD intensity of cisPt-treated FL-Par-4 and the untreated control. This produces a molar ellipticity value of approximately to -3e^5 deg·cm^2·dmol^{-1}. This difference in CD intensity for cisPt-treated FL-Par-4 could be related to the S-Pt dichroism, comparable to the global shift in dichroism intensity observed for cisPt-treated cl-Par-4.

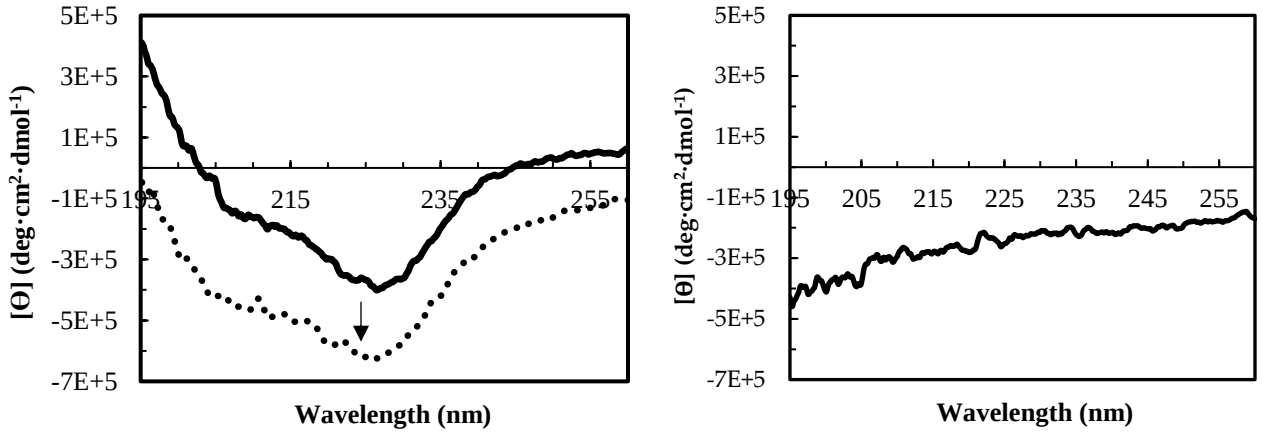

Fig. 27. Outlier experiment: increased intensity of negative dichroism upon cisPt treatment of 4.1 µM FL-Par-4 was seen with one sample. (a) CD of 4.1 µM FL-Par-4 without (solid) and with (dotted line) 1 molar equivalent of cisPt in 30 mM NaCl, pH 7 buffer. (b) Difference plot of the two plots in panel (a). Pathlength used was 0.1 cm.

Formation of Pt-induced covalent FL-Par-4 oligomers

Human FL-Par-4 is 36.5 kilodaltons based on amino acid sequence; however, disordered proteins due to their intrinsic disorder and non-globular conformation often have slower

electrophoretic mobility and run higher on SDS-PAGE. Platinated FL-Par-4 oligomers were detected in a denaturing gel after treatment with 5 to 20 molar equivalents of cisPt (Figure 28a).

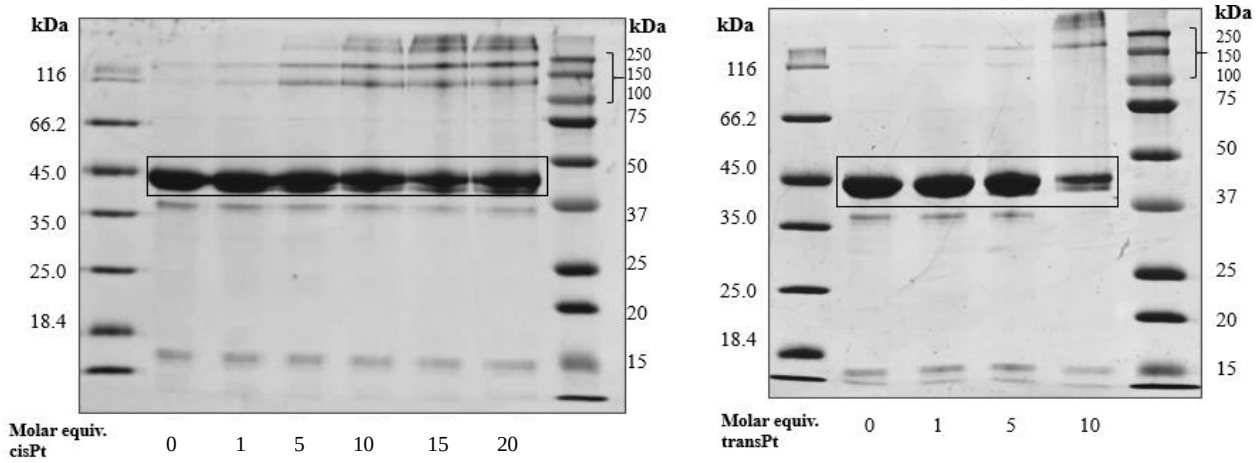

(a) (b)

Fig. 28. At high concentration, cisplatin and transplatin cross-link FL-Par-4. SDS-PAGE of 27 µM FL-Par-4 treated with (a) cisPt and (b) transPt prepared in pH 7 buffer containing 195 mM NaCl.

Intensity of the bands near 116 and 200 kDa increased with increasing cisPt concentration. Platinated FL-Par-4 oligomers were detected when treated with 10 molar equivalents of transPt (Figure 28b) In both denaturing gels, the intensity of bands near the sample loading wells also increased with increasing Pt concentration, consistent with a large oligomeric species. Bands near 116 and 200 kDa could possibly represent tetramer and possibly hexamer, respectively.

Since Pt-induced FL-Par-4 cross-links were also detected, chromatographic studies were performed to assess changes in FL-Par-4 oligomerization upon Pt treatment. FL-Par-4 at a concentration of 16 µM was treated with freshly prepared cisPt versus aged cisPt prepared in buffer containing low [Cl^-] (30 mM NaCl).

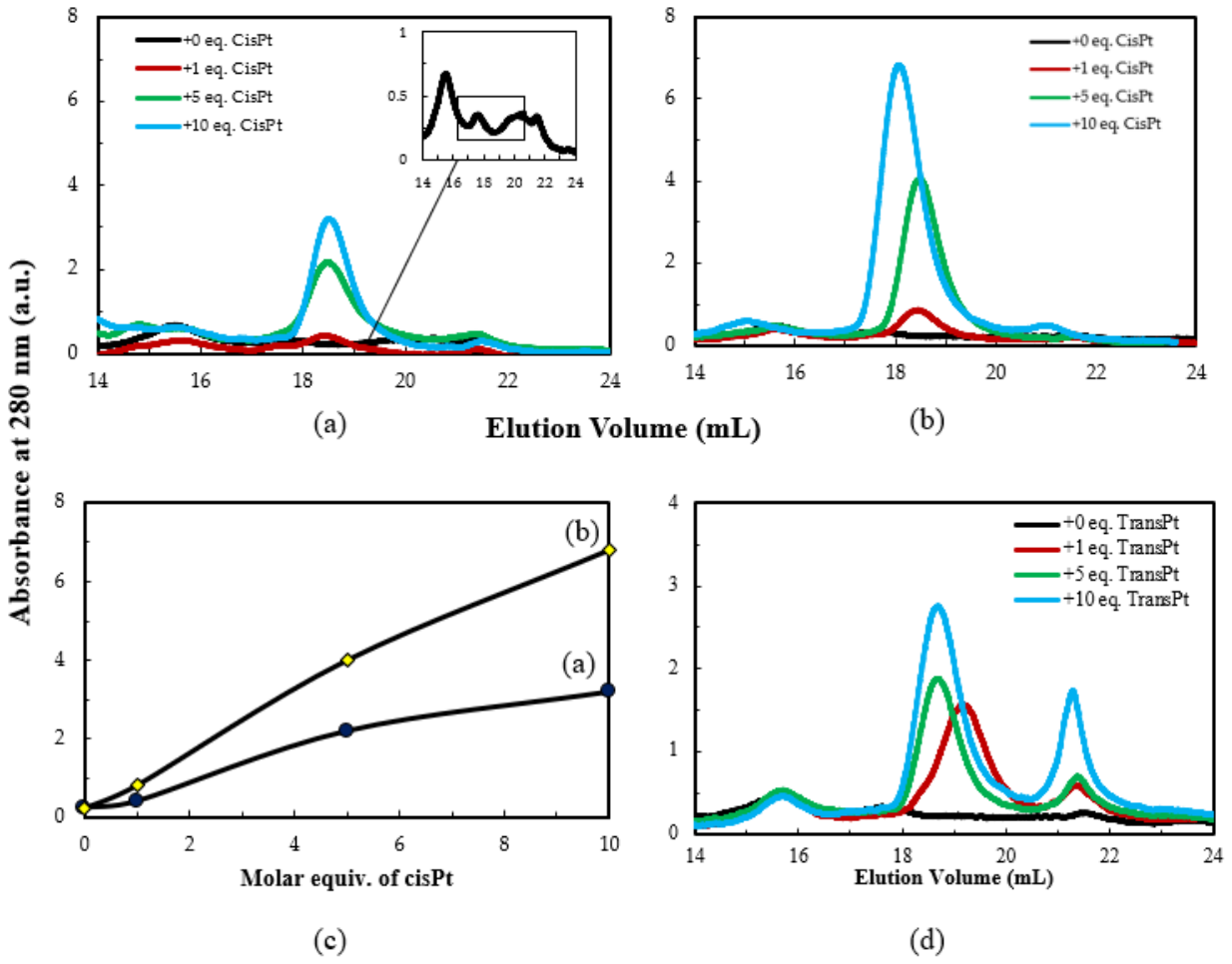

Fig. 29. Gel filtration of FL-Par-4 treated with cisplatin and transplatin. FL-Par-4 at 16 µM was treated with varying molar equivalents of cisPt in low ionic strength conditions (30 mM NaCl) at pH 7. (a) FL-Par-4 treated with freshly prepared cisplatin (less reactive). Insert in (a) is elution profile of untreated FL-Par-4. (b) FL-Par-4 treated with aged cisplatin (more reactive) (c) Differing effect of fresh (less reactive) vs. aged (more reactive) cisplatin. Shown is A280 for the peak that eluted at 19 mL in (a) and (b). (d) FLPar-4 treated with varying molar equivalents of transplatin.

Retention times for untreated FL-Par-4 are 15, 17.5, and 20-22 mL (Figure 29a, insert). Upon cisPt treatment, the retention time for the major peak increased to 19 mL and A280 values increased proportionally to cisPt treatment. Next, the experiment was repeated with cisPt that had

been in aqueous solution longer (Figure 29b). A similar trend was observed, except that the peak intensity at 19 mL was approximately double that of Figure 29a for all the molar ratios of cisPt tested. In both elution profiles, one platinated FL-Par-4 adduct was detected. Shown in Figure 29c is the relationship between A280 and cisPt concentration for the peak eluting at 19 mL in Figures 29a,b. Treatment of FL-Par-4 with transPt produced two platinated adducts with retention times of 19 and 21.5 mL and the A280 of these peaks increased upon transPt treatment (Figure 29d).

Preliminary ITC analysis of cisPt-FL-Par-4 interaction

ITC was used to study the thermodynamics and kinetics of the Par-4-Pt interaction. Figure 30 shows the titration profile of cisPt binding with 16 µM FL-Par-4 at 23 °C. Each peak represents one injection of cisPt into the protein solution and the plot below represents amount of heat released per injection. The interaction of cisPt with FL-Par-4 is exothermic in nature, evident by the negative peaks at each injection. Listed in Table 3 are the thermodynamic parameters obtained from the titration : the enthalpy change was $-1.114e^4$ cal/mol, the entropy change was -8.54 cal/mol/deg, and the binding constant was $3.6e^5$ M^{-1}. Additional ITC experiments of FL-Par-4 titrated with cisPt are also characteristic of an exothermic reaction.

[Par-4] µM	[cisPt] µM	Temp (°C)	Enthalpy change	Entropy change	Binding constant
16	320	23	$-1.114e^4$ cal/mol	-8.54 cal/mol/deg	$3.6e^5$ M^{-1}

Table 3. Interaction of cisplatin with 16 µM FL-Par-4 by ITC. Listed are the kinetic/thermodynamic parameters.

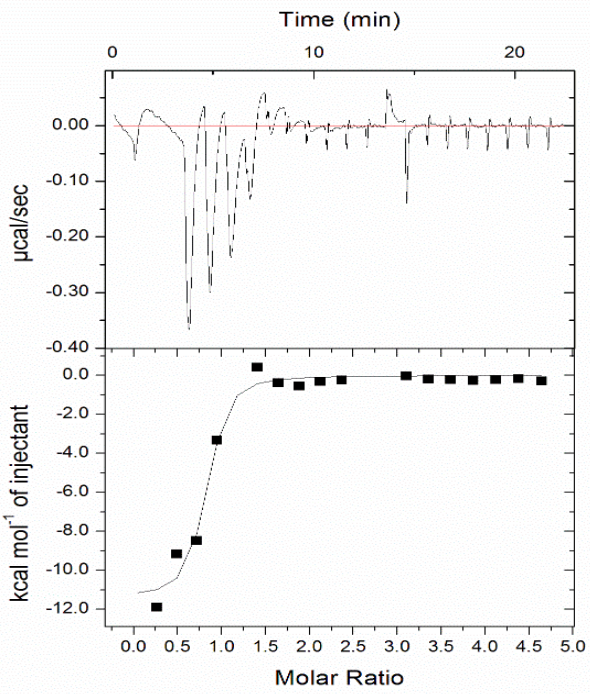

Fig. 30. Preliminary ITC analysis of the interaction of 16 µM FL-Par-4 with cisplatin. (a) Thermogram and (b) binding isotherm for the titration of cisPt with FL-Par-4.

Evidence of dimer and trimer formation by FL-Par-4 with increased ionic strength

Oligomerization is important for many biologically active proteins [146, 158, 163, 164], and Par-4 is known to self-associate [38, 39]. Therefore, SEC-MALS experiments were performed to study the oligomeric association of 16 µM FL-Par-4 (not treated with cisPt or transPt) in high ionic strength of 300 mM NaCl at pH 7 (Figure 31). The peak area between 11-13 mL was analyzed by MALS to obtain values for molar mass (MM) for two separate experiments. Figure 31a shows a plot of refractive index and light scattering versus elution volume for the two experiments (labeled as sample 1 and sample 2). Sample 1 scattered more light but had lower RI measurements. Sample 2 had substantially larger RI measurements, but decreased LS.

Figures 31b,c presents a simultaneous plot of RI (blue curve) and molar mass (MM; dotted line) vs. elution time (11-13 mL) from the SEC column for sample 1 (Figure 31b) and sample 2

(Figure 31c). The variation in Figure 31b suggests a somewhat heterogeneous sample, with a minimum and dominant MM near 104 kDa in the center of the peak, which is consistent with trimer formation (monomeric FL-Par-4 is 36.5 kDa). Other parts of the peak produce MM values as high as 350 kDa.

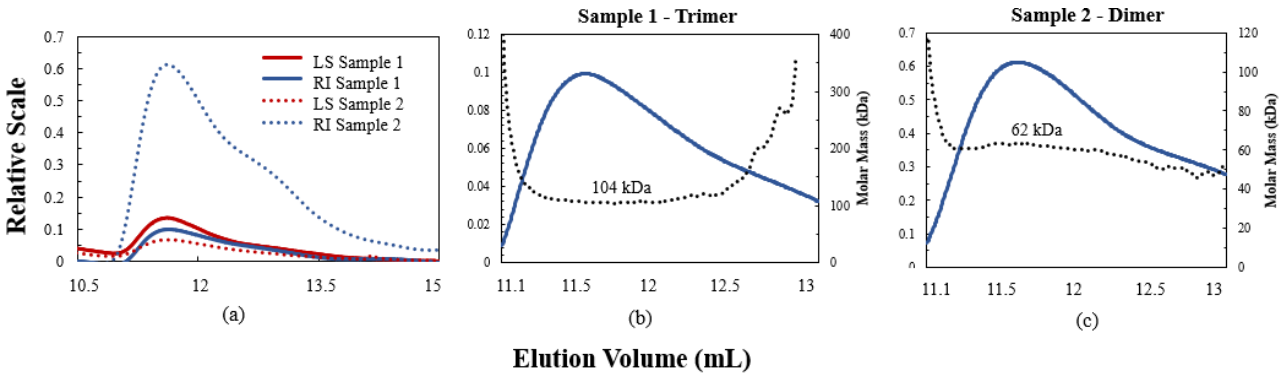

Fig. 31. Trimer and dimer formation by FL-Par-4 with increased ionic strength. SEC-MALS analysis of 16 µM FL-Par-4 in 300 mM NaCl, 10 mM Tris, pH 7 buffer from two separate experiments labeled as sample 1 and sample 2. (a) Refractive index (blue) and light scattering (red) for each experiment, vs column retention time. Solid is sample 1 and dotted is sample 2. Panels (b) and (c) show plots of molar mass (dotted) and refractive index (solid blue) for (b) sample 1, indicating a trimer and (c) sample 2, indicating a dimer.

In Figure 31c, the MM at the center of the peak is 62 kDa, consistent with dimer formation. The largest MM value was detected as the peak started to elute, with a size near 120 kDa (trimer), suggesting possible trimer-dimer interconversion. However, the dominant conformation appears to be a trimer or dimer under these conditions. Further experiments would be required to better understand what factors may tip the balance in favor of trimer or in favor of dimer.

DISCUSSION

Interaction of Par-4 and metallodrugs: potential physiological significance

The use of metallodrugs in platinum-based cancer therapy is limited due to metabolic deactivation which occurs when the drug interacts with sulfur-containing biomolecules such as proteins [69, 70]. This binding interaction can influence both the protein structure and function along with the activity of the drug [74, 76, 81, 165-167]. Additionally, these interactions can contribute to some of the toxic side effects that are associated with platinum-based cancer therapy [168, 169].

Previous studies have demonstrated a synergistic anti-cancer effect between Par-4 and cisPt [71-73]; however, direct binding had not been studied. In this study, we investigated the hypothesis that cisPt and transPt directly bind the Par-4 tumor suppressor, specifically the full-length protein and the caspase-cleaved fragment. Results showed that cisPt and transPt do in fact directly bind both cl-Par-4 and FL-Par-4 and this is the first evidence of direction interaction between Pt cancer drugs and the Par-4 tumor suppressor.

Both cl-Par-4 and FL-Par-4 are important in cancer cell apoptosis [57, 58]. Prior studies have found that the cisplatin-albumin complexes are toxic to carcinoma cells [170, 171], infusion of cisPt-HSA complexes increased patient survival times [170, 172], and that albumin binding could result in decreased negative side effects of cisPt treatment such as nephrotoxicity [172, 173]. While it is unclear the effect cisPt and transPt binding has on Par-4 apoptotic activity, it is plausible the complex could have antitumor activity comparable to HSA. Further analysis is needed to determine the effect of cisPt and transPt binding on Par-4 structure and function, and ultimately how this relates to cancer cell apoptosis and resistance processes.

Biophysical analysis of Pt-Par-4 interactions

The change in negative dichroism intensity in the disulfide range of 250-260 nm (Figure 20c) for cisPt-treated cl-Par-4 in 150 mM NaCl is likely due to the formation of Pt-S bonds. The platinum center of one cisPt molecule could be interacting with sulfur groups from one or two residues, inducing changes in dichroism in the disulfide bond region. Disulfide bonds absorb in the near UV region and can produce negative or positive dichroism in the range of 250 to 260 nm depending on the dihedral angle of the bond [174]. Additional experiments have shown increased and decreased intensity of negative dichroism in the disulfide region (Figure 22). The global shift in dichroism intensity is likely related to S-Pt coordination mentioned above. Changes in the intensity of negative dichroism upon cisPt treatment have been observed for other proteins such as alpha-2-macroglobulin [166] and atox 1 [175]. There was no substantial change in UV-visible absorbance spectra or hydrodynamic size upon cisPt treatment. CisPt treated cl-Par-4 in 1 M NaCl did not vary substantially from the untreated sample (Figure 21). This could be related to the protein already being in a stable conformation and high [Cl^-] can decrease the reactivity of cisPt.

Circular dichroism experiments of FL-Par-4 treated with cisPt and transPt showed no substantial change in dichroism and produced spectra characteristic of a predominantly alpha helical conformation (Figure 26a). CisPt binding does not always induce a change in protein secondary structure. For example, Far UV-CD of platinated RNase A showed that even with cisPt treatment, the protein remained correctly folded and was moderately thermostable [176]. Additionally, DLS experiments showed only minor decrease in Rs upon cisPt and transPt treatment. Pt-treated FL-Par-4 was consistent with a large oligomeric species (Figure 26c). However, in one experiment, the intensity of negative dichroism increased upon cisPt treatment (Figure 27). The CD spectra of the untreated control (Figure 27a) showed less intense negative

dichroism compared to Figure 26a, suggesting a change in initial protein conformation which likely influenced cisPt binding.

As an IDP, it is likely that intrinsic disorder and conformational flexibility affect the accessibility of S-containing residues for Pt-binding. Therefore, this does not exclude the possibility of other results obtained from Pt treatment of Par-4 and the effect of cisPt or transPt treatment on Par-4 is likely dependent on initial protein conformation.

Gel electrophoresis and chromatographic studies

Inter-molecular cl-Par-4 and FL-Par-4 cross-links were detected by SDS-PAGE when treated with increased molar ratios of cisPt or transPt (Figures 23, 28). Some Coomassie staining near the wells suggests that cross-linking by transPt produces oligomers too large to fully enter the gel. Platinated cl-Par-4 oligomers were not resistant to thermal denaturation and cl-Par-4 treated with transPt seemed more susceptible to heat denaturation than when treated with cisPt (Figure 24). CisPt-induced protein cross-links have been detected via polyacrylamide gel electrophoresis for other proteins such as holo-Atox1, the BRCA1 ring domain, and RNase A [167, 176, 177]. For example, incubation of cisPt with the copper chaperone Atox1 produced a faint dimeric band on SDS-PAGE in addition to the monomeric band [177]. Additional studies with holo-Atox1 found increased dimers and trimers on SDS-PAGE upon incubation with cisPt [76]. Oligomeric Atox1 species were detected after incubation with transPt and Pt-induced oligomerization was time dependent [76]. In this study, oligomeric bands were detected after one hour of incubation, suggesting the reaction occurs quickly.

Since cl-Par-4 and FL-Par-4 cross-links were detected via SDS-PAGE, the oligomers were further characterized by chromatographic studies. Chromatographic profiles obtained for cl-Par-4

treated with cisPt and transPt show increased absorbance at 280 nm upon treatment with 10 molar equivalents cisPt and both equivalents tested of transPt (Figure 25). The retention time did not change and remained near 21.5 mL, suggesting the platinated species is a large cl-Par-4 oligomer and similar cisPt and transPt binding sites. Interestingly, cisPt and transPt have been shown to have different binding sites in other proteins [79, 84]. Based on these results, cisPt and transPt treatment do not prevent the formation of large cl-Par-4 oligomers.

One platinated FL-Par-4 species was detected upon treatment with varying molar ratios of cisPt. Platinated FL-Par-4 had a slightly increased retention time and increased A280 values compared to the untreated control (Figure 29a,b). Interestingly, FL-Par-4 treatment with cisPt that had been in aqueous solution longer produced greater A280 values (Figure 29c). Substitution of the chloro ligands by the aqua ligand is a two-step process (Figure S3), yielding either monoaquo (+1) or diaquo (+2) cisPt. It is possible that Figures 29a,b represent the interaction of monoaquo (+1) and diaquo (+2) cisPt with Par-4, respectively, although further studies would be needed to confirm this. Gel filtration of FL-Par-4 treated with transPt showed two platinated adducts, evident by increased A280 values (Figure 29d).

Sulfur-platinum coordination can be detected by monitoring changes in absorbance at 280 nm because the charge transfer between sulfur and platinum absorbs at 280 nm. Coordination of the platinum center to other amino acid side chains is not detected at 280 nm. The interaction of cisPt with cox17 increased the A280 value of the eluting peak compared to the untreated protein [165]. Gel filtration of cisPt-treated RNase A showed increased A280 for specific peaks when incubated with greater molar equivalents of cisPt [176]. A methionine residue was found to be the primary cisPt binding site in RNase A [176].

Protein metalation is a complex process that is dependent on many factors including the protein, the nature of the metal in the compound, and the environmental conditions. Figure 25 shows increased A280 values for cl-Par-4 upon cisPt or transPt treatment; however, Figure 20a shows no variation in A280 upon cisPt treatment. This could be related to variation in ionic strength of the buffer or protein concentration. The UV-vis experiment in Figure 20a was performed with buffer containing 150 mM NaCl, while gel filtration experiments were performed with buffer containing 30 mM NaCl. While the ratios of cl-Par-4 to cisPt or transPt remained constant, cl-Par-4 was ten times less concentrated in the UV-vis experiment in Figure 20a. Previous experiments have shown that the conformation of cl-Par-4 has some dependence on protein concentration and therefore, it is likely that cisPt-binding is dependent on cl-Par-4 conformation and the accessibility of S-containing residues. Although there was no change in A280 in Figure 20a, the CD spectra in Figure 20c does show a change in dichroism intensity, possibly correlated to Pt-S coordination. Further UV-vis experiments could be utilized to study S-Pt coordination in cl-Par-4 and further gel filtration experiments could be used to assess how the conformation of cl-Par-4 is influenced by protein concentration.

Since cisPt and transPt have a high affinity for sulfur donors and gel filtration results are consistent with S-Pt coordination, it is plausible the Pt-crosslinking site is a sulfur-containing residue [74]. FL-Par-4 has six sulfur-containing residues while cl-Par-4 retains three of those residues (Figure 19). Shown in Figure S1 (Appendix) is a model of the Par-4 C-terminus cross-linked by cisPt at methionine 293, one of the potential cisPt binding sites in Par-4. Shown in Figure S2 are changes in backbone dihedral angles observed in the theoretical Par-4 model after introduction of the M293-Pt-M293 crosslink.

However, the exact cisPt and transPt binding site(s) in FL-Par-4 and cl-Par-4 are yet to be determined; therefore, further structural studies are necessary to identify the specific binding site(s) and characterize any subsequent changes in Par-4 structure. For example, mass spectrometry could be utilized to further characterize the Pt-S unit in cl-Par-4 and FL-Par-4. Mass spectrometry has been used to identify and characterize the cisplatin binding sites in proteins such as hen egg white lysozyme, ubiquitin, myoglobin, among others [77-79, 178-180]. Additionally, crystallographic studies could also be used to further study and characterize Pt-S coordination in cl-Par-4 and FL-Par-4 [180].

Preliminary ITC Analysis

ITC experiments are useful in providing thermodynamic information about protein-ligand interactions [181]. The titration profile of cisPt binding Par-4 (Figure 30) shows the reaction is exothermic in nature with one interaction jump. Values obtained for both entropy and enthalpy change were negative (Table 3). Other studies have found cisPt-protein interactions to be exothermic, such as the case with alpha-2-macroglobulin [166]. Similar results were observed for the reaction of BSA titrated with naproxen: exothermic in nature, one interaction jump, and negative enthalpy and entropy change [182].

FL-Par-4 forms both dimers and trimers with increasing ionic strength

SEC-MALS experiments showed variation in the oligomeric association of FL-Par-4 (Figure 31). Sample 1 had a molar mass consistent with trimer, while sample 2 had a molar mass consistent with dimer formation. Other studies have reported octamer formation in Par-4 isolated from HeLa cells [183], homodimerization of the racine Par-4 coiled coil [42], tetramer formation in cl-Par-4

[162], and conformational equilibrium in the racine Par-4 coiled coil domain between monomer and dimer [38].

Oligomeric proteins can undergo dissociation as they traverse the column, as seen with the SecA protein which exists in monomer-dimer equilibria [184]. Results from this study show that FL-Par-4 exists in dynamic equilibria between oligomeric associations and that FL-Par-4 can form both dimers and trimers. RNase A has been shown to self-associate through 3D-domain swapping forming many diverse oligomers: dimers, trimers, tetramers, pentamers, and hexamers [185-187].

The formation of functional protein oligomers is a highly regulated process; however, protein misfolding and the formation of protein aggregates often contribute to disease [6, 188]. Oligomerization is considered an inevitable step in protein aggregation [188, 189]. Association-prone monomers can associate to form early oligomers, late oligomers, and ultimately amorphous aggregates, globular oligomers, or amyloid fibrils [188, 189]. However, RNase A aggregates are cytotoxic to non-solid tumors [190]. This raises the possibility that oligomerization of FL-Par-4 and cl-Par-4 could have both functional and pathogenic roles.

CHAPTER V

CONCLUSIONS AND FUTURE WORK

The work in this dissertation has characterized the intrinsically disordered Par-4 tumor suppressor using biophysical and analytical techniques. There is an abundance of IDPs in pathological conditions such as cancer [6]. Therefore, characterizing the induced folding process of IDPs as well as the interactions of metallodrugs with tumor suppressor proteins is important to further our understanding of the structure-function relationship of IDPs and additionally cancer resistance processes.

Results showed that the caspase-cleaved fragment of Par-4 is highly susceptible to environment, forming a predominantly helical conformation in conditions of either acidic pH or high ionic strength at neutral pH. Cl-Par-4 is highly susceptible to aggregation and forms large oligomers in physiological conditions of low ionic strength and neutral pH. Studies provided the first evidence of tetramer formation in cl-Par-4, which could be the active conformation capable of killing cancer cells. Additional studies showed that the platinum chemotherapeutic cisplatin and its trans isomer transplatin are capable of binding both full length Par-4 and cl-Par-4. Pt binding induces the formation of platinated Par-4 oligomers and cross-linking likely occurs through coordination to sulfur ligands.

Further structural analysis such as nuclear magnetic resonance (NMR) spectroscopy, cryo-EM, or mass spectrometry are needed to identify the cisPt and transPt binding site(s) in FL-Par-4 and cl-Par-4. Additionally, the effect of cisPt and transPt-binding on the apoptotic function of FL-Par-4 and cl-Par-4 is yet to be determined. There could be applications of the binding interaction in cancer therapy if the Par-4-Pt complex is shown to be cytotoxic to cancer cells.

Additional ongoing Par-4 studies in the Pascal Laboratory include investigating how scattering of large oligomers could influence biophysical analysis along with the identification of new Par-4-protein interactions using the LexA system. In conclusion, the Par-4 tumor suppressor is crucial to cancer cell apoptosis and further structural knowledge of this protein along with binding interactions, both with other cellular proteins and anti-cancer drugs, will provide a better understanding of the structure-function relationship in this intrinsically disordered tumor suppressor.

REFERENCES

1. Dunker, A. K., Lawson, J. D., Brown, C. J., Williams, R. M., Romero, P., Oh, J. S., Oldfield, C. J., Campen, A. M., Ratliff, C. M., Hipps, K. W., Ausio, J., Nissen, M. S., Reeves, R., Kang, C., Kissinger, C. R., Bailey, R. W., Griswold, M. D., Chiu, W., Garner, E. C. & Obradovic, Z. (2001) Intrinsically disordered protein, *Journal of Molecular Graphics and Modelling.* **19**, 26-59.
2. Tompa, P. (2002) Intrinsically unstructured proteins, *Trends in Biochemical Sciences.* **27**, 527-533.
3. Wright, P. E. & Dyson, H. J. (1999) Intrinsically unstructured proteins: re-assessing the protein structure-function paradigm, *Journal of Molecular Biology.* **293**, 321-331.
4. Uversky, V. N. (2013) Unusual biophysics of intrinsically disordered proteins, *Biochimica et Biophysica Acta (BBA) - Proteins and Proteomics.* **1834**, 932-951.
5. Uversky, V. N., Gillespie, J. R. & Fink, A. L. (2000) Why are "natively unfolded" proteins unstructured under physiologic conditions?, *Proteins: Structure, Function, and Bioinformatics.* **41**, 415-427.
6. Uversky, V. N., Oldfield, C. J. & Dunker, A. K. (2008) Intrinsically Disordered Proteins in Human Diseases: Introducing the D2 Concept, *Annual Review of Biophysics.* **37**, 215-246.
7. Xue, B., Dunker, A. K. & Uversky, V. N. (2012) Orderly order in protein intrinsic disorder distribution: disorder in 3500 proteomes from viruses and the three domains of life, *Journal of Biomolecular Structure and Dynamics.* **30**, 137-149.
8. Ward, J. J., Sodhi, J. S., McGuffin, L. J., Buxton, B. F. & Jones, D. T. (2004) Prediction and Functional Analysis of Native Disorder in Proteins from the Three Kingdoms of Life, *Journal of Molecular Biology.* **337**, 635-645.
9. Dunker, A. K., Garner, E., Guilliot, S., Romero, P., Albrecht, K., Hart, J., Obradovic, Z., Kissinger, C. & Villafranca, J. E. (1998) Protein disorder and the evolution of molecular recognition: theory, predictions and observations, *Pacific Symposium on Biocomputing Pacific Symposium on Biocomputing*, 473-84.
10. Uversky, V. N. & Dunker, A. K. (2010) Understanding protein non-folding, *Biochimica et biophysica acta.* **1804**, 1231-64.
11. Keith Dunker, A., Brown, C. J. & Obradovic, Z. (2002) Identification and functions of usefully disordered proteins in *Advances in Protein Chemistry* pp. 25-49, Academic Press.
12. Iakoucheva, L. M., Brown, C. J., Lawson, J. D., Obradović, Z. & Dunker, A. K. (2002) Intrinsic Disorder in Cell-signaling and Cancer-associated Proteins, *Journal of Molecular Biology.* **323**, 573-584.
13. Wright, P. E. & Dyson, H. J. (2015) Intrinsically disordered proteins in cellular signalling and regulation, *Nature reviews Molecular cell biology.* **16**, 18-29.
14. Uversky, V. N. (2002) What does it mean to be natively unfolded?, *European Journal of Biochemistry.* **269**, 2-12.
15. Dyson, H. J. & Wright, P. E. (2002) Coupling of folding and binding for unstructured proteins, *Current Opinion in Structural Biology.* **12**, 54-60.
16. Fuxreiter, M., Simon, I., Friedrich, P. & Tompa, P. (2004) Preformed Structural Elements Feature in Partner Recognition by Intrinsically Unstructured Proteins, *Journal of Molecular Biology.* **338**, 1015-1026.
17. Kriwacki, R. W., Hengst, L., Tennant, L., Reed, S. I. & Wright, P. E. (1996) Structural studies of p21Waf1/Cip1/Sdi1 in the free and Cdk2-bound state: conformational disorder mediates binding diversity, *Proceedings of the National Academy of Sciences.* **93**, 11504-11509.

18. Fink, A. L. (1995) Compact Intermediate States in Protein Folding, *Annual Review of Biophysics and Biomolecular Structure.* **24**, 495-522.
19. Uversky, V. N. (2009) Intrinsically disordered proteins and their environment: effects of strong denaturants, temperature, pH, counter ions, membranes, binding partners, osmolytes, and macromolecular crowding, *The protein journal.* **28**, 305-25.
20. Tantos, A., Han, K.-H. & Tompa, P. (2012) Intrinsic disorder in cell signaling and gene transcription, *Molecular and Cellular Endocrinology.* **348**, 457-465.
21. Dunker, A. K. & Obradovic, Z. (2001) The protein trinity--linking function and disorder, *Nature biotechnology.* **19**, 805-6.
22. Wells, M., Tidow, H., Rutherford, T. J., Markwick, P., Jensen, M. R., Mylonas, E., Svergun, D. I., Blackledge, M. & Fersht, A. R. (2008) Structure of tumor suppressor p53 and its intrinsically disordered N-terminal transactivation domain, *Proc Natl Acad Sci U S A.* **105**, 5762-7.
23. Mark, W. Y., Liao, J. C., Lu, Y., Ayed, A., Laister, R., Szymczyna, B., Chakrabartty, A. & Arrowsmith, C. H. (2005) Characterization of segments from the central region of BRCA1: an intrinsically disordered scaffold for multiple protein-protein and protein-DNA interactions?, *J Mol Biol.* **345**, 275-87.
24. Ng, K. P., Potikyan, G., Savene, R. O., Denny, C. T., Uversky, V. N. & Lee, K. A. (2007) Multiple aromatic side chains within a disordered structure are critical for transcription and transforming activity of EWS family oncoproteins, *Proc Natl Acad Sci U S A.* **104**, 479-84.
25. Uversky, V. N. (2015) Intrinsically disordered proteins and their (disordered) proteomes in neurodegenerative disorders, *Front Aging Neurosci.* **7**, 18-18.
26. Wells, M., Tidow, H., Rutherford, T. J., Markwick, P., Jensen, M. R., Mylonas, E., Svergun, D. I., Blackledge, M. & Fersht, A. R. (2008) Structure of tumor suppressor p53 and its intrinsically disordered N-terminal transactivation domain, *Proceedings of the National Academy of Sciences of the United States of America.* **105**, 5762-5767.
27. Mark, W.-Y., Liao, J. C. C., Lu, Y., Ayed, A., Laister, R., Szymczyna, B., Chakrabartty, A. & Arrowsmith, C. H. (2005) Characterization of Segments from the Central Region of BRCA1: An Intrinsically Disordered Scaffold for Multiple Protein–Protein and Protein–DNA Interactions?, *Journal of Molecular Biology.* **345**, 275-287.
28. Malaney, P., Pathak, R. R., Xue, B., Uversky, V. N. & Davé, V. (2013) Intrinsic disorder in PTEN and its interactome confers structural plasticity and functional versatility, *Scientific reports.* **3**, 2035-2035.
29. (2003) A Protein-Chameleon: Conformational Plasticity of α-Synuclein, a Disordered Protein Involved in Neurodegenerative Disorders AU - Uversky, Vladimir N, *Journal of Biomolecular Structure and Dynamics.* **21**, 211-234.
30. Sells, S. F., Wood Jr., D. P., Joshi-Barve, S. S., Muthukumar, S., Jacob, R. J., Crist, S. A., Humphreys, S. & Rangnekar, V. M. (1994) Commonality of the Gene Programs Induced by Effectors of Apoptosis in Androgen-dependent and -independent Prostate Cells, *Cell Growth and Differentiation.* **5**, 457-466.
31. Sells, S. F., Han, S. S., Muthukkumar, S., Maddiwar, N., Johnstone, R., Boghaert, E., Gillis, D., Liu, G., Nair, P., Monnig, S., Collini, P., Mattson, M. P., Sukhatme, V. P., Zimmer, S. G., Wood, D. P., Jr., McRoberts, J. W., Shi, Y. & Rangnekar, V. M. (1997) Expression and function of the leucine zipper protein Par-4 in apoptosis, *Molecular and cellular biology.* **17**, 3823-3832.
32. Boghaert, E., Sells, S., Walid, A., Malone, P., Williams, N., Weinstein, M., Strange, R. & Rangnekar, V. (1997) Immunohistochemical analysis of the proapoptotic protein Par-4 in normal rat tissues, *Cell Growth Differ.* **8**, 881-890.

33. Burikhanov, R., Zhao, Y., Goswami, A., Qiu, S., Schwarze, S. R. & Rangnekar, V. M. (2009) The Tumor Suppressor Par-4 Activates an Extrinsic Pathway for Apoptosis, *Cell.* **138**, 377-388.
34. El-Guendy, N. & Rangnekar, V. M. (2003) Apoptosis by Par-4 in cancer and neurodegenerative diseases, *Experimental Cell Research.* **283**, 51-66.
35. El-Guendy, N., Zhao, Y., Gurumurthy, S., Burikhanov, R. & Rangnekar, V. M. (2003) Identification of a Unique Core Domain of Par-4 Sufficient for Selective Apoptosis Induction in Cancer Cells, *Molecular and Cellular Biology.* **23**, 5516-5525.
36. Goswami, A., Burikhanov, R., de Thonel, A., Fujita, N., Goswami, M., Zhao, Y., Eriksson, J. E., Tsuruo, T. & Rangnekar, V. M. (2005) Binding and Phosphorylation of Par-4 by Akt Is Essential for Cancer Cell Survival, *Molecular Cell.* **20**, 33-44.
37. Zhao, Y., Burikhanov, R., Qiu, S., Lele, S. M., Jennings, C. D., Bondada, S., Spear, B. & Rangnekar, V. M. (2007) Cancer Resistance in Transgenic Mice Expressing the SAC Module of Par-4, *Cancer Research.* **67**, 9276-9285.
38. Schwalbe, M., Dutta, K., Libich, D. S., Venugopal, H., Claridge, J. K., Gell, D. A., Mackay, J. P., Edwards, P. J. B. & Pascal, S. M. (2010) Two-state conformational equilibrium in the Par-4 leucine zipper domain, *Proteins: Structure, Function, and Bioinformatics.* **78**, 2433-2449.
39. Libich, D. S., Schwalbe, M., Kate, S., Venugopal, H., Claridge, J. K., Edwards, P. J. B., Dutta, K. & Pascal, S. M. (2009) Intrinsic disorder and coiled-coil formation in prostate apoptosis response factor 4, *The FEBS Journal.* **276**, 3710-3728.
40. Dutta, K., Alexandrov, A., Huang, H. & Pascal, S. M. (2001) pH-induced folding of an apoptotic coiled coil, *Protein Science.* **10**, 2531-2540.
41. Dutta, K., Engler, F. A., Cotton, L., Alexandrov, A., Bedi, G. S., Colquhoun, J. & Pascal, S. M. (2003) Stabilization of a pH-sensitive apoptosis-linked coiled coil through single point mutations, *Protein Science.* **12**, 257-265.
42. Tiruttani Subhramanyam, U. K., Kubicek, J., Eidhoff, U. B. & Labahn, J. (2017) Structural basis for the regulatory interactions of proapoptotic Par-4, *Cell Death And Differentiation.* **24**, 1540.
43. Díaz-Meco, M. T., Municio, M. M., Frutos, S., Sanchez, P., Lozano, J., Sanz, L. & Moscat, J. (1996) The Product of par-4, a Gene Induced during Apoptosis, Interacts Selectively with the Atypical Isoforms of Protein Kinase C, *Cell.* **86**, 777-786.
44. Cheema, S. K., Mishra, S. K., Rangnekar, V. M., Tari, A. M., Kumar, R. & Lopez-Berestein, G. (2003) Par-4 Transcriptionally Regulates Bcl-2 through a WT1-binding Site on the bcl-2 Promoter, *Journal of Biological Chemistry.* **278**, 19995-20005.
45. Johnstone, R. W., See, R. H., Sells, S. F., Wang, J., Muthukkumar, S., Englert, C., Haber, D. A., Licht, J. D., Sugrue, S. P., Roberts, T., Rangnekar, V. M. & Shi, Y. (1996) A novel repressor, par-4, modulates transcription and growth suppression functions of the Wilms' tumor suppressor WT1, *Molecular and Cellular Biology.* **16**, 6945-6956.
46. Page, G., Kögel, D., Rangnekar, V. & Scheidtmann, K. H. (1999) Interaction partners of Dlk/ZIP kinase: co-expression of Dlk/ZIP kinase and Par-4 results in cytoplasmic retention and apoptosis, *Oncogene.* **18**, 7265.
47. Roussigne, M., Cayrol, C., Clouaire, T., Amalric, F. & Girard, J.-P. (2003) THAP1 is a nuclear proapoptotic factor that links prostate-apoptosis-response-4 (Par-4) to PML nuclear bodies, *Oncogene.* **22**, 2432.
48. Ortega, G., Diercks, T. & Millet, O. (2015) Halophilic Protein Adaptation Results from Synergistic Residue-Ion Interactions in the Folded and Unfolded States, *Chemistry & Biology.* **22**, 1597-1607.

49. Dominy, B. N., Perl, D., Schmid, F. X. & Brooks, C. L. (2002) The Effects of Ionic Strength on Protein Stability: The Cold Shock Protein Family, *Journal of Molecular Biology.* **319**, 541-554.
50. Beauchamp, D. L. & Khajehpour, M. (2012) Studying salt effects on protein stability using ribonuclease t1 as a model system, *Biophysical Chemistry.* **161**, 29-38.
51. Clark, A. M., Ponniah, K., Warden, M. S., Raitt, E. M., Yawn, A. C. & Pascal, S. M. (2018) pH-Induced Folding of the Caspase-Cleaved Par-4 Tumor Suppressor: Evidence of Structure Outside of the Coiled Coil Domain, *Biomolecules.* **8**, 162.
52. Grigoryan, G. & Keating, A. E. (2008) Structural specificity in coiled-coil interactions, *Curr Opin Struct Biol.* **18**, 477-483.
53. Lee, A. S. (2007) GRP78 Induction in Cancer: Therapeutic and Prognostic Implications, *Cancer Research.* **67**, 3496-3499.
54. Shrestha-Bhattarai, T. & Rangnekar, V. M. (2010) Cancer-selective apoptotic effects of extracellular and intracellular Par-4, *Oncogene.* **29**, 3873-3880.
55. Chakraborty, M., Qiu, S. G., Vasudevan, K. M. & Rangnekar, V. M. (2001) Par-4 Drives Trafficking and Activation of Fas and FasL to Induce Prostate Cancer Cell Apoptosis and Tumor Regression, *Cancer Research.* **61**, 7255-7263.
56. Gurumurthy, S., Goswami, A., Vasudevan, K. M. & Rangnekar, V. M. (2005) Phosphorylation of Par-4 by Protein Kinase A Is Critical for Apoptosis, *Molecular and Cellular Biology.* **25**, 1146-1161.
57. Chaudhry, P., Singh, M., Parent, S. & Asselin, E. (2012) Prostate Apoptosis Response 4 (Par-4), a Novel Substrate of Caspase-3 during Apoptosis Activation, *Molecular and Cellular Biology.* **32**, 826-839.
58. Thayyullathil, F., Pallichankandy, S., Rahman, A., Kizhakkayil, J., Chathoth, S., Patel, M. & Galadari, S. (2013) Caspase-3 mediated release of SAC domain containing fragment from Par-4 is necessary for the sphingosine-induced apoptosis in Jurkat cells, *Journal of molecular signaling.* **8**, 2-2.
59. Treude, F., Kappes, F., Fahrenkamp, D., Müller-Newen, G., Dajas-Bailador, F., Krämer, O. H., Lüscher, B. & Hartkamp, J. (2014) Caspase-8-mediated PAR-4 cleavage is required for TNFα-induced apoptosis, *Oncotarget.* **5**, 2988-2998.
60. Johnstone, R. W., Tommerup, N., Hansen, C., Vissing, H. & Shi, Y. (1998) Mapping of the Human PAWR (par-4) Gene to Chromosome 12q21, *Genomics.* **53**, 241-243.
61. Mabe, N. W., Fox, D. B., Lupo, R., Decker, A. E., Phelps, S. N., Thompson, J. W. & Alvarez, J. V. (2018) Epigenetic silencing of tumor suppressor Par-4 promotes chemoresistance in recurrent breast cancer, *The Journal of Clinical Investigation.* **128**, 4413-4428.
62. Kögel, D., Reimertz, C., Mech, P., Poppe, M., Frühwald, M. C., Engemann, H., Scheidtmann, K. H. & Prehn, J. H. M. (2001) Dlk/ZIP kinase-induced apoptosis in human medulloblastoma cells: requirement of the mitochondrial apoptosis pathway, *British Journal Of Cancer.* **85**, 1801.
63. Cook, J., Krishnan, S., Ananth, S., Sells, S. F., Shi, Y., Walther, M. M., Linehan, W. M., Sukhatme, V. P., Weinstein, M. H. & Rangnekar, V. M. (1999) Decreased expression of the pro-apoptotic protein Par-4 in renal cell carcinoma, *Oncogene.* **18**, 1205.
64. Moreno-Bueno, G., Fernandez-Marcos, P. J., Collado, M., Tendero, M. J., Rodriguez-Pinilla, S. M., Garcia-Cao, I., Hardisson, D., Diaz-Meco, M. T., Moscat, J., Serrano, M. & Palacios, J. (2007) Inactivation of the Candidate Tumor Suppressor Par-4 in Endometrial Cancer, *Cancer Research.* **67**, 1927-1934.
65. Zapata-Benavides, P., Méndez-Vázquez, J. L., González-Rocha, T. R., Zamora-Avila, D. E., Franco-Molina, M. A., Garza-Garza, R. & Rodriguez-Padilla, C. (2009) Expression of Prostate

Apoptosis Response (Par-4) Is Associated with Progesterone Receptor in Breast Cancer, *Archives of Medical Research.* **40**, 595-599.
66. RANGANATHAN, P. & RANGNEKAR, V. M. (2005) Regulation of Cancer Cell Survival by Par-4, *Ann N Y Acad Sci.* **1059**, 76-85.
67. Zhao, Y., Burikhanov, R., Brandon, J., Qiu, S., Shelton, B. J., Spear, B., Bondada, S., Bryson, S. & Rangnekar, V. M. (2011) Systemic Par-4 inhibits non-autochthonous tumor growth, *Cancer Biology & Therapy.* **12**, 152-157.
68. Kim, K., Araujo, P., Hebbar, N., Zhou, Z., Zheng, X., Zheng, F., Rangnekar, V. M. & Zhan, C.-G. (2019) Development of a novel prostate apoptosis response-4 (Par-4) protein entity with an extended duration of action for therapeutic treatment of cancer, *Protein Engineering, Design and Selection.* **32**, 159-166.
69. Barabas, K., Milner, R., Lurie, D. & Adin, C. (2008) Cisplatin: a review of toxicities and therapeutic applications, *Veterinary and Comparative Oncology.* **6**, 1-18.
70. Dasari, S. & Bernard Tchounwou, P. (2014) Cisplatin in cancer therapy: Molecular mechanisms of action, *European Journal of Pharmacology.* **740**, 364-378.
71. Tan, J., You, Y., Xu, T., Yu, P., Wu, D., Deng, H., Zhang, Y. & Bie, P. (2014) Par-4 downregulation confers cisplatin resistance in pancreatic cancer cells via PI3K/Akt pathway-dependent EMT, *Toxicology Letters.* **224**, 7-15.
72. Wang, J., Li, Y., Ma, F., Zhou, H., Ding, R., Lu, B., Zou, L., Li, J. & Lu, R. (2017) Inhibitory effect of Par-4 combined with cisplatin on human Wilms' tumor cells, *Tumor Biology.* **39**, 1010428317716689.
73. Brasseur, K., Fabi, F., Adam, P., Parent, S., Lessard, L. & Asselin, E. (2016) Post-translational regulation of the cleaved fragment of Par-4 in ovarian and endometrial cancer cells, *Oncotarget.* **7**, 36971-36987.
74. Messori, L. & Merlino, A. (2016) Cisplatin binding to proteins: A structural perspective, *Coordination Chemistry Reviews.* **315**, 67-89.
75. Ivanov, A. I., Christodoulou, J., Parkinson, J. A., Barnham, K. J., Tucker, A., Woodrow, J. & Sadler, P. J. (1998) Cisplatin Binding Sites on Human Albumin, *Journal of Biological Chemistry.* **273**, 14721-14730.
76. Palm, M. E., Weise, C. F., Lundin, C., Wingsle, G., Nygren, Y., Björn, E., Naredi, P., Wolf-Watz, M. & Wittung-Stafshede, P. (2011) Cisplatin binds human copper chaperone Atox1 and promotes unfolding in vitro, *Proceedings of the National Academy of Sciences of the United States of America.* **108**, 6951-6956.
77. Zhao, T. & King, F. L. (2011) Mass-spectrometric characterization of cisplatin binding sites on native and denatured ubiquitin, *JBIC Journal of Biological Inorganic Chemistry.* **16**, 633-639.
78. Casini, A., Mastrobuoni, G., Temperini, C., Gabbiani, C., Francese, S., Moneti, G., Supuran, C. T., Scozzafava, A. & Messori, L. (2007) ESI mass spectrometry and X-ray diffraction studies of adducts between anticancer platinum drugs and hen egg white lysozyme, *Chemical Communications*, 156-158.
79. Zhao, T. & King, F. L. (2010) A mass spectrometric comparison of the interactions of cisplatin and transplatin with myoglobin, *Journal of Inorganic Biochemistry.* **104**, 186-192.
80. Neault, J. F. & Tajmir-Riahi, H. A. (1998) Interaction of cisplatin with human serum albumin. Drug binding mode and protein secondary structure, *Biochimica et Biophysica Acta (BBA) - Protein Structure and Molecular Enzymology.* **1384**, 153-159.
81. Ferraro, G., Massai, L., Messori, L. & Merlino, A. (2015) Cisplatin binding to human serum albumin: a structural study, *Chemical Communications.* **51**, 9436-9439.

82. Giraud-Panis, M.-J. & Leng, M. (2000) Transplatin-modified oligonucleotides as modulators of gene expression, *Pharmacology & Therapeutics.* **85**, 175-181.
83. Boudvillain, M., Dalbiès, R., Aussourd, C. & Leng, M. (1995) Intrastrand cross-links are not formed in the reaction between transplatin and native DNA: relationm with the clinical inefficency of transplatin, *Nucleic Acids Research.* **23**, 2381-2388.
84. Peleg-Shulman, T., Najajreh, Y. & Gibson, D. (2002) Interactions of cisplatin and transplatin with proteins: Comparison of binding kinetics, binding sites and reactivity of the Pt-protein adducts of cisplatin and transplatin towards biological nucleophiles, *Journal of Inorganic Biochemistry.* **91**, 306-311.
85. Du, W., Han, W., Li, Z. & Wang, B. (2000) Urease conformational change induced by transplatin: A comparison on the interaction of urease with transplatin and cisplatin, *Thermochimica Acta.* **359**, 55-60.
86. Hebbar, N., Burikhanov, R., Shukla, N., Qiu, S., Zhao, Y., Elenitoba-Johnson, K. S. J. & Rangnekar, V. M. (2017) A Naturally Generated Decoy of the Prostate Apoptosis Response-4 Protein Overcomes Therapy Resistance in Tumors, *Cancer Research*.
87. Ano Bom, A. P. D., Freitas, M. S., Moreira, F. S., Ferraz, D., Sanches, D., Gomes, A. M. O., Valente, A. P., Cordeiro, Y. & Silva, J. L. (2010) The p53 Core Domain Is a Molten Globule at Low pH: FUNCTIONAL IMPLICATIONS OF A PARTIALLY UNFOLDED STRUCTURE, *Journal of Biological Chemistry.* **285**, 2857-2866.
88. Wang, G., Dinkins, M., He, Q., Zhu, G., Poirier, C., Campbell, A., Mayer-Proschel, M. & Bieberich, E. (2012) Astrocytes Secrete Exosomes Enriched with Proapoptotic Ceramide and Prostate Apoptosis Response 4 (PAR-4): POTENTIAL MECHANISM OF APOPTOSIS INDUCTION IN ALZHEIMER DISEASE (AD), *Journal of Biological Chemistry.* **287**, 21384-21395.
89. Kowal, J., Tkach, M. & Théry, C. (2014) Biogenesis and secretion of exosomes, *Current Opinion in Cell Biology.* **29**, 116-125.
90. Chen, Y. & Arriaga, E. A. (2006) Individual Acidic Organelle pH Measurements by Capillary Electrophoresis, *Analytical Chemistry.* **78**, 820-826.
91. Alexandrov, A., Dutta, K. & Pascal, S. M. (2001) MBP Fusion Protein with a Viral Protease Cleavage Site: One-Step Cleavage/Purification of Insoluble Proteins, *BioTechniques.* **30**, 1194-1198.
92. Linding, R., Jensen, L. J., Diella, F., Bork, P., Gibson, T. J. & Russell, R. B. (2003) Protein Disorder Prediction: Implications for Structural Proteomics, *Structure.* **11**, 1453-1459.
93. Garnier, J., Osguthorpe, D. J. & Robson, B. (1978) Analysis of the accuracy and implications of simple methods for predicting the secondary structure of globular proteins, *Journal of Molecular Biology.* **120**, 97-120.
94. Whitmore, L. & Wallace, B. A. (2004) DICHROWEB, an online server for protein secondary structure analyses from circular dichroism spectroscopic data, *Nucleic Acids Research.* **32**, W668-W673.
95. Ko, J., Park, H., Heo, L. & Seok, C. (2012) GalaxyWEB server for protein structure prediction and refinement, *Nucleic Acids Research.* **40**, W294-W297.
96. Uversky, V. N. (2002) Natively unfolded proteins: A point where biology waits for physics, *Protein Science.* **11**, 739-756.
97. Garnier, J., Gibrat, J.-F. & Robson, B. (1996) [32] GOR method for predicting protein secondary structure from amino acid sequence in *Methods in Enzymology* pp. 540-553, Academic Press.

98. Hu, C. C. & Ghabrial, S. A. (1995) The conserved, hydrophilic and arginine-rich N-terminal domain of cucumovirus coat proteins contributes to their anomalous electrophoretic mobilities in sodium dodecylsulfate-polyacrylamide gels, *Journal of Virological Methods.* **55**, 367-379.
99. Receveur-Bréchot, V., Bourhis, J.-M., Uversky, V. N., Canard, B. & Longhi, S. (2006) Assessing protein disorder and induced folding, *Proteins: Structure, Function, and Bioinformatics.* **62**, 24-45.
100. Tcherkasskaya, O. & Uversky, V. N. (2001) Denatured collapsed states in protein folding: Example of apomyoglobin, *Proteins: Structure, Function, and Bioinformatics.* **44**, 244-254.
101. Uversky, V. N. (1993) Use of fast protein size-exclusion liquid chromatography to study the unfolding of proteins which denature through the molten globule, *Biochemistry.* **32**, 13288-13298.
102. Burkhard, P., Stetefeld, J. & Strelkov, S. V. (2001) Coiled coils: a highly versatile protein folding motif, *Trends in Cell Biology.* **11**, 82-88.
103. Vinson, C., Myakishev, M., Acharya, A., Mir, A. A., Moll, J. R. & Bonovich, M. (2002) Classification of Human B-ZIP Proteins Based on Dimerization Properties, *Molecular and Cellular Biology.* **22**, 6321-6335.
104. Murre, C., McCaw, P. S. & Baltimore, D. (1989) A new DNA binding and dimerization motif in immunoglobulin enhancer binding, daughterless, MyoD, and myc proteins, *Cell.* **56**, 777-783.
105. Timm, D. E., Vissavajjhala, P., Ross, A. H. & Neet, K. E. (1992) Spectroscopic and chemical studies of the interaction between nerve growth factor (NGF) and the extracellular domain of the low affinity NGF receptor, *Protein Science.* **1**, 1023-1031.
106. Kim, T. D., Ryu, H. J., Cho, H. I., Yang, C.-H. & Kim, J. (2000) Thermal Behavior of Proteins: Heat-Resistant Proteins and Their Heat-Induced Secondary Structural Changes, *Biochemistry.* **39**, 14839-14846.
107. Roy, S., Bayly, C. I., Gareau, Y., Houtzager, V. M., Kargman, S., Keen, S. L. C., Rowland, K., Seiden, I. M., Thornberry, N. A. & Nicholson, D. W. (2001) Maintenance of caspase-3 proenzyme dormancy by an intrinsic "safety catch" regulatory tripeptide, *Proceedings of the National Academy of Sciences.* **98**, 6132-6137.
108. Park, H. J., Lyons, J. C., Ohtsubo, T. & Song, C. W. (1999) Acidic environment causes apoptosis by increasing caspase activity, *British journal of cancer.* **80**, 1892-1897.
109. Johansson, A. C., Steen, H., Öllinger, K. & Roberg, K. (2003) Cathepsin D mediates cytochrome c release and caspase activation in human fibroblast apoptosis induced by staurosporine, *Cell Death And Differentiation.* **10**, 1253.
110. Matsuyama, S., Llopis, J., Deveraux, Q. L., Tsien, R. Y. & Reed, J. C. (2000) Changes in intramitochondrial and cytosolic pH: early events that modulate caspase activation during apoptosis, *Nature Cell Biology.* **2**, 318.
111. Segal, M. S. & Beem, E. (2001) Effect of pH, ionic charge, and osmolality on cytochromec-mediated caspase-3 activity, *American Journal of Physiology-Cell Physiology.* **281**, C1196-C1204.
112. Freitas, N. & Cunha, C. (2009) Mechanisms and signals for the nuclear import of proteins, *Current genomics.* **10**, 550-557.
113. Silver, P. A. (1991) How proteins enter the nucleus, *Cell.* **64**, 489-497.
114. Donninger, H., Hesson, L., Vos, M., Beebe, K., Gordon, L., Sidransky, D., Liu, J. W., Schlegel, T., Payne, S., Hartmann, A., Latif, F. & Clark, G. J. (2010) The Ras Effector RASSF2 Controls the PAR-4 Tumor Suppressor, *Molecular and Cellular Biology.* **30**, 2608-2620.

115. Quistgaard, E. M., Löw, C., Moberg, P., Guettou, F., Maddi, K. & Nordlund, P. (2013) Structural and Biophysical Characterization of the Cytoplasmic Domains of Human BAP29 and BAP31, *PLOS ONE.* **8**, e71111.
116. Uversky, V. N., Gillespie, J. R., Millett, I. S., Khodyakova, A. V., Vasiliev, A. M., Chernovskaya, T. V., Vasilenko, R. N., Kozlovskaya, G. D., Dolgikh, D. A., Fink, A. L., Doniach, S. & Abramov, V. M. (1999) Natively Unfolded Human Prothymosin α Adopts Partially Folded Collapsed Conformation at Acidic pH, *Biochemistry.* **38**, 15009-15016.
117. Uversky, V. N., Li, J. & Fink, A. L. (2001) Evidence for a Partially Folded Intermediate in α-Synuclein Fibril Formation, *Journal of Biological Chemistry.* **276**, 10737-10744.
118. Weinreb, P. H., Zhen, W., Poon, A. W., Conway, K. A. & Lansbury, P. T. (1996) NACP, A Protein Implicated in Alzheimer's Disease and Learning, Is Natively Unfolded, *Biochemistry.* **35**, 13709-13715.
119. Gottlieb, R. A., Nordberg, J., Skowronski, E. & Babior, B. M. (1996) Apoptosis induced in Jurkat cells by several agents is preceded by intracellular acidification, *Proceedings of the National Academy of Sciences of the United States of America.* **93**, 654-658.
120. Sharma, K. & Srikant, C. B. (1998) G Protein Coupled Receptor Signaled Apoptosis Is Associated with Activation of a Cation Insensitive Acidic Endonuclease and Intracellular Acidification, *Biochemical and Biophysical Research Communications.* **242**, 134-140.
121. Xie, Z., Schendel, S., Matsuyama, S. & Reed, J. C. (1998) Acidic pH Promotes Dimerization of Bcl-2 Family Proteins, *Biochemistry.* **37**, 6410-6418.
122. Nilsson, C., Johansson, U., Johansson, A.-C., Kågedal, K. & Öllinger, K. (2006) Cytosolic acidification and lysosomal alkalinization during TNF-α induced apoptosis in U937 cells, *Apoptosis.* **11**, 1149.
123. Yuan, X.-M., Li, W., Dalen, H., Lotem, J., Kama, R., Sachs, L. & Brunk, U. T. (2002) Lysosomal destabilization in p53-induced apoptosis, *Proceedings of the National Academy of Sciences.* **99**, 6286-6291.
124. Putz, U., Howitt, J., Doan, A., Goh, C.-P., Low, L.-H., Silke, J. & Tan, S.-S. (2012) The Tumor Suppressor PTEN Is Exported in Exosomes and Has Phosphatase Activity in Recipient Cells, *Science Signaling.* **5**, ra70-ra70.
125. Parolini, I., Federici, C., Raggi, C., Lugini, L., Palleschi, S., De Milito, A., Coscia, C., Iessi, E., Logozzi, M., Molinari, A., Colone, M., Tatti, M., Sargiacomo, M. & Fais, S. (2009) Microenvironmental pH is a key factor for exosome traffic in tumor cells, *The Journal of biological chemistry.* **284**, 34211-34222.
126. Azmi, A. S., Bao, B. & Sarkar, F. H. (2013) Exosomes in cancer development, metastasis, and drug resistance: a comprehensive review, *Cancer and Metastasis Reviews.* **32**, 623-642.
127. Février, B. & Raposo, G. (2004) Exosomes: endosomal-derived vesicles shipping extracellular messages, *Current Opinion in Cell Biology.* **16**, 415-421.
128. Colombo, M., Raposo, G. & Théry, C. (2014) Biogenesis, Secretion, and Intercellular Interactions of Exosomes and Other Extracellular Vesicles, *Annual Review of Cell and Developmental Biology.* **30**, 255-289.
129. Nilsson, C., Kågedal, K., Johansson, U. & Öllinger, K. (2004) Analysis of cytosolic and lysosomal pH in apoptotic cells by flow cytometry, *Methods in Cell Science.* **25**, 185-194.
130. Mellman, I., Fuchs, R. & Helenius, A. (1986) Acidification of the Endocytic and Exocytic Pathways, *Annual Review of Biochemistry.* **55**, 663-700.
131. Tycko, B. & Maxfield, F. R. (1982) Rapid acidification of endocytic vesicles containing α2-macroglobulin, *Cell.* **28**, 643-651.

132. van Renswoude, J., Bridges, K. R., Harford, J. B. & Klausner, R. D. (1982) Receptor-mediated endocytosis of transferrin and the uptake of fe in K562 cells: identification of a nonlysosomal acidic compartment, *Proceedings of the National Academy of Sciences of the United States of America.* **79**, 6186-6190.
133. Chang, S., Kim, J. H. & Shin, J. (2002) p62 forms a ternary complex with PKCζ and PAR-4 and antagonizes PAR-4-induced PKCζ inhibition, *FEBS Letters.* **510**, 57-61.
134. Sanchez, P., De Carcer, G., Sandoval, I. V., Moscat, J. & Diaz-Meco, M. T. (1998) Localization of Atypical Protein Kinase C Isoforms into Lysosome-Targeted Endosomes through Interaction with p62, *Molecular and Cellular Biology.* **18**, 3069-3080.
135. Diering, G. H. & Numata, M. (2014) Endosomal pH in neuronal signaling and synaptic transmission: role of Na(+)/H(+) exchanger NHE5, *Frontiers in physiology.* **4**, 412-412.
136. Denzer, K., Kleijmeer, M. J., Heijnen, H. F., Stoorvogel, W. & Geuze, H. J. (2000) Exosome: from internal vesicle of the multivesicular body to intercellular signaling device, *Journal of Cell Science.* **113**, 3365-3374.
137. Warburg, O. (1956) On the Origin of Cancer Cells, *Science.* **123**, 309-314.
138. Griffiths, J. R. (1991) Are cancer cells acidic?, *British journal of cancer.* **64**, 425-427.
139. Li, J. & Eastman, A. (1995) Apoptosis in an Interleukin-2-dependent Cytotoxic T Lymphocyte Cell Line Is Associated with Intracellular Acidification: ROLE OF THE Na/H-ANTIPORT, *Journal of Biological Chemistry.* **270**, 3203-3211.
140. Matsuyama, S. & Reed, J. C. (2000) Mitochondria-dependent apoptosis and cellular pH regulation, *Cell Death And Differentiation.* **7**, 1155.
141. Thangaraju, M., Sharma, K., Leber, B., Andrews, D. W., Shen, S.-H. & Srikant, C. B. (1999) Regulation of Acidification and Apoptosis by SHP-1 and Bcl-2, *Journal of Biological Chemistry.* **274**, 29549-29557.
142. Rothschild, L. J. & Mancinelli, R. L. (2001) Life in extreme environments, *Nature.* **409**, 1092.
143. Rampelotto, P. H. (2013) Extremophiles and extreme environments, *Life (Basel, Switzerland).* **3**, 482-485.
144. Sievers, F., Wilm, A., Dineen, D., Gibson, T. J., Karplus, K., Li, W., Lopez, R., McWilliam, H., Remmert, M., Söding, J., Thompson, J. D. & Higgins, D. G. (2011) Fast, scalable generation of high-quality protein multiple sequence alignments using Clustal Omega, *Molecular systems biology.* **7**, 539-539.
145. Sievers, F. & Higgins, D. G. (2018) Clustal Omega for making accurate alignments of many protein sequences, *Protein science : a publication of the Protein Society.* **27**, 135-145.
146. Drazic, A., Gebendorfer, K. M., Mak, S., Steiner, A., Krause, M., Bepperling, A. & Winter, J. (2014) Tetramers Are the Activation-competent Species of the HOCl-specific Transcription Factor HypT, *Journal of Biological Chemistry.* **289**, 977-986.
147. Melby, T. E., Ciampaglio, C. N., Briscoe, G. & Erickson, H. P. (1998) The Symmetrical Structure of Structural Maintenance of Chromosomes (SMC) and MukB Proteins: Long, Antiparallel Coiled Coils, Folded at a Flexible Hinge, *The Journal of Cell Biology.* **142**, 1595-1604.
148. Xi, Z., Gao, Y., Sirinakis, G., Guo, H. & Zhang, Y. (2012) Single-molecule observation of helix staggering, sliding, and coiled coil misfolding, *Proceedings of the National Academy of Sciences.* **109**, 5711-5716.

149. Kon, T., Imamula, K., Roberts, A. J., Ohkura, R., Knight, P. J., Gibbons, I. R., Burgess, S. A. & Sutoh, K. (2009) Helix sliding in the stalk coiled coil of dynein couples ATPase and microtubule binding, *Nature structural & molecular biology.* **16**, 325-333.
150. O'Shea, E., Klemm, J., Kim, P. & Alber, T. (1991) X-ray structure of the GCN4 leucine zipper, a two-stranded, parallel coiled coil, *Science.* **254**, 539-544.
151. Dempsey, C. E. (1990) The actions of melittin on membranes, *Biochimica et Biophysica Acta (BBA) - Reviews on Biomembranes.* **1031**, 143-161.
152. Bello, J., Bello, H. R. & Granados, E. (1982) Conformation and aggregation of melittin: dependence of pH and concentration, *Biochemistry.* **21**, 461-465.
153. Derewenda, U., Tarricone, C., Choi, W. C., Cooper, D. R., Lukasik, S., Perrina, F., Tripathy, A., Kim, M. H., Cafiso, D. S., Musacchio, A. & Derewenda, Z. S. (2007) The Structure of the Coiled-Coil Domain of Ndel1 and the Basis of Its Interaction with Lis1, the Causal Protein of Miller-Dieker Lissencephaly, *Structure.* **15**, 1467-1481.
154. Nicholls, C. D., McLure, K. G., Shields, M. A. & Lee, P. W. K. (2002) Biogenesis of p53 Involves Cotranslational Dimerization of Monomers and Posttranslational Dimerization of Dimers: IMPLICATIONS ON THE DOMINANT NEGATIVE EFFECT, *Journal of Biological Chemistry.* **277**, 12937-12945.
155. Lee, W., Harvey, T. S., Yin, Y., Yau, P., Litchfield, D. & Arrowsmith, C. H. (1994) Solution structure of the tetrameric minimum transforming domain of p53, *Nature Structural Biology.* **1**, 877-890.
156. Stommel, J. M., Marchenko, N. D., Jimenez, G. S., Moll, U. M., Hope, T. J. & Wahl, G. M. (1999) A leucine-rich nuclear export signal in the p53 tetramerization domain: regulation of subcellular localization and p53 activity by NES masking, *The EMBO Journal.* **18**, 1660-1672.
157. Dewson, G., Kratina, T., Czabotar, P., Day, C. L., Adams, J. M. & Kluck, R. M. (2009) Bak Activation for Apoptosis Involves Oligomerization of Dimers via Their α6 Helices, *Molecular Cell.* **36**, 696-703.
158. Hayashi, M. K., Ames, H. M. & Hayashi, Y. (2006) Tetrameric Hub Structure of Postsynaptic Scaffolding Protein Homer, *The Journal of Neuroscience.* **26**, 8492-8501.
159. Kostova, I. (2006) Platinum Complexes as Anticancer Agents, *Recent patents on anti-cancer drug discovery.* **1**, 1-22.
160. Paciotti, R., Corinti, D., De Petris, A., Ciavardini, A., Piccirillo, S., Coletti, C., Re, N., Maitre, P., Bellina, B., Barran, P., Chiavarino, B., Elisa Crestoni, M. & Fornarini, S. (2017) Cisplatin and transplatin interaction with methionine: bonding motifs assayed by vibrational spectroscopy in the isolated ionic complexes, *Physical Chemistry Chemical Physics.* **19**, 26697-26707.
161. Alexandrov, A., Dutta, K. & Pascal, S. (2001) MBP Fusion Protein with a Viral Protease Cleavage Site: One-Step Cleavage/Purification of Insoluble Proteins, *BioTechniques.* **30**, 1194-8.
162. Clark, A. M., Ponniah, K., Warden, M. S., Raitt, E. M., Smith, B. G. & Pascal, S. M. (2019) Tetramer formation by the caspase-activated fragment of the Par-4 tumor suppressor, *The FEBS Journal.* **286**, 4060-4073.
163. Chène, P. (2001) The role of tetramerization in p53 function, *Oncogene.* **20**, 2611-2617.
164. Kraiss, S., Quaiser, A., Oren, M. & Montenarh, M. (1988) Oligomerization of oncoprotein p53, *J Virol.* **62**, 4737-4744.
165. Zhao, L., Cheng, Q., Wang, Z., Xi, Z., Xu, D. & Liu, Y. (2014) Cisplatin binds to human copper chaperone Cox17: the mechanistic implication of drug delivery to mitochondria, *Chemical Communications.* **50**, 2667-2669.

166. Zia, M. K., Siddiqui, T., Ali, S. S., Ahsan, H. & Khan, F. H. (2018) Interaction of anti-cancer drug-cisplatin with major proteinase inhibitor-alpha-2-macroglobulin: Biophysical and thermodynamic analysis, *International Journal of Biological Macromolecules.* **116**, 721-727.
167. Atipairin, A., Canyuk, B. & Ratanaphan, A. (2010) Cisplatin Affects the Conformation of Apo Form, not Holo Form, of BRCA1 RING Finger Domain and Confers Thermal Stability, *Chemistry & Biodiversity.* **7**, 1949-1967.
168. Safirstein, R., Winston, J., Goldstein, M., Moel, D., Dikman, S. & Guttenplan, J. (1986) Cisplatin Nephrotoxicity, *American Journal of Kidney Diseases.* **8**, 356-367.
169. Wang, X. & Guo, Z. (2007) The Role of Sulfur in Platinum Anticancer Chemotherapy, *Anti-Cancer Agents in Medicinal Chemistry- Anti-Cancer Agents).* **7**, 19-34.
170. DeSimone, P., Brennan, L., Cattaneo, M. & Zucca, E. (1987). Phase I evaluation and pharmacokinetics of cis-platin (cis Pt) complexed to albumin (cis Pt A). Paper presented at the *Proc Am Soc Clin Oncol*.
171. Hoshino, T., Misaki, M., Yamamoto, M., Shimizu, H., Ogawa, Y. & Toguchi, H. (1995) In Vitro Cytotoxicities and In Vivo Distribution of Transferrin–Platinum(II) Complex, *Journal of Pharmaceutical Sciences.* **84**, 216-221.
172. Holding, J., Lindup, W., van Laer, C., Vreeburg, G., Schilling, V., Wilson, J. & Stell, P. (1992) Phase I trial of a cisplatin-albumin complex for the treatment of cancer of the head and neck, *British Journal of Clinical Pharmacology.* **33**, 75-81.
173. Nanji, A. A., Stewart, D. J. & Mikhael, N. Z. (1986) Hyperuricemia and hypoalbuminemia predispose to cisplatin-induced nephrotoxicity, *Cancer Chemotherapy and Pharmacology.* **17**, 274-276.
174. Sharon, M. K. & Nicholas, C. P. (2000) The Use of Circular Dichroism in the Investigation of Protein Structure and Function, *Current Protein & Peptide Science.* **1**, 349-384.
175. Palm-Espling, M. E. & Wittung-Stafshede, P. (2012) Reaction of platinum anticancer drugs and drug derivatives with a copper transporting protein, Atox1, *Biochemical Pharmacology.* **83**, 874-881.
176. Picone, D., Donnarumma, F., Ferraro, G., Russo Krauss, I., Fagagnini, A., Gotte, G. & Merlino, A. (2015) Platinated oligomers of bovine pancreatic ribonuclease: Structure and stability, *Journal of Inorganic Biochemistry.* **146**, 37-43.
177. Arnesano, F., Banci, L., Bertini, I., Felli, I. C., Losacco, M. & Natile, G. (2011) Probing the Interaction of Cisplatin with the Human Copper Chaperone Atox1 by Solution and In-Cell NMR Spectroscopy, *Journal of the American Chemical Society.* **133**, 18361-18369.
178. Möltgen, S., Piumatti, E., Massafra, G. M., Metzger, S., Jaehde, U. & Kalayda, G. V. (2020) Cisplatin Protein Binding Partners and Their Relevance for Platinum Drug Sensitivity, *Cells.* **9**, 1322.
179. Li, H., Zhao, Y., Phillips, H. I. A., Qi, Y., Lin, T.-Y., Sadler, P. J. & O'Connor, P. B. (2011) Mass Spectrometry Evidence for Cisplatin As a Protein Cross-Linking Reagent, *Analytical Chemistry.* **83**, 5369-5376.
180. Merlino, A. (2021) Recent advances in protein metalation: structural studies, *Chemical Communications.* **57**, 1295-1307.
181. Damian, L. (2013) Isothermal Titration Calorimetry for Studying Protein–Ligand Interactions in *Protein-Ligand Interactions: Methods and Applications* (Williams, M. A. & Daviter, T., eds) pp. 103-118, Humana Press, Totowa, NJ.
182. Ràfols, C., Zarza, S. & Bosch, E. (2014) Molecular interactions between some non-steroidal anti-inflammatory drugs (NSAIDʹs) and bovine (BSA) or human (HSA) serum albumin estimated

by means of isothermal titration calorimetry (ITC) and frontal analysis capillary electrophoresis (FA/CE), *Talanta.* **130**, 241–250.
183. Gao, S., Wang, H., Lee, P., Melamed, J., Li, C. X., Zhang, F., Wu, H., Zhou, L. & Wang, Z. Androgen receptor and prostate apoptosis response factor-4 target the c-FLIP gene to determine survival and apoptosis in the prostate gland. **36**, 463.
184. Woodbury, R. L., Hardy, S. J. S. & Randall, L. L. (2002) Complex behavior in solution of homodimeric SecA, *Protein Sci.* **11**, 875-882.
185. Gotte, G., Bertoldi, M. & Libonati, M. (1999) Structural versatility of bovine ribonuclease A, *European Journal of Biochemistry.* **265**, 680-687.
186. Gotte, G., Laurents, D. V. & Libonati, M. (2006) Three-dimensional domain-swapped oligomers of ribonuclease A: identification of a fifth tetramer, pentamers and hexamers, and detection of trace heptameric, octameric and nonameric species, *Biochimica et Biophysica Acta (BBA) - Proteins and Proteomics.* **1764**, 44-54.
187. Gotte, G., Laurents, D. V., Merlino, A., Picone, D. & Spadaccini, R. (2013) Structural and functional relationships of natural and artificial dimeric bovine ribonucleases: New scaffolds for potential antitumor drugs, *FEBS Letters.* **587**, 3601-3608.
188. Uversky, V. N. (2010) Mysterious oligomerization of the amyloidogenic proteins, *The FEBS Journal.* **277**, 2940-2953.
189. Morris, A. M., Watzky, M. A. & Finke, R. G. (2009) Protein aggregation kinetics, mechanism, and curve-fitting: A review of the literature, *Biochimica et Biophysica Acta (BBA) - Proteins and Proteomics.* **1794**, 375-397.
190. Matousek, J., Gotte, G., Pouckova, P., Soucek, J., Slavik, T., Vottariello, F. & Libonati, M. (2003) Antitumor Activity and Other Biological Actions of Oligomers of Ribonuclease A, *Journal of Biological Chemistry.* **278**, 23817-23822.
191. Tyn, M. T. & Gusek, T. W. (1990) Prediction of diffusion coefficients of proteins, *Biotechnology and bioengineering.* **35**, 327-38.
192. Smilgies, D.-M. & Folta-Stogniew, E. (2015) Molecular weight-gyration radius relation of globular proteins: a comparison of light scattering, small-angle X-ray scattering and structure-based data, *J Appl Crystallogr.* **48**, 1604-1606.
193. Erickson, H. P. (2009) Size and shape of protein molecules at the nanometer level determined by sedimentation, gel filtration, and electron microscopy, *Biol Proced Online.* **11**, 32-51.

APPENDIX

COMPUTATIONAL ANALYSIS OF M293-PT-M293 CROSSLINKED CL-PAR-4 COILED COIL DIMER

In order to assess whether cross-linking by cisPt could potentially be introduced without major disruption of the coiled coil, a theoretical model of the cl-Par-4 coiled coil with platinum cross-linking between M293 of each molecule of the coiled coil dimer was developed by Professor Bayse. Peptides were created from point mutations of the coiled coil Par-4 x-ray structure (PDB: 5FIY). The simulations were performed using AMBER 16 and the *ff14sb* force field. Parameters for the $[Pt(NH_3)_2Met_2]$ fragment were created using the Metal Center Parameter Builder (MCPB). The protein system was neutralized with Na^+ ions and solvated with a 10-angstrom rectangular box of TIP3P water molecules. The solvated system was warmed and equilibrated to 300 K prior to 1-3 microsecond production runs.

A depiction of the resulting cross-linked dimer is shown in Figure S1. The platinum atom is shown as a sphere, and the coordinating sulfur atoms from M293 of each chain are yellow. Note that the platinum atom is not positioned centrally and symmetrically in this model: it is to one side of the dimer axis. This necessitates that asymmetry will be introduced into the dimer. However, note that the coiled coil remains largely intact, as shown by the broad cartoon shape for each chain, which is deployed only if the backbone angles are within the alpha helix range. A break in the helix is seen for molecule B, directly at the M293 residue itself. An overall curve and some other kinks and irregularities are also introduced. However, the largest alteration near the site of the platinum is at M293, and the coiled coil remains intact.

Figure S2 presents the numerical values of changes in the backbone introduced into the model by the M293-platinum-M293 crosslink. These changes were derived by subtracting the dihedral angles of the un-coordinated coiled coil (PDB 5FIY) from the dihedral angles of the cross-linked dimer model shown in Figure S1. The largest changes are compensating alterations in phi and psi angles of M293 of molecule B (marked by * in Figure S2, bottom two panels). These changes are phi (-84 degrees) and psi (+89 degrees). Other changes are seen, the largest nearby ones being two residues away in either direction, at R291 phi (-47 degrees) and D295 psi (+41 degrees). In general, lesser changes are seen in chain A than in chain B. However, some large changes are seen near the C-terminus of molecule A, far from the M293 site, but these may not be directly related to the crosslink. Large changes were also seen at the chain termini (residues 262-265 and residues 338-340). These changes are highly influenced by natural instability at chain termini rather than by the crosslink, and so these terminal residues have been omitted from the graphs in Figure S2.

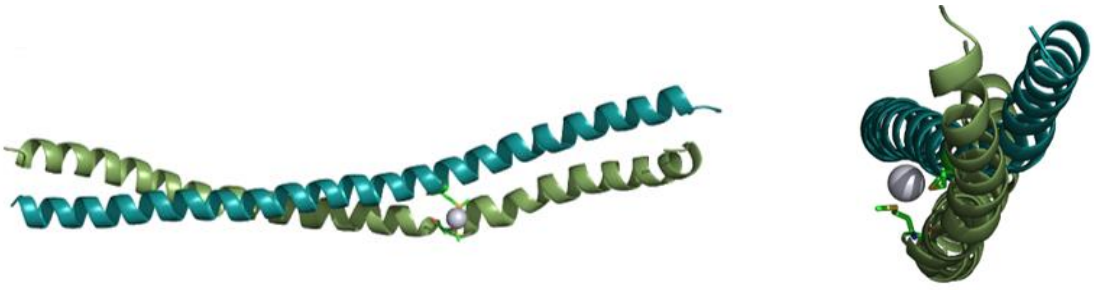

(a) (b)

Fig. S1. Computational model of M293-Pt-M293 crosslinked cl-Par-4 coiled coil dimer. Chain A of the dimer is colored teal, while chain B is olive. The platinum atom is shown as a grey sphere. The M293 side chain of each molecule is shown as sticks, with the coordinating sulfur atoms drawn in yellow.

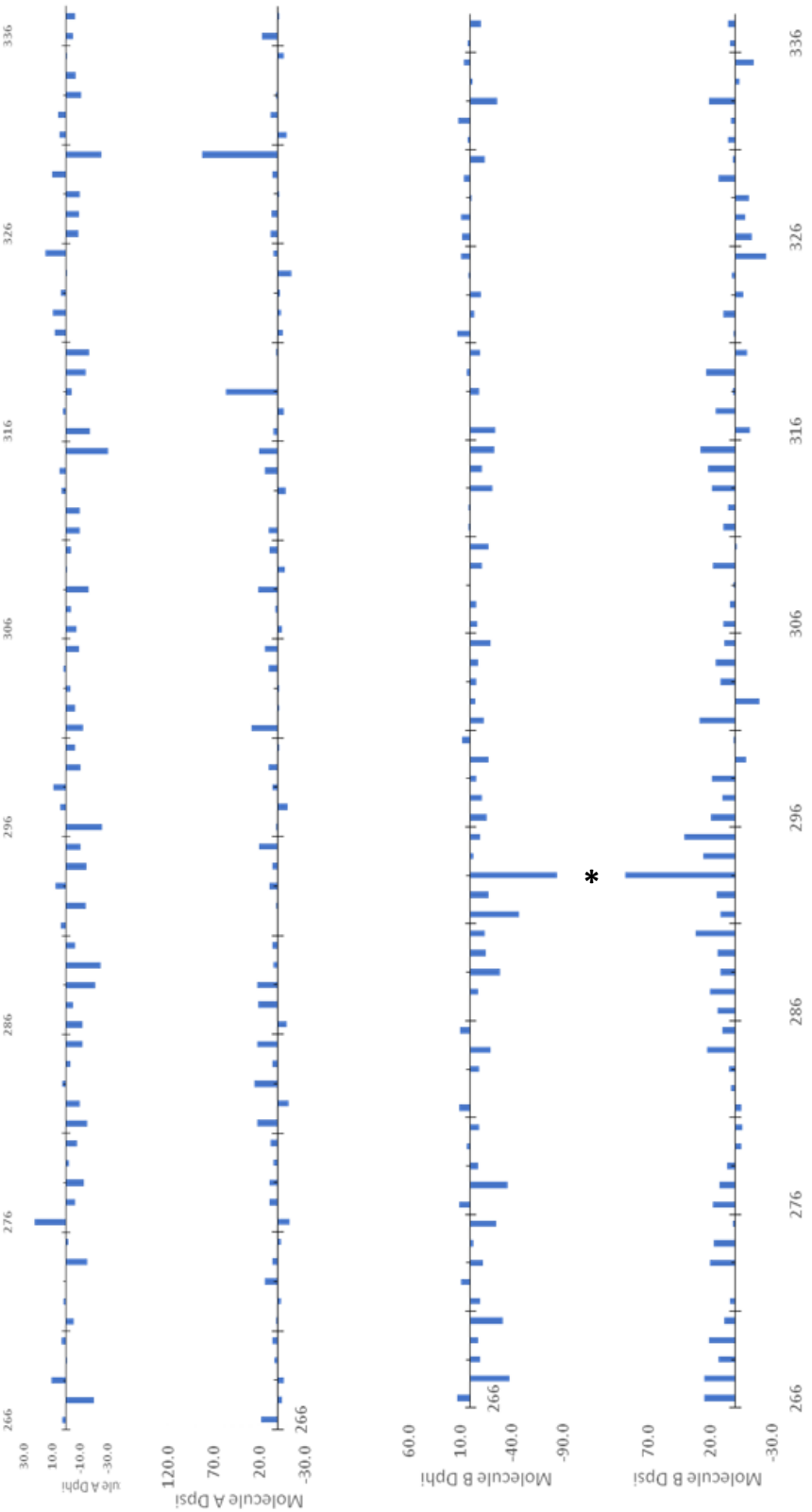

Fig. S2. Changes in backbone dihedral angles observed in the cl-Par-4 model after introduction of the M293-Pt-M293 crosslink. Changes in phi and psi for residues 266-337 are shown for each chain. The M293 residue of chain B is marked by an asterisk (*).

In summary, computational analysis supports the experimental result that cisplatin-induced crosslinking could occur in Par-4 without major disruption of secondary structure. However, the exact cisPt and transPt binding site(s) in FL-Par-4 and cl-Par-4 are yet to be determined. Therefore, further structural studies are needed to identify the cisPt and transPt binding site(s) in Par-4 and assess how these binding interactions affect Par-4 structure.

DETERMINING MOLARITY OF A PROTEIN FROM THE MASS CONCENTRATION

To determine the molarity of a protein from the mass concentration, the following relationship is used: mM = (mg/mL) / (MW in kDa)

For Par-4:

1 mM cl-Par-4 = 24 mg/mL (cl-Par-4 is a 24 kDa protein)

1 mM FL-Par-4 = 36.5 mg/mL (FL-Par-4 is a 36.5 kDa protein)

Example: Convert 1 mg/mL cl-Par-4 (24 kDa protein) to molarity.

X mM cl-Par-4 = 1 mg/mL cl-Par-4 / 24 kDa = 0.042 mM (1 M / 1000 mM) = $4.2e^{-5}$ M cl-Par-4

Example: Convert 1 mg/mL FL-Par-4 (36.5 kDa protein) to molarity.

X mM FL-Par-4 = 1 mg/mL FL-Par-4 / 36.5 kDa = 0.027 mM (1 M / 1000 mM) = $2.7e^{-5}$ M FL-Par-4

RELATIONSHIP BETWEEN RADIUS AND MOLECULAR WEIGHT OF A SPHERICAL PROTEIN

For a fully folded protein, the relationship of volume to molecular weight is $R_{min} = (3V/4\Pi)^{1/3} = 0.066M^{1/3}$ [191-193]. R_{min} is in units of nm and M is in units of Daltons. R_{min} refers to the minimum radius of a sphere that could contain the specified mass of protein (M). A partial specific volume of $v_2 = 0.73$ cm^3/g is assumed. The estimated radius of a spherical 10 kDa protein is 1.42 nm, 3.05 nm for a 100 kDa spherical protein, and 5.21 nm for a spherical 500 kDa protein complex. The hydrodynamic radius increases as molecular weight of the protein (or complex) increases. However, a protein of the same molecular weight would display a larger radius if in a non-globular conformation.

LIGAND DISPLACEMENT REACTION OF CISPLATIN WITH WATER

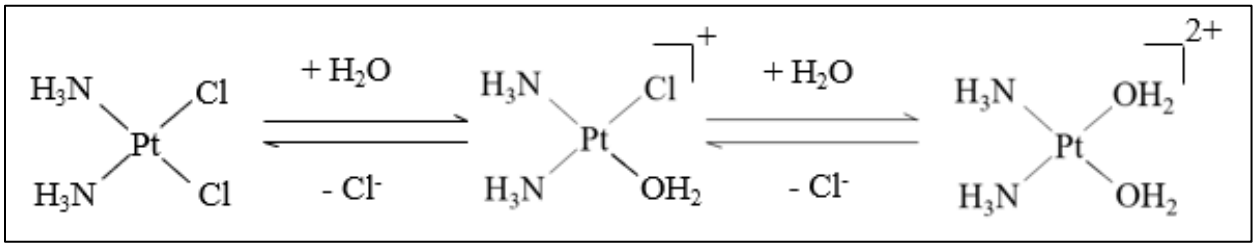

Fig. S3. Ligand displacement reaction of cisplatin with water to form a highly reactive cationic species, capable of crosslinking DNA and interacting with other biomolecules (US patent number 756906B2, mechanism reproduced from Long et al. 1981)

VITA

Andrea Megan Clark

akorell@odu.edu

Department of Chemistry and Biochemistry, Old Dominion University, Norfolk, VA 23529

Education

Old Dominion University, PhD, Chemistry (May 2021)

Old Dominion University , MS non-thesis, Chemistry (August 2020)

Salisbury University, BS, *magna cum laude*, Biology (May 2016)

Select Presentations

A. Clark, K. Ponniah, M. Warden, E. Raitt, B. Smith, and S. Pascal, "Ionic strength-induced tetramer formation in the Par-4 tumor suppressor" Oral presentation delivered at Virginia Academy of Science, Norfolk, VA, May 2019.

A. Clark and S. Pascal, "Folding of the intrinsically disordered Par-4 tumor suppressor under native and extreme conditions" Oral presentation delivered at the Virginia Space Grant Consortium Spring Meeting, Hampton, VA. April 2019.

A. Clark, K. Ponniah, M. Warden, E. Raitt, A. Yawn, and S. Pascal, "Acid-induced folding of caspase-activated Par-4 tumor suppressor" Oral presentation delivered at the American Chemical Society National Meeting, Orlando, FL. April 2019.

Peer Reviewed Publications

Alexander Bowitch, Ansuman Sahoo, **Andrea M. Clark**, Christiana Ntangka, Krishna K. Raut, Paul Gollnick, Michael C. Yu, Steven M. Pascal, Sarah E. Walker, and Denise M. Ferkey. Methylation of the D2 dopamine receptor affects binding with regulatory proteins Par-4 and Calmodulin. *microPublication Biology*, 2021

Wortman, M.J., Dagdanova, A.V., **Clark, A.M**., Godfrey, E.W., Pascal, S.M., Johnson, E.M., and Daniel, D.C. A synthetic Pur-based peptide binds and alters G-quadruplex secondary structure present in the expanded RNA repeat of C9orf72 ALS/FTD. *BBA- Molecular Cell Research*, 2020, 118674

Clark, A.M., Ponniah, K. Warden, M.S., Raitt, E.M., Smith, B.G., and Pascal, S.M. Tetramer formation by the caspase-activated fragment of the Par-4 tumor suppressor. *The FEBS Journal*, 2019, 286 (20), 4060-4073

Clark, A.M., Ponniah, K., Warden, M.S., Raitt, E.M., Yawn, A.C., and Pascal, S.M. pH-induced folding of the caspase-cleaved Par-4 tumor suppressor: evidence of structure outside of the coiled-coil domain. *Biomolecules*, 2018, 8(4): 162

Professional Positions

Regulatory Specialist, US FDA Drug Division Department – Registrar Corp, Hampton, VA (July 2020 – present)

Graduate Teaching Assistant, Department of Chemistry and Biochemistry – Old Dominion University, Norfolk, VA (Fall 2016 – Summer 2020)